Article

Immunity

Age-Related Dopaminergic Innervation Augments T Helper 2-Type Allergic Inflammation in the Postnatal Lung

Graphical Abstract

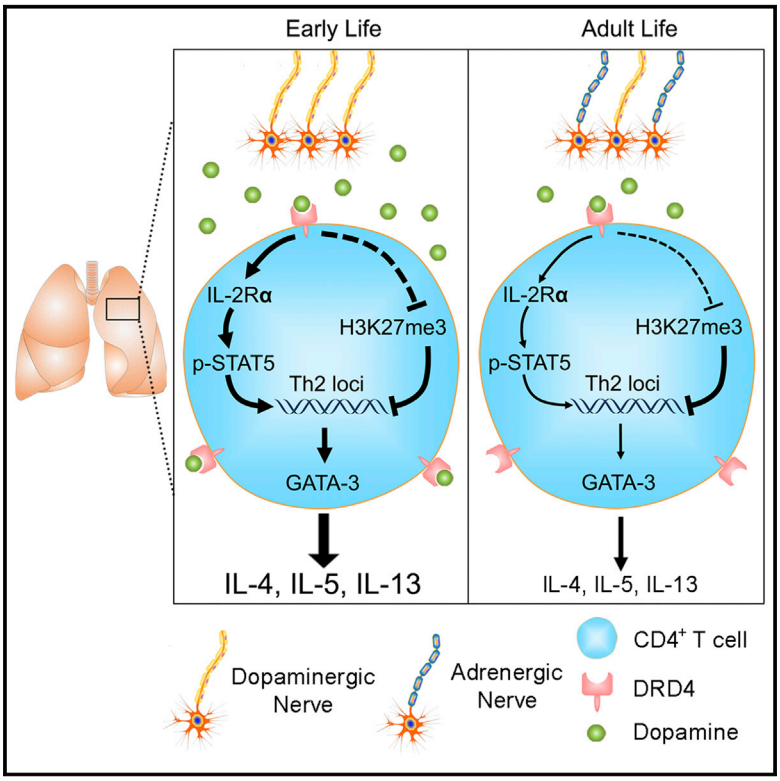

Authors

Wei Wang, Jonathan A. Cohen, Antonia Wallrapp, ..., Alan Fine, Yan Bai, Xingbin Ai

Correspondence

xai@partners.org

In Brief

Children are more prone to developing allergic asthma than adults. Wang et al. find that sympathetic nerves undergo a dopaminergic-to-adrenergic transition during post-natal development of the lung. Dopamine signaling in CD4$^+$ T cells promotes a Th2 phenotype, which makes young mice more susceptible to allergy. These findings provide an age-related mechanism underlying the susceptibility of the young to allergic inflammation.

Highlights

- Sympathetic innervation in the lung undergoes a dopaminergic-to-adrenergic transition
- Dopamine signals through DRD4 in CD4$^+$ T cells to induce a Th2 phenotype
- Dopaminergic nerves in the early lung foster susceptibility to allergic inflammation

Wang et al., 2019, Immunity *51*, 1102–1118
December 17, 2019 © 2019 Elsevier Inc.
https://doi.org/10.1016/j.immuni.2019.10.002

CellPress

CellPress

Immunity
Article

Age-Related Dopaminergic Innervation Augments T Helper 2-Type Allergic Inflammation in the Postnatal Lung

Wei Wang,[1] Jonathan A. Cohen,[1] Antonia Wallrapp,[2] Kenneth G. Trieu,[1] Juliana Barrios,[3] Fengzhi Shao,[3] Nandini Krishnamoorthy,[1] Vijay K. Kuchroo,[2] Matthew R. Jones,[3] Alan Fine,[3,4] Yan Bai,[1] and Xingbin Ai[1,5,6,*]
[1]Division of Pulmonary and Critical Care Medicine, Department of Medicine, Brigham and Women's Hospital, Boston, MA, USA
[2]Evergrande Center for Immunologic Diseases, Harvard Medical School and Brigham and Women's Hospital, Boston, MA, USA
[3]The Pulmonary Center, Department of Medicine, Boston University School of Medicine, Boston, MA, USA
[4]The West Roxbury Veteran's Hospital, West Roxbury, MA, USA
[5]Present address: Division of Newborn Medicine, Department of Pediatrics, Massachusetts General Hospital for Children, Boston, MA, USA
[6]Lead Contact
*Correspondence: xai@partners.org
https://doi.org/10.1016/j.immuni.2019.10.002

SUMMARY

Young children are more susceptible to developing allergic asthma than adults. As neural innervation of the peripheral tissue continues to develop after birth, neurons may modulate tissue inflammation in an age-related manner. Here we showed that sympathetic nerves underwent a dopaminergic-to-adrenergic transition during post-natal development of the lung in mice and humans. Dopamine signaled through a specific dopamine receptor (DRD4) to promote T helper 2 (Th2) cell differentiation. The dopamine-DRD4 pathway acted synergistically with the cytokine IL-4 by upregulating IL-2-STAT5 signaling and reducing inhibitory histone trimethylation at Th2 gene loci. In murine models of allergen exposure, the dopamine-DRD4 pathway augmented Th2 inflammation in the lungs of young mice. However, this pathway operated marginally after sympathetic nerves became adrenergic in the adult lung. Taken together, the communication between dopaminergic nerves and CD4$^+$ T cells provides an age-related mechanism underlying the susceptibility to allergic inflammation in the early lung.

INTRODUCTION

The nervous system communicates with the immune system to regulate inflammation. Pathogen exposure and tissue injury stimulate immune cells and trigger a neural reflex (Chavan et al., 2017). Activation of the neural reflex causes release of neurotransmitters from the innervating afferent and efferent neurons. These neurotransmitters can signal to immune cells, thereby modulating innate and adaptive immune responses. For example, the cholinergic vagal system is activated in sepsis and, by releasing acetylcholine, represses tumor necrosis factor production in spleen macrophages (Borovikova et al., 2000; Wang et al., 2003). In other organs, such as the gut, cholinergic and sympathetic nerves play opposing roles in modulating innate lymphoid type 2 cell (ILC2)-mediated type 2 inflammation by secreting neuromedin U and epinephrine, respectively (Cardoso et al., 2017; Klose et al., 2017; Moriyama et al., 2018).

Allergic asthma is a common airway disease characterized by eosinophilia, mucus overproduction, airway hyperreactivity, and tissue remodeling (Becerra-Díaz et al., 2017; Fahy, 2015). These hallmarks are driven by type 2 cytokines, including interleukin-4 (IL-4), IL-5, and IL-13. Major effector cells in asthma are T helper 2 (Th2) cells. These cells are differentiated from naive CD4$^+$ T cells through a well-orchestrated process that involves priming in the lymph nodes and maturation in the lungs (Van Dyken et al., 2016). Th2 cell differentiation requires IL-4 and IL-2. IL-4 induces differentiation and maintains the Th2 phenotype (Le Gros et al., 1990), whereas IL-2, which is expressed by T cells upon activation, promotes proliferation and Th2 differentiation by transcriptionally activating expression of the *Il2ra*, *Il4*, and *Il4ra* genes via STAT5 (Cote-Sierra et al., 2004; Zhu et al., 2003). Apart from cytokines, neurotransmitters modulate type 2 inflammation. Neuropeptides are known to enhance the antigen-presenting activity of dendritic cells in adult murine models of allergic asthma (Buttari et al., 2014; Ohtake et al., 2015; Talbot et al., 2015). Dopamine has also been shown to induce a Th2 phenotype in CD4$^+$ T cells in culture (Huang et al., 2010; Nakano et al., 2009). However, the intracellular signaling mechanism of dopamine driving Th2 cell differentiation is unknown. In addition, there are conflicting reports regarding the identity of the dopamine receptors involved and the role of dopamine in disease models (Contreras et al., 2016; Franz et al., 2015; Huang et al., 2010; Ilani et al., 2004; Mori et al., 2013; Nakano et al., 2009).

To date, studies related to neural regulation of type 2 inflammation have been limited to mature tissues in adult disease models. As neurons undergo dynamic changes in the abundance and phenotype during post-natal maturation, neuron-immune cell communication may differ with age, contributing to disease susceptibility in a tissue-specific and age-related manner. This age-related communication may be particularly important in asthma because young children are more susceptible to developing allergic asthma than adults (Stern et al., 2008).

 © 2019 Elsevier Inc.

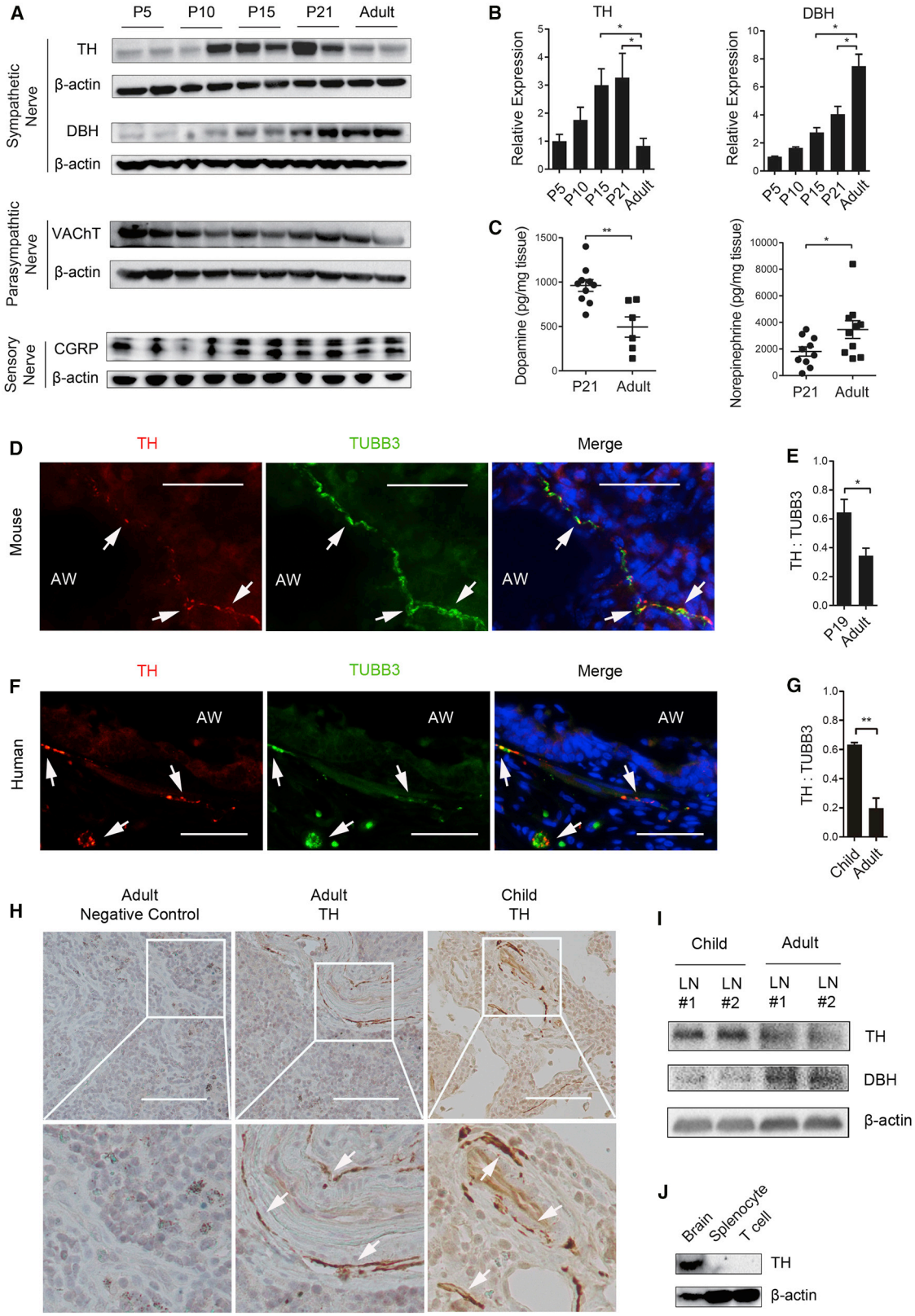

(legend on next page)

In the lungs, nerves innervate the smooth muscle compartment in the airway and vasculature. These nerves are mostly derived from neurons whose cell bodies are located outside of the pulmonary tract in the nodose ganglion, sympathetic ganglion, and brain stem. Nodose sensory afferents and cholinergic and sympathetic efferents are connected through brain stem neurons to form a neurocircuitry that controls fundamental respiratory functions, such as breathing and coughing (Aven and Ai, 2013). Development of the neurocircuitry requires locally produced neurotrophins, such as brain-derived neurotrophic factor and neurotrophin 4 (Aven et al., 2014; Patel et al., 2016; Radzikinas et al., 2011). Temporal expression of these neurotrophins dynamically regulates the process of airway innervation during embryogenesis and post-natal maturation. In the murine lung, neural innervation peaks around post-natal day 14 (P14), followed by a decline in the third post-natal week before it reaches the mature configuration in adults (Aven et al., 2014).

In this study, we characterized the post-natal development of the 3 major types of nerves in the murine lung and discovered that sympathetic nerves transitioned from a predominantly dopamine-producing (dopaminergic) phenotype in early post-natal life to a norepinephrine-producing (adrenergic) phenotype in adult life. We investigated dopamine signaling in T cells and in murine models of allergic inflammation. We found that dopaminergic nerves in the early lung augmented Th2 inflammation by communicating with $CD4^+$ T cells via the dopamine-DRD4 pathway, whereas adrenergic nerves in the adult lung had no Th2-inducing activities. Our findings provide evidence of the development of sympathetic innervation as an age-related modulatory mechanism in Th2 inflammation in the lung, which has implications for the susceptibility and etiology of allergic asthma in young children.

RESULTS

Sympathetic Nerves in the Lung Undergo a Dopaminergic-to-Adrenergic Transition during Post-natal Development

We characterized the developmental dynamics of the 3 major types of nerves in the murine lung after birth. Western blot analysis showed that the relative abundance of sensory and cholinergic nerves, identified by calcitonin gene-related peptide (CGRP) and vesicular acetylcholine transporter (VAChT), respectively, remained mostly unchanged by age (Figure 1A). For sympathetic nerves, however, tyrosine hydroxylase (TH), a specific marker and the rate-limiting enzyme for the biosynthesis of dopamine, peaked around P15–P21, followed by a decline in the adult lung, whereas the amount of dopamine β-hydroxylase (DBH), an enzyme that converts dopamine to norepinephrine, increased with age (Figures 1A and 1B). These changes in tyrosine hydroxylase and DBH were associated with a 50% reduction in the amount of dopamine from P21 (961.9 ± 66.72 pg/mg lung weight) to adults (494.0 ± 114.7 pg/mg lung weight), with a reciprocal increase in norepinephrine (1,815 ± 349 pg/mg lung weight at P21 versus 3,469 ± 669 pg/mg lung weight in adults) (Figure 1C).

Previous studies detected tyrosine hydroxylase in a subset of immune cells, mostly by gene expression assays (Cosentino et al., 2007; Flierl et al., 2007; Papa et al., 2017). To address whether the age-related reduction in tyrosine hydroxylase expression in the post-natal lung was caused by a change in sympathetic innervation, we investigated the source of tyrosine hydroxylase in both mouse and human lungs. Because the lung samples in western blot and dopamine measurement assays likely included lymph nodes associated with bronchi, we separately examined the lung and associated lymph nodes. Because of technical difficulties of dissecting lymph nodes associated with mouse lungs, especially in neonates, we resorted to lymph nodes associated with human donor lungs for the assay. Double-staining for tyrosine hydroxylase and a pan-neural marker, neuron-specific class III β-tubulin (TUBB3), detected tyrosine hydroxylase exclusively in $TUBB3^+$ structures along the airway and blood vessel in mice and humans (Figures 1D and 1F). In addition, tyrosine hydroxylase and DBH were found selectively in nerves along the lymphatic vessel in lymph nodes associated with adult donor lungs (Figures 1H and S1A). DBH was also found only in nerves in the mouse lung (Figure S1B). Furthermore, tyrosine hydroxylase in isolated mouse splenocytes and purified $CD4^+$ T cells was below detection compared with robust expression in neurons (Figure 1J).

After validating the nerve as the major source of tyrosine hydroxylase, we quantified the abundance of sympathetic nerves

Figure 1. Sympathetic Nerves in the Lung Transition from Dopaminergic to Adrenergic Phenotypes from Early Life to Adult Life

(A and B) Western blot analyses (A) of the markers of sympathetic nerves (tyrosine hydroxylase [TH] and dopamine β-hydroxylase [DBH]), parasympathetic nerves (vesicular acetylcholine transporter [VAChT]), and sensory nerves (calcitonin gene-related peptide [CGRP]) in mouse lungs at different post-natal ages. β-Actin was a loading control. Each lane represents one sample. The expression of TH and DBH is presented as fold change relative to post-natal day 5 (P5) in (B). N = 6 from 2 independent experiments.

(C) The amount of dopamine and norepinephrine in the lungs of P21 and adult mice. Results were normalized to the lung weight. Each mark represents one sample.

(D and F) Double-fluorescent staining for TH and neuron-specific class III β-tubulin (TUBB3) in the lungs of mice (D) and humans (F). To visualize nerves, frozen sections (15 μm in thickness) were used for double staining. Nuclei were labeled with Hoechst dye. Arrows mark TH^+TUBB3^+ nerves. AW, airway. Scale bars, 30 μm.

(E and G) Relative abundance of TH^+ nerves in the lungs of mice (E) and humans (G) of two age groups. For quantification, the immunoreactivity of TH was normalized to TUBB3 in double-stained tissue sections. Airways with a diameter of 0.2–0.5 mm in P19 and adult mice and human mid-sized airways with a diameter of 1–2 mm in children (0–13 years of age) and adults (40–65 years of age) were quantified. Data represent mean ± SEM from 5 non-overlapping images from each sample and a total of 3 mouse samples and 4 human samples of each age group.

(H) Representative images of TH staining of lymph nodes associated with donor lungs. Bottom panels: enlarged images outlined in the top panels. Arrows point to TH^+ nerves. Similar results were obtained from 3 donors for each age group.

(I) The expression of TH and DBH in human lymph nodes of each age group, assayed by western blot (see also Figure S1).

(J) The amount of TH in mouse brain, splenocytes, and purified $CD4^+$ T cells, assayed by western blot. Data represent the results from 3 independent experiments. $^*p < 0.05$ and $^{**}p < 0.01$ by two-tailed Student's t test.

See also Figure S1.

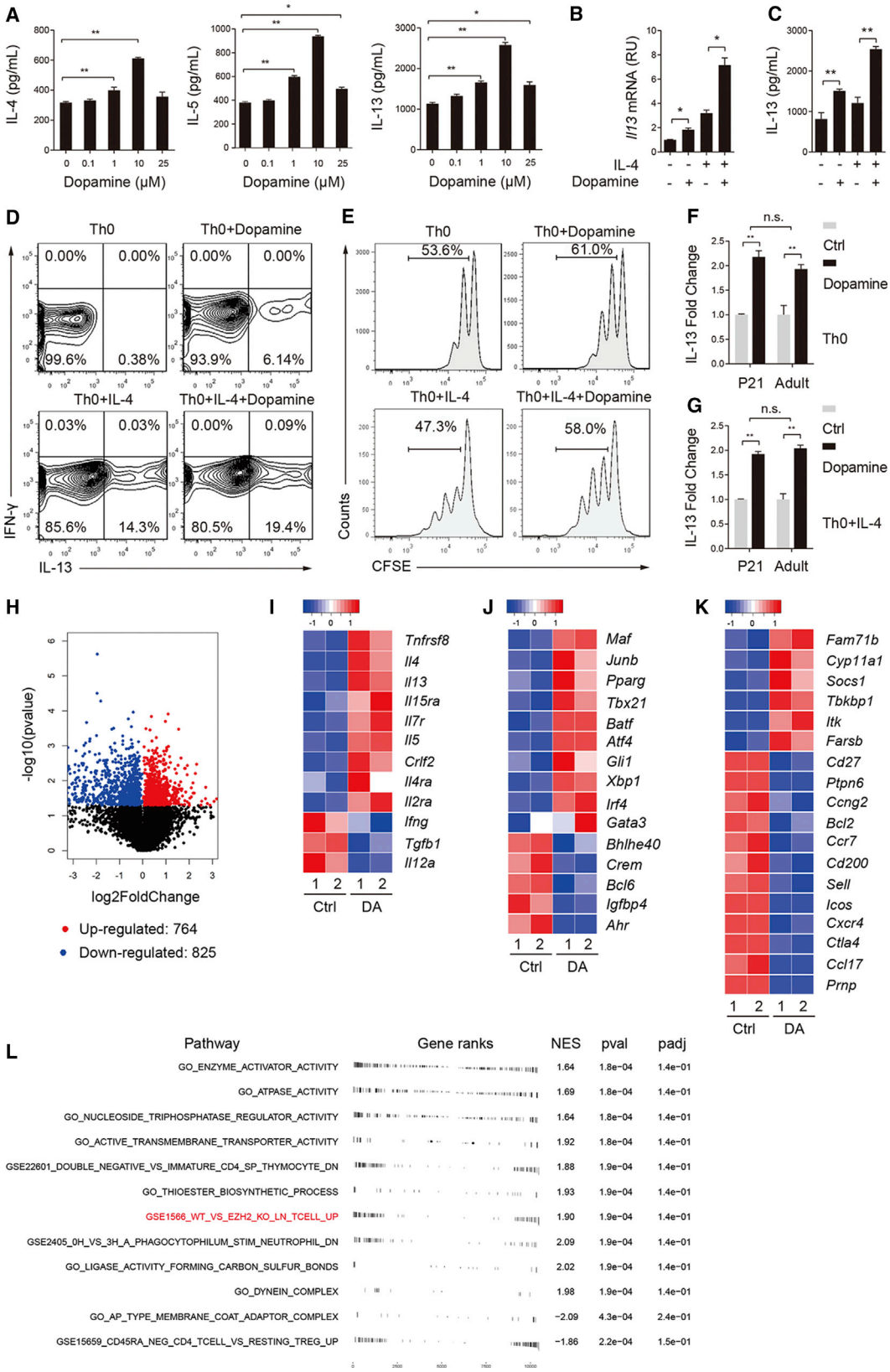

(legend on next page)

in immature and adult lungs. To control for variations caused by the size of the airway, we normalized the immunoreactivity of tyrosine hydroxylase to TUBB3. We found that the extent of tyrosine hydroxylase$^+$ innervation was a fold higher in P19 mice and children (0–13 years of age) compared with the adult counterparts (3–4 months of age in mice and 40–65 years of age in humans) (Figures 1E and 1G). In addition, lymph nodes associated with donor lungs had more abundant tyrosine hydroxylase but less DBH in children compared with adults, as shown by western blot and antibody staining (Figures 1I and S1A). Taken together, sympathetic nerves that innervate the lung and associated lymph nodes transition from a predominantly dopaminergic phenotype in early post-natal life to an adrenergic phenotype in adulthood. In accordance, the sympathetic nervous system in the adult lung is known to be mostly adrenergic (Felten et al., 1985).

Dopamine Promotes a Th2 Phenotype of Naive CD4$^+$ T Cells

We tested whether sympathetic nerves played an age-related role in inflammation by releasing dopamine in the early lung. Dopamine has been shown previously to induce Th2 cytokine expression *in vitro* (Huang et al., 2010; Nakano et al., 2009). To investigate the mechanism of dopamine signaling in Th2 cell differentiation, we isolated naive CD4$^+$ T cells from mouse spleen using a negative selection kit. Cells were stimulated with αCD3 and αCD28 alone (Th0) and in the presence of IL-4 (Th0+IL-4). Dopamine dose-dependently elevated the expression of IL-4, IL-5, and IL-13 in Th0 cultures (Figure 2A). In contrast, norepinephrine and epinephrine, two neurotransmitters that are enzymatically converted from dopamine, had no Th2-inducing activities (Figures S1E and S1F). The activity of dopamine peaked at 10 μM by doubling the amount of Th2 cytokines in Th0 and Th0+IL-4 cultures on day 4 (Figures 2A–2C and S1C) while repressing Th1 cytokines such as *Ifng* (Figure S1D). We thus used 10 μM dopamine for all *in vitro* studies. We noted that the extent of increase in *Il4* and IL-13 expression by dopamine+IL-4 was greater than single treatments combined (Figures 2B and 2C and S1C). In addition, dopamine induced the appearance of IL-13$^+$ cells in Th0 cultures (6.14%) and increased the percentage of IL-13$^+$ cells in Th0+IL-4 cultures from 14.3% to 19.4% (Figure 2D). Furthermore, dopamine promoted T cell proliferation by ~20% in both Th0 and Th0+IL-4 cultures (Figure 2E). Because of the effect of dopamine on cell proliferation, the total number of IL-13$^+$ cells in dopamine-treated Th0+IL-4 culture was slightly higher than the combined effect of single treatments. Taken together, dopamine promotes Th2 cell differentiation in synergy with IL-4.

To evaluate whether age affected T cell responses to dopamine, we compared IL-13 expression in dopamine-treated CD4$^+$ T cells isolated from neonatal and adult mice. We found no difference in the extent of IL-13 induction by dopamine between neonatal and adult cultures (Figures 2F and 2G). In addition, dopamine similarly elevated *Il13* expression in human CD4$^+$ T cells isolated from lymph nodes associated with donor lungs from children and adults (Figure S1G). Furthermore, after identifying DRD4 as the functional dopamine receptor on CD4$^+$ T cells (Figure 3), we showed that age had no effect on DRD4 expression (Figure S2C). Therefore, dopamine promotes Th2 cell differentiation independent of age.

Dopamine Promotes Th2 Cell Differentiation through a Global Transcriptional Program

To gain insights into the mechanism of dopamine signaling in Th2 cell differentiation, we performed RNA sequencing (RNA-seq) of day 4 Th0 cultures. Among a total of 1,589 differentially expressed genes with an adjusted $p < 0.05$ (Figure 2H), dopamine elevated the expression of Th2 cytokine genes such as *Il4*, *Il5*, and *Il13* while repressing Th1 cytokine genes such as *Ifng* and *Il12a* (Figure 2I). These findings were consistent with the results of qPCR and ELISA in culture (Figures 2A–2C, S1C, and S1D). Dopamine also increased the expression of receptor genes for IL-2 and IL-4 (Figure 2I), suggesting a feedforward mechanism for these two essential cytokines in Th2 differentiation. Furthermore, dopamine upregulated expression of the Th2-specifying gene *Gata3* as well as other transcriptional factors known to play a role in Th2 differentiation, including *Maf* and *Pparg* (Chen et al., 2017; Henriksson et al., 2019; Ho et al., 1998; Zheng and Flavell, 1997; Figure 2J). Genes involved in T cell activation during Th2 differentiation (Aki et al., 2018; Henriksson et al.,

Figure 2. Dopamine Promotes a Th2 Phenotype in Naive CD4$^+$ T Cell Cultures

Naive CD4$^+$ T cells isolated from mouse spleens were stimulated with αCD3 and αCD28 (Th0) and IL-4 (Th0+IL-4). Cultures were analyzed on day 4. Except for (A), all other cultures were treated with 10 μM dopamine.

(A) Production of IL-4, IL-5, and IL-13 by Th0 cultures treated with increasing concentrations of dopamine. Data represent mean ± SEM of 3 independent experiments.

(B and C) *Il13* mRNA (B) and protein expression (C) in cultures with and without dopamine and IL-4 (10 ng/mL). Data are representative of at least 5 independent experiments.

(D) Flow cytometry analyses of CD4$^+$ T cell cultures for IL-13 and IFN-γ expression. Data are representative of 2 independent experiments.

(E) Flow cytometry analyses of cell proliferation under each culture condition. Data are representative of 3 independent experiments.

(F and G) IL-13 production in dopamine-treated neonatal and adult cultures relative to the untreated baseline control. Data represent mean ± SEM from 3 independent experiments.

(H) Volcano plot of transcripts with fragments per kilobase (FPKM) > 1 in RNA-seq of Th0 cultures with and without dopamine. Red dots represent significantly upregulated genes, and blue dots represent significantly downregulated genes.

(I–K) Heatmaps of differential gene expression of cytokines and receptors (I), transcriptional factors (J), and other genes involved in T cell activation and Th2 differentiation (K). Each column represents one sample. Genes were ranked by fold change. All listed genes have an adjusted $p < 0.05$. DA, dopamine.

(L) Pathway analyses of gene set enrichment in dopamine-treated Th0 cultures. Pathways that had a false discovery rate (FDR) < 0.05 are shown. NES, normalized enrichment score (a positive score indicates gene set enrichment at the top of the ranked list or those that were upregulated by dopamine); pval, enriched p value; padj, Benjamini-Hochberg-adjusted p value set to < 0.25.

*$p < 0.05$ and **$p < 0.01$ by two-tailed Student's t test.

See also Figure S1.

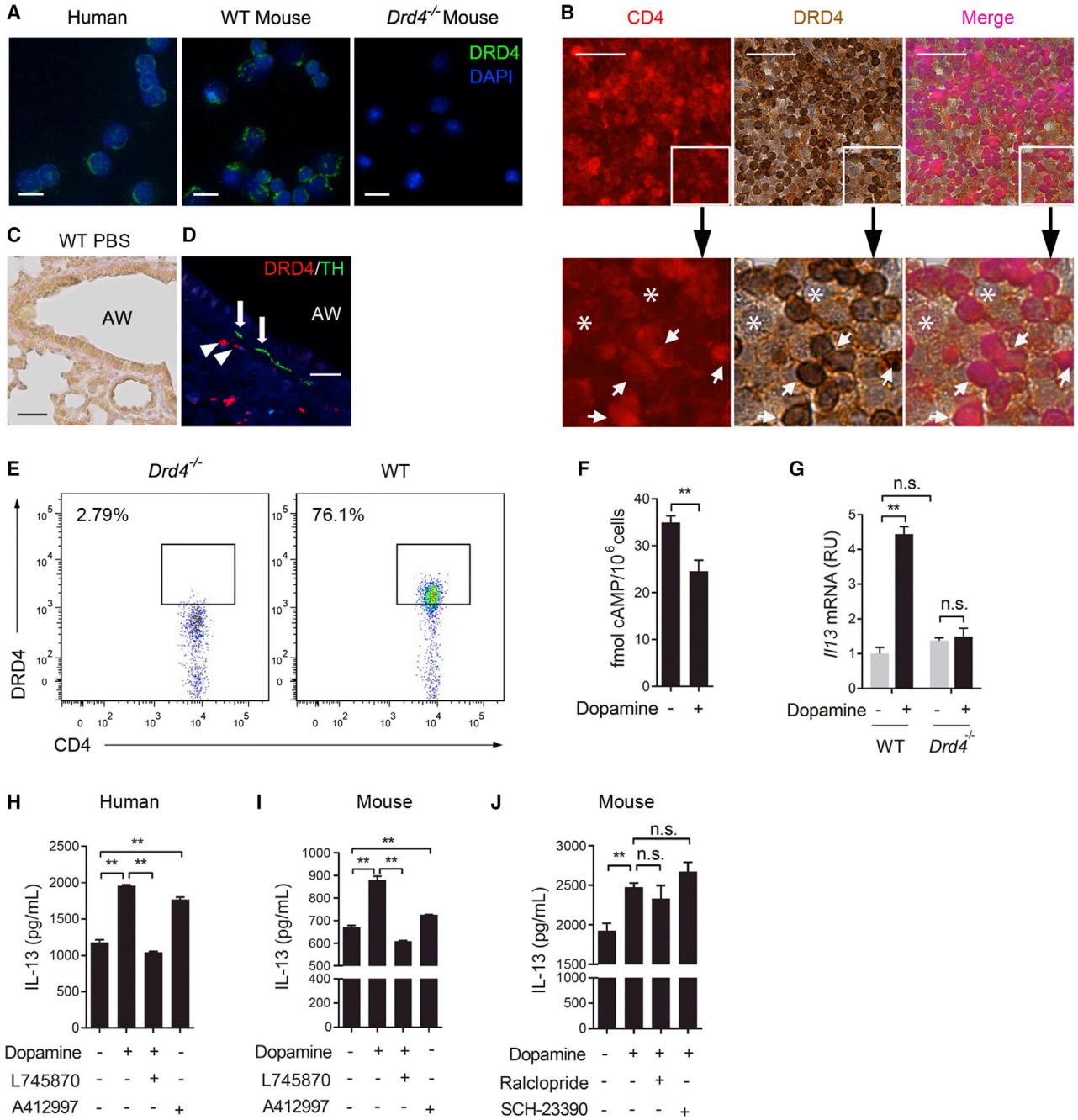

Figure 3. Dopamine Signals through a Major DRD4 Receptor on CD4$^+$ T Cells to Promote the Th2 Phenotype

(A) Staining for DRD4 in mouse and human CD4$^+$ T cell cultures. Nuclei were labeled with Hoechst dye.

(B) Double staining for CD4 and DRD4 using histological sections of lymph nodes associated with adult human donor lungs. The outlined area is enlarged in the bottom panel. Arrows mark CD4$^+$DRD4$^+$ cells. Asterisks mark cells that are double negative. Images show representative results of 3 donors.

(C) DRD4 staining of lung sections of P21 mice at baseline.

(D) Double staining for DRD4 and TH in P21 mouse lungs following OVA exposure. Arrowheads mark DRD4$^+$ cells, and arrows mark TH$^+$ nerves.

(A–D) Images are representative of the results of 3 independent experiments.

(E) Flow cytometry analyses of DRD4 expression in CD4$^+$ T cells in mouse lungs following allergen exposure at P21. Similar results were obtained in 2 independent experiments.

(F) The amount of intracellular cAMP in control and dopamine-treated Th0 cultures. Data represent mean ± SEM of 3 independent experiments.

(G) *Il13* mRNA expression in wild-type and *Drd4*$^{-/-}$ CD4$^+$ T cells with or without dopamine treatment. Data represent fold change relative to WT cultures at baseline of 3 independent experiments.

(H–J) IL-13 production by CD4$^+$ T cells of mouse (H) and human (I) in each treatment group (the DRD4 antagonist L-745870 [300 nM], the DRD4 agonist A412997 [100 nM], the DRD2/3 antagonist raclopride [50 nM], and the DRD1/5 antagonist SCH-23390 [50 nM]). (J) IL-13 production by mouse CD4$^+$ T cells in each

(legend continued on next page)

2019) were also changed by dopamine (Figure 2K). Notably, dopamine had no effect on expression of the *Il6*, *Il9*, *Il10*, and *Il17* genes. Therefore, dopamine signaling selectively promotes Th2 cytokine expression in naive CD4$^+$ T cells by activating a transcriptional program.

We generated a list of all genes detected in the samples ranked on the t-statistic followed by pathway analyses. We found that dopamine regulated energy consumption, ion channel activity, and cell cycle pathways (Figure 2L). These findings are consistent with the positive effect of dopamine on T cell proliferation (Figure 2E). We also found a significant overlap of differentially expressed genes between dopamine treatment and EZH2 deficiency in CD4$^+$ T cells (Figure 2L). EZH2 is a histone methyltransferase within Polycomb Repressive Complex 2 (PRC2). EZH2 enzymatically catalyzes histone 3 trimethylation at lysine 27 (H3K27me3) to induce epigenetic silencing of gene expression (Margueron and Reinberg, 2011). These findings suggest that epigenetic mechanisms may be involved in dopamine-induced Th2 cell differentiation.

DRD4 Is the Functional Dopamine Receptor on CD4$^+$ T Cells

Among the 5 dopamine receptor genes (*Drd1–Drd5*), qPCR of naive mouse CD4$^+$ T cells and RNA-seq of T cell cultures detected mRNA expression of *Drd1*, *Drd4*, and *Drd5*, and *Drd4* gene expression was the highest (Figure S2A). To confirm DRD4 expression by CD4$^+$ T cells, we stained the Th0 culture with a DRD4 antibody. The specificity of this DRD4 antibody was confirmed by negative staining of *Drd4*$^{-/-}$ CD4$^+$ T cells (Figures 3A and 3E). DRD4 was detected on the surface of CD4$^+$ T cells in culture from mice and humans (Figure 3A), and its expression was unchanged by T cell differentiation, age, and the location of CD4$^+$ T cells (in circulation or in tissue) (Figures S2B–S2D). A majority of CD4$^+$ T cells (97%) in human lymph nodes were DRD4$^+$ (Figure 3B).

DRD4 was not detected in the normal mouse lung by antibody staining, likely because of a low abundance of CD4$^+$ T cells at baseline (Figure 3C). However, following allergen exposure of neonatal mice, DRD4$^+$ cells appeared in close proximity to tyrosine hydroxylase$^+$ nerves around airways and blood vessels where immune cells were recruited into the lung (Figure 3D). To extensively characterize DRD4 expression in immune cells, we employed flow cytometry analyses. Because there is no commercially available flow antibody for DRD4, we used the DRD4 antibody for immunohistochemistry and included *Drd4*$^{-/-}$ cells as a negative control. CD4$^+$ T cells accounted for ~18% of all immune cell recruits following allergen exposure. DRD4 was expressed by a majority of the recruited CD4$^+$ T cells (76%) (Figure 3E). In contrast, other immune cells involved in type 2 inflammation, such as ILCs, B cells, mast cells, eosinophils, and antigen-presenting cells (macrophages and dendritic cells), had no detectable DRD4 expression (Figures S2A and S2E). Given a significant role of ILCs in type 2 inflammation, we evaluated the other four dopamine receptor genes and found no expression of any dopamine receptor genes in ILCs (Figure S2A). In accordance, dopamine had no effect on type 2 cytokine expression by ILCs or differentiated ILC2 cells in culture (Figures S2F–S2K). Last, ~20% of DRD4$^+$ cells were CD4$^-$, and these DRD4$^+$ CD4$^-$ cells likely included CD8$^+$ T cells (Figure S2E).

DRD4 belongs to the D2 receptor subfamily that blocks adenylate cyclase, whereas DRD1 and DRD5 are D1 receptors that activate adenylate cyclase (Beaulieu and Gainetdinov, 2011). Dopamine reduced the amount of intracellular cyclic AMP (cAMP) from 35 fmol to 23 fmol per one million CD4$^+$ T cells (Figure 3F), further supporting DRD4 being the major dopamine receptor.

To test whether DRD4 was required for dopamine-induced Th2 differentiation, we first compared the effect of dopamine on *Il13* mRNA expression in cultures from wild-type and *Drd4*$^{-/-}$ mice. Dopamine increased *Il13* gene expression in wild-type cells; however, it had no effect in *Drd4*$^{-/-}$ cells (Figure 3G). Notably, we found no baseline difference in *Il13* mRNA between wild-type and *Drd4*$^{-/-}$ cultures (Figure 3G). This finding is consistent with a lack of tyrosine hydroxylase expression by T cells (Figure 1J) and, hence, no baseline dopamine signaling. Second, a specific DRD4 antagonist, L745870 (300 nM; Patel et al., 1997), completely blocked the effect of dopamine on IL-13 expression in mouse and human CD4$^+$ T cells, whereas a DRD4-specific agonist, A412997 (100 nM; Moreland et al., 2005), increased IL-13 expression (Figures 3H and 3I). Third, SCH-23390 (50 nM, an inhibitor of DRD1/5; Hyttel, 1983), and raclopride (50 nM, an inhibitor of DRD2/3; Ogren et al., 1986), had no effect on dopamine-induced IL-13 expression (Figure 3J). These findings demonstrate that DRD4 is the functional receptor on CD4$^+$ T cells that mediates dopamine signaling in Th2 differentiation.

The Dopamine-DRD4 Pathway Promotes Th2 Cell Differentiation by Enhancing IL-2-STAT5 Signaling

Among the key regulators of Th2 cell differentiation, the expression of *Il2ra* is known to be repressed by cAMP (Anastassiou et al., 1992). Therefore, the dopamine-DRD4 pathway may increase the expression of IL-2Rα (also called CD25) by repressing cAMP production, promoting IL-2 signaling and Th2 differentiation. In support of this hypothesis, dopamine elevated *Il2ra* gene expression, as shown by RNA-seq (Figure 2I). Dopamine also increased CD4$^+$ T cell proliferation (Figure 2E), consistent with an enhanced, proliferative role of IL-2.

To test whether dopamine upregulated IL-2Rα expression and signaling by reducing cAMP production, we compared CD4$^+$ T cell cultures treated with dopamine alone and in combination with forskolin (Fsk, 1 μM), an agonist of adenylate cyclase. Fsk completely prevented dopamine-induced increases in *Il2ra* gene expression and the percentage of CD25$^+$CD4$^+$ T cells in both Th0 and Th0+IL-4 cultures (Figures 4A, 4B, S3A, and S3E). Consistent with increased IL-2Rα expression, dopamine significantly elevated the signaling activity of IL-2, as shown by increased STAT5 phosphorylation (p-STAT5) in Th0+IL-4

treatment group (the DRD2/3 antagonist raclopride [50 nM] and the DRD1/5 antagonist SCH-23390 [50 nM]). Data represent mean ± SEM of 3 independent experiments.

**$p < 0.01$ by two-tailed Student's t test. n.s., not significant. Scale bars, 10 μm in (A) and 50 μm in (B)–(D).

See also Figures S2 and S3.

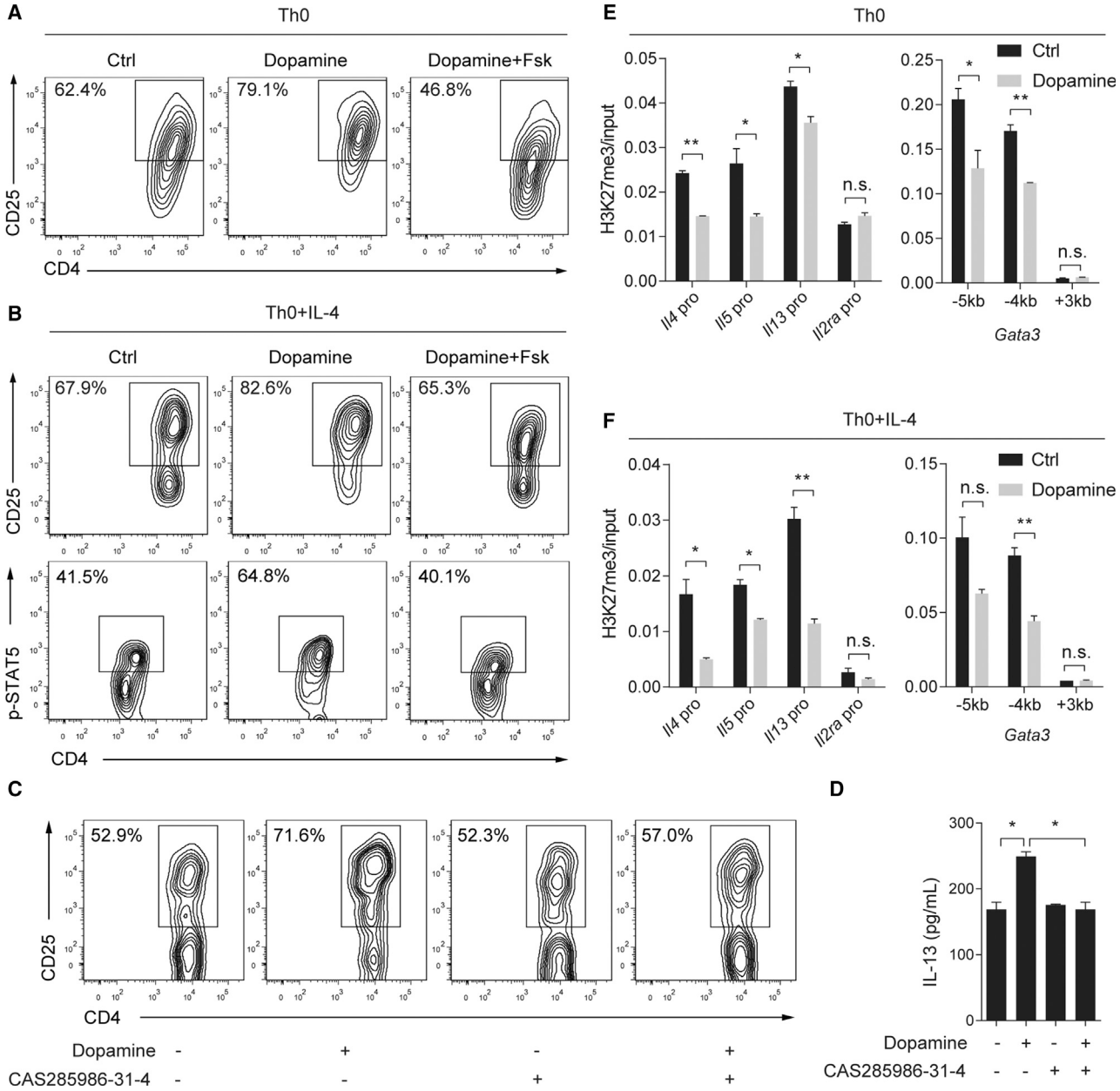

Figure 4. Dopamine Promotes Th2 Differentiation by Upregulating IL-2 Signaling and Reducing H3K27me3 at Th2 Gene Loci

(A) Flow cytometry analyses of IL-2Rα (also called CD25) in Th0 cultures treated with dopamine alone and in combination with forskolin (Fsk; 1 μM). Similar results were obtained in 3 independent experiments.

(B) Flow cytometry analyses of CD25 and p-STAT5 in Th0+IL-4 cultures of each treatment group. Similar results were obtained in 5 independent experiments.

(C) Flow cytometry analyses of CD25 expression in day 2 Th0 cultures following treatment with dopamine and a STAT5-specific inhibitor, CAS285986-31-4 (20 μM). Data are representative of 3 independent experiments.

(D) IL-13 production in day 2 Th0 cultures in each treatment group, measured by ELISA.

(E and F) The relative amount of H3K27me3 at the promoters of *Il4*, *Il5*, *Il13*, *Il2ra*, and *Gata3* genes in Th0 and Th0+IL-4 cultures by quantitative ChIP analyses. Bar graphs (D–F) represent mean ± SEM of three independent experiments. *$p < 0.05$, **$p < 0.01$ by two-tailed Student's t test.

See also Figure S3.

cultures (Figures 4B and S3I). However, the amount of p-STAT5 was reduced almost to baseline by Fsk (Figures 4B and S3I). We then tested whether elevated IL-2 signaling by dopamine was required for the increase in Th2 cytokine expression. For this assay, we treated Th0 cultures with a specific STAT5 inhibitor, CAS285986-31-4 (Müller et al., 2008). To diminish the side effect of the inhibitor on cell survival, we tested different concentrations of the inhibitor and the duration of treatment. The STAT5 inhibitor at 20 μM had no detectable effect on cell growth and baseline expression of CD25 and IL-13 in day 2 cultures (Figures 4C,

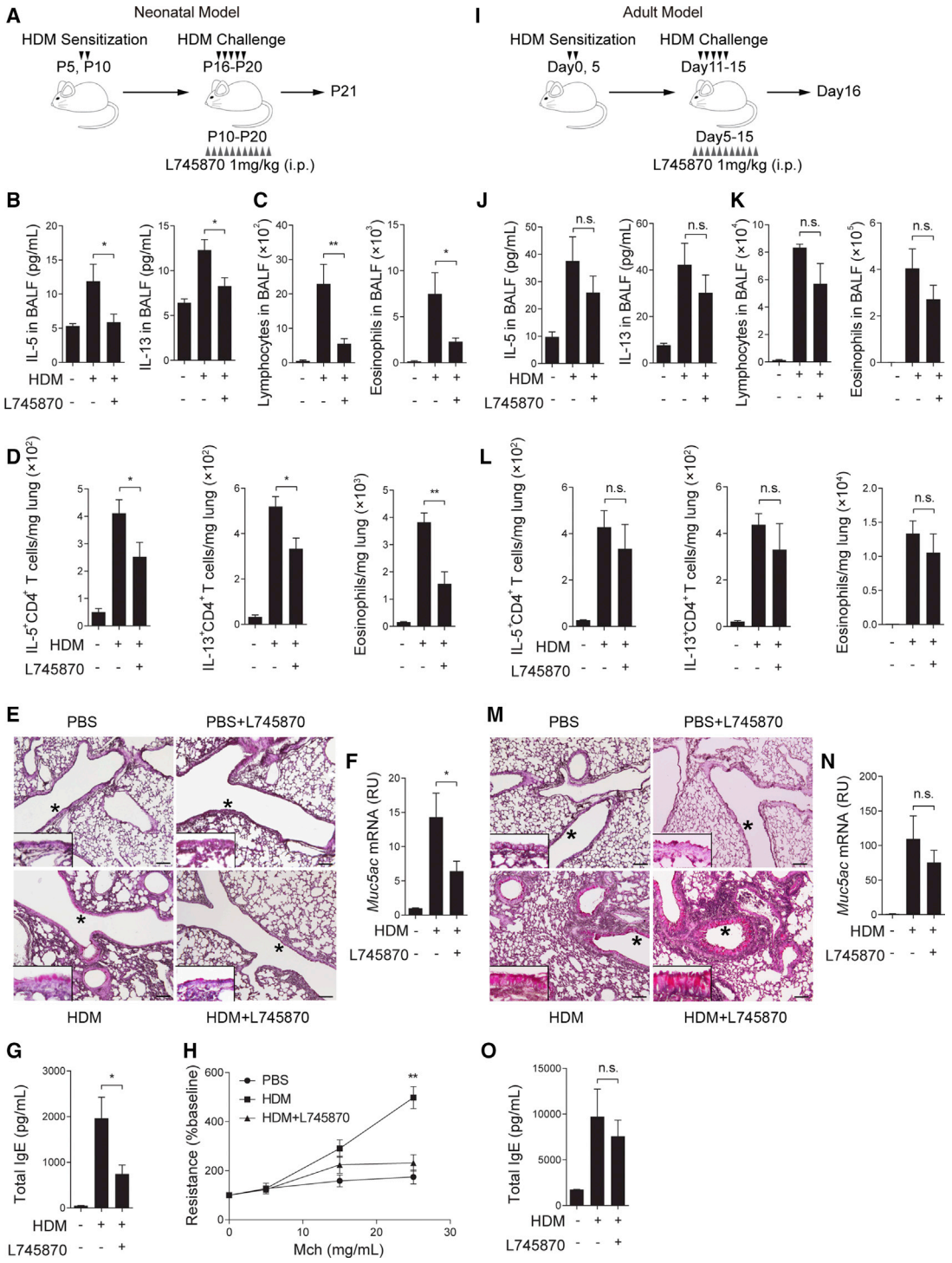

Figure 5. The Dopamine-DRD4 Pathway Plays a Significant Role in Th2 Inflammation in Neonatal Mice

(A and I) Schemes of HDM allergen sensitization and challenge with L745870 treatment in neonatal mice (A) and adult mice (I). Mice were analyzed 1 day after the last challenge.

(B and J) The amounts of IL-5 and IL-13 in BALF of neonatal and adult mice in each group. N = 12 from 3 independent experiments in (B) and N = 5 from 2 independent experiments in (J).

(C and K) The abundance of lymphocytes and eosinophils in BALF of neonatal and adult mice. N = 12 from 3 independent experiments in (C) and N = 5 from 2 independent experiments in (K).

(D and L) The abundance of IL-5$^+$ and IL-13$^+$ CD4$^+$ T cells and eosinophils in the lungs of neonatal and adult mice. Data were normalized to the lung weight. N = 8 from 2 independent experiments in (D) and N = 5 from 2 independent experiments in (L).

(legend continued on next page)

4D, S3J, and S3K); however, the STAT5 inhibitor abolished induction of CD25 and IL-13 expression by dopamine (Figures 4C, 4D, S3J, and S3K). Last, to link cAMP production and Th2 cytokine gene regulation in the dopamine-DRD4 pathway, we analyzed IL-13 and *Il4* expression in Th0 and Th0+IL-4 cultures that were treated with dopamine alone or dopamine+Fsk. The combined treatment diminished the increase in IL-13 and *Il4* expression in dopamine-treated cultures (Figures S3B–S3D and S3F–S3H). Therefore, the dopamine-DRD4 pathway blocks cAMP production to upregulate IL-2Rα expression, elevating IL-2 signaling activities to promote Th2 differentiation.

Dopamine Transcriptionally Upregulates Th2 Genes with an Associated Reduction in H3K27me3 at These Th2 Gene Loci

Pathway analysis of RNA-seq data suggested that dopamine signaling in $CD4^+$ T cells may involve epigenetic mechanisms by counteracting the activity of EZH2 (Figure 2L). EZH2 is known to bind directly to the promoters of Th2 genes such as *Gata3*, *Il4*, *Il5*, and *Il13* and repress gene transcription by causing H3K27me3 (Tumes et al., 2013). To test whether dopamine reduced H3K27me3 at the Th2 gene loci, we performed chromatin immunoprecipitation (ChIP) with a specific H3K27me3 antibody, followed by qPCR using primers flanking the established EZH2-binding sites within the promoter of the Th2 genes (Tumes et al., 2013). Compared with the untreated control, dopamine reduced H3K27me3 at the promoters of the *Il4*, *Il5*, and *Il13* genes in Th0 and Th0+IL-4 cultures (Figures 4E and 4F). For the *Gata3* promoter, dopamine decreased H3K27me3 at the −5 kb and −4 kb sites but not at the +3 kb site (Figures 4E and 4F). In contrast, dopamine had no effect on H3K27me3 in the promoter of *Il2ra*, a gene that exhibited little EZH2 binding (Tumes et al., 2013; Figures 4E and 4F). Taken together, dopamine signaling decreases epigenetic silencing of selected Th2 genes, which may facilitate Th2 cell differentiation.

To test whether dopamine opposed EZH2 to mediate epigenetic modification, we showed that dopamine reduced the expression of *Ezh2* and 3 regulatory subunit genes within PRC2, *Eed*, *Jarid2*, and *Aebp2* (Figure S3L). In addition, blockade of EZH2 activity with a specific inhibitor, 3-deazaneplanocin A (DZNep), promoted Th2 cytokine expression similarly as dopamine (Figures S3M and S3N; Tumes et al., 2013). Importantly, DZNep blunted the effect of dopamine on *Il4* and *Il13* gene expression in culture (Figures S3M and S3N). As a control for the functional specificity of DZNep, we showed that DZNep had no effect on the *Il2ra* gene with or without dopamine (Figure S3O). These findings support that dopamine-induced Th2 differentiation involves epigenetic regulation at key Th2 gene loci by repressing EZH2 and other components within PRC2.

The Dopamine-DRD4 Pathway Plays a Critical, Augmenting Role in Th2 Inflammation Following Allergen Exposure in Neonatal Mice but Not in Adult Mice

The dopaminergic-to-adrenergic transition of the sympathetic nervous system during post-natal development was associated with more dopamine in the early lung than the adult lung (Figure 1). We reasoned that, if dopamine served as an age-related neural signal to augment Th2 cell differentiation, then blockade of dopamine-DRD4 signaling would preferentially ameliorate Th2 inflammation in early life. To test this hypothesis, we assessed the effect of DRD4 inhibition on Th2 inflammation in neonatal and adult mice following exposure to house dust mites (HDMs) or ovalbumin (OVA) (Figures 5 and S4–S6). To block DRD4, we employed a specific DRD4 inhibitor (L745870) and *Drd4*$^{-/-}$ mice. Notably, *Drd4*$^{-/-}$ mice have no previously reported phenotypes except for addictive behavior (Rubinstein et al., 1997). Consistently, no baseline lung phenotype was found in L745870-treated mice and *Drd4*$^{-/-}$ mice without allergen exposure (PBS condition) (Figures 5E, 5M, S5C–S5I, and S5S).

Neonatal mice were sensitized and challenged intranasally with HDMs and treated with L745870 between P10 and P20 (Figure 5A), a time period when tyrosine hydroxylase expression increased sharply in the lung (Figure 1A). Because of technical issues with neonatal intranasal delivery that often causes variations in efficacy, we chose to deliver L745870 by intraperitoneal injection. At P21, compared with solvent, L745870 reduced the amount of IL-5 and IL-13 (Figure 5B) and diminished the abundance of lymphocytes and eosinophils in bronchoalveolar lavage fluid (BALF) (Figure 5C). L745870 also significantly decreased the number of IL-5- and IL-13-expressing $CD4^+$ T cells and eosinophils in the lung (Figures 5D and S4A). In addition, L745870 decreased HDM-induced mucus overproduction and the amount of total immunoglobulin E (IgE) in serum and ameliorated airway hyperresponsiveness to methacholine (Figures 5E–5H). Furthermore, L745870 improved pathological scores in the HDM-exposed lungs, as assayed by the thickness of airway epithelium and peri-vascular nuclear density (Figures S4B and S4C). Last, similar to L745870 treatment, genetic disruption of DRD4 reduced Th2 inflammation in neonatal mice following HDM exposure (Figures S4D–S4F).

We assessed the effect of L745870 in the adult HDM mouse model (Figure 5I). The dosage of HDMs was adjusted to the body weight of adult mice. Adult mice that were treated with L745870 for the same duration as neonates exhibited no significant difference in Th2 inflammation compared with solvent treatment (Figures 5J–5O and S4G–S4I).

As a complementary model of allergic inflammation, we subjected neonatal and adult mice to OVA sensitization and

(E and M) Representative image of periodic acid–Schiff (PAS) staining in lung sections of neonatal and adult mice. The epithelial areas marked by asterisks are enlarged and shown in the insets. Scale bars, 100 μm.

(F and N) Mucus production in neonatal and adult lungs, assayed by *Muc5ac* qPCR. N = 12 from 3 independent experiments in (F) and N = 5 in 2 independent experiments in (N).

(G and O) The amount of total IgE in serum from neonatal and adult mice. N = 12 from 3 independent experiments in (G) and N = 5 from 2 independent experiments in (O).

(H) Airway resistance in neonatal mice of each group relative to the baseline. N = 4–5 in 2 independent experiments.

**$p < 0.01$ by one-way ANOVA followed by Tukey's post-hoc test in (H). For all other panels, *$p < 0.05$, **$p < 0.01$ by two-tailed Student's t test.

See also Figures S4–S6.

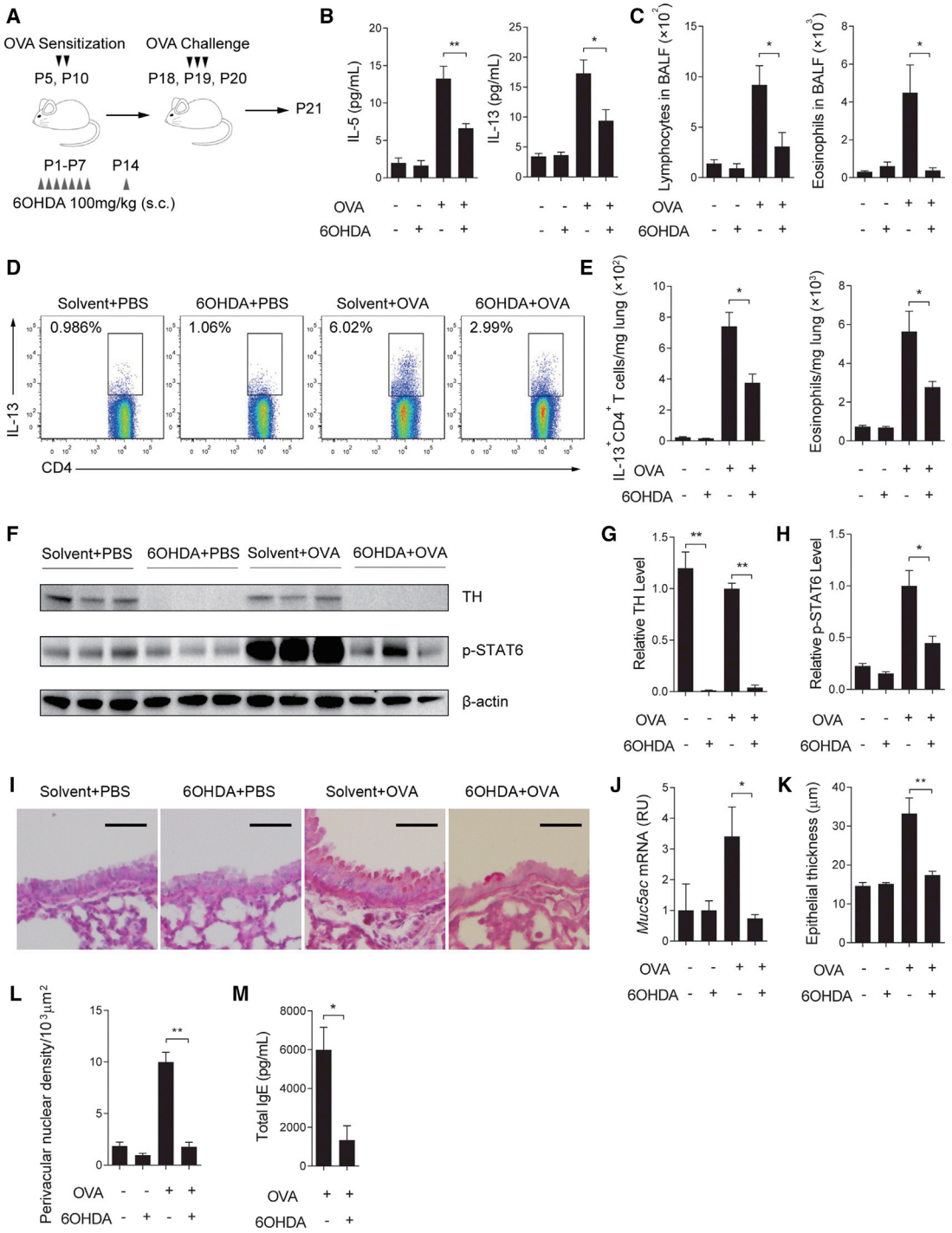

Figure 6. Ablation of Dopaminergic Nerves Ameliorates Allergic Inflammation in Young Mice

(A) Scheme of 6OHDA treatment during OVA sensitization and challenge in neonatal mice. Mice were analyzed 1 day after the last challenge at P21.

(B) The amount of IL-5 and IL-13 in BALF in each group. N = 5–7 from 2 independent experiments.

(C) Quantification of lymphocytes and eosinophils in BALF at P21. N = 5–7 from 2 independent experiments.

(D) Flow cytometry analyses of IL-13$^+$CD4$^+$ T cells in the lungs in each group. Similar results were obtained from 2 independent experiments.

(E) The abundance of IL-13$^+$CD4$^+$ T cells and eosinophils in the lungs in each group. Data were normalized to the lung weight. N = 5–7 in 2 independent experiments.

(F) Western blot analyses of relative expression of tyrosine hydroxylase (TH) and phosphorylated STAT6 (p-STAT6) in the lung of each group. β-actin was loading control. Each lane represents one sample.

(G and H) Quantification of the relative level of TH (G) and p-STAT6 (H) based on western blot. N = 5–7 in 2 independent experiments.

(legend continued on next page)

challenge (Figures S5 and S6). We showed that L745870 treatment and DRD4 deficiency profoundly reduced Th2 inflammation, airway hypercontractility, and mucus overproduction following OVA exposure in neonates while having a marginal effect in adult mice (Figures S5 and S6). Taken together, the dopamine-DRD4 pathway plays an age-related role in augmenting Th2 inflammation in early life.

Allergen exposure had no effect on the age-related reduction in expression of tyrosine hydroxylase (Figure S5B) and neonatal DBH expression (Figure S5M). In accordance, the amount of dopamine remained unchanged in allergen-exposed mouse lungs at P21 (898.2 ± 95.57 pg/mg lung weight [OVA] versus 961.9 ± 66.72 pg/mg lung weight [PBS]). However, DBH expression in the adult lung was elevated by allergen exposure (Figure S5M). This was associated with a decrease in the already lower amount of dopamine (229.4 ± 73.08 pg/mg lung weight [OVA] versus 494.0 ± 114.7 pg/mg lung weight [PBS]). Therefore, allergen exposure potentiates the age-related difference in dopamine.

Dopamine in the Lungs Is a Critical, Age-Related Regulator of Th2 Inflammation

To provide further evidence that the age-related role of dopamine-DRD4 signaling in allergic inflammation was determined by the amount of dopamine, we assessed the effect of dopaminergic neuron ablation on Th2 inflammation in neonates following allergen exposure. For this assay, mice were treated with 6-hydroxydopamine (6OHDA), a specific neurotoxin for dopaminergic neurons during the first 2 weeks after birth (Angeletti and Levi-Montalcini, 1972; Figure 6A). 6OHDA diminished tyrosine hydroxylase$^+$ nerves in the lung at P21 (Figures 6F and 6G). 6OHDA treatment had no detectable effect on inflammation at baseline (Figures 6B–6L). However, following OVA exposure, mice treated with 6OHDA exhibited a significant reduction in IL-5 and IL-13 (Figure 6B) and the abundance of lymphocytes and eosinophils in the BALF (Figure 6C). 6OHDA also reduced the abundance of IL-13$^+$CD4$^+$ T cells and eosinophils in the lungs (Figures 6D and 6E), the amount of p-STAT6 (Figures 6F and 6H), mucus overproduction (Figures 6I and 6J), and the amount of total IgE in serum (Figures 6M). Furthermore, 6OHDA improved pathological scores in OVA-exposed lungs, as measured by airway epithelial thickness and perivascular nuclear density (Figures 6K and 6L).

6OHDA has a broad effect on the sympathetic nervous system. To alleviate the concern of side effects of 6OHDA, we took a complementary gain-of-function approach by treating adult mice with a specific DRD4 agonist, A412997 (Moreland et al., 2005), to offset the low dopamine activity in the adult lung (Figure S7A). DRD4 activation alone was insufficient to induce inflammation (Figure S7B). Following OVA exposure, the DRD4 agonist substantially worsened Th2 inflammation and mucus overproduction in adult mice (Figures S7C–S7G). Taken together, the amount of dopamine is a critical regulator of Th2 inflammation in the lung.

CD4$^+$ T Cells Mediate Dopamine-DRD4 Signaling in Early Life to Augment Th2 Inflammation

To establish that CD4$^+$ T cells were the critical mediator of dopamine-DRD4 signaling in the early lung, we performed an adoptive transfer assay using CD4$^+$ T cells isolated from OT-II mice. OT-II mice express a transgenic T cell receptor for OVA. OVA sensitization of OT-II mice stimulated T cell activation and proliferation (Church et al., 2012; Kim et al., 2018), as evident by a 3-fold increase in the number of splenic CD4$^+$ T cells with a significant, activated CD44^{high}CD62L^{low} subpopulation (~25%). Because age had no effect on the T cell response to dopamine (Figures 2F, 2G, S1G), we isolated CD4$^+$ T cells from 5-week-old OT-II mice for the adoptive transfer assay because the spleen at this age is fully grown and contains more CD4$^+$ T cells than the neonatal spleen. Purified splenic CD4$^+$ T cells from OVA-sensitized OT-II mice were intratracheally transferred into wild-type and *Drd4*$^{-/-}$ recipients at P14, followed by OVA challenge (Figure 7A). Because the recipients were not sensitized, OVA challenge induced allergic inflammation only through the transferred OT-II cells. At P21, wild-type and *Drd4*$^{-/-}$ recipients exhibited comparable Th2 inflammation, as assayed by the amount of IL-5 and IL-13 and the number of eosinophils in BALF (Figures 7B and 7C), infiltrating IL-13$^+$CD4$^+$ T cells and eosinophils in the lungs (Figures 7D and 7E), the amount of p-STAT6 (Figures 7F and 7G), mucus overproduction (Figures 7H and 7I), and pathological scores (Figure 7J). These findings indicate that adoptively transferred CD4$^+$ T cells from OVA-sensitized OT-II mice are sufficient to induce allergic inflammation in neonates independent of the genotype of the recipient.

After validating the adoptive transfer approach in neonatal allergic inflammation, we went on to evaluate the contribution of the transferred OT-II cells and the recipient to dopamine-augmented allergic inflammation. For this assay, we treated wild-type and *Drd4*$^{-/-}$ recipient mice with the DRD4 inhibitor L745870 immediately after adoptive transfer at P14 (Figure 7A). We reasoned if cells from recipient mice played a role in DRD4 regulation of allergic inflammation, then L745870 treatment would have a greater inhibitory effect on wild-type littermates than on *Drd4*$^{-/-}$ mice. However, we found that L745870 treatment similarly reduced Th2 inflammation regardless of the recipient genotype, as shown by immunological assays of Th2 inflammation, mucus overproduction, and pathological scores (Figures 7B–7J). Therefore, transferred CD4$^+$ T cells from OVA-sensitized OT-II mice primarily mediate dopamine-DRD4 signaling in the early lung to augment Th2 inflammation. These findings, together with selective expression of DRD4 in CD4$^+$ T cells, but not ILCs and other immune cells involved in type 2 inflammation (Figures 3A, 3B, S2A, and S2E), provide strong evidence that CD4$^+$ T cells

(I and J) Mucus overproduction in the lung of each group assayed by PAS staining (I) and qPCR (J). N = 5 from 2 independent experiments. Scale bars, 100 μm.
(K and L) Pathological assays of epithelial thickness (K) and perivascular nuclear density (L). Data represent mean ± SEM of 3 non-overlapping histological areas in each mouse; 3–5 mice in each group from 2 independent experiments.
(M) The amount of total IgE in serum from each group. N = 5–7 in 2 independent experiments.
*$p < 0.05$ and **$p < 0.01$ by two-tailed Student's t test.
See also Figure S7.

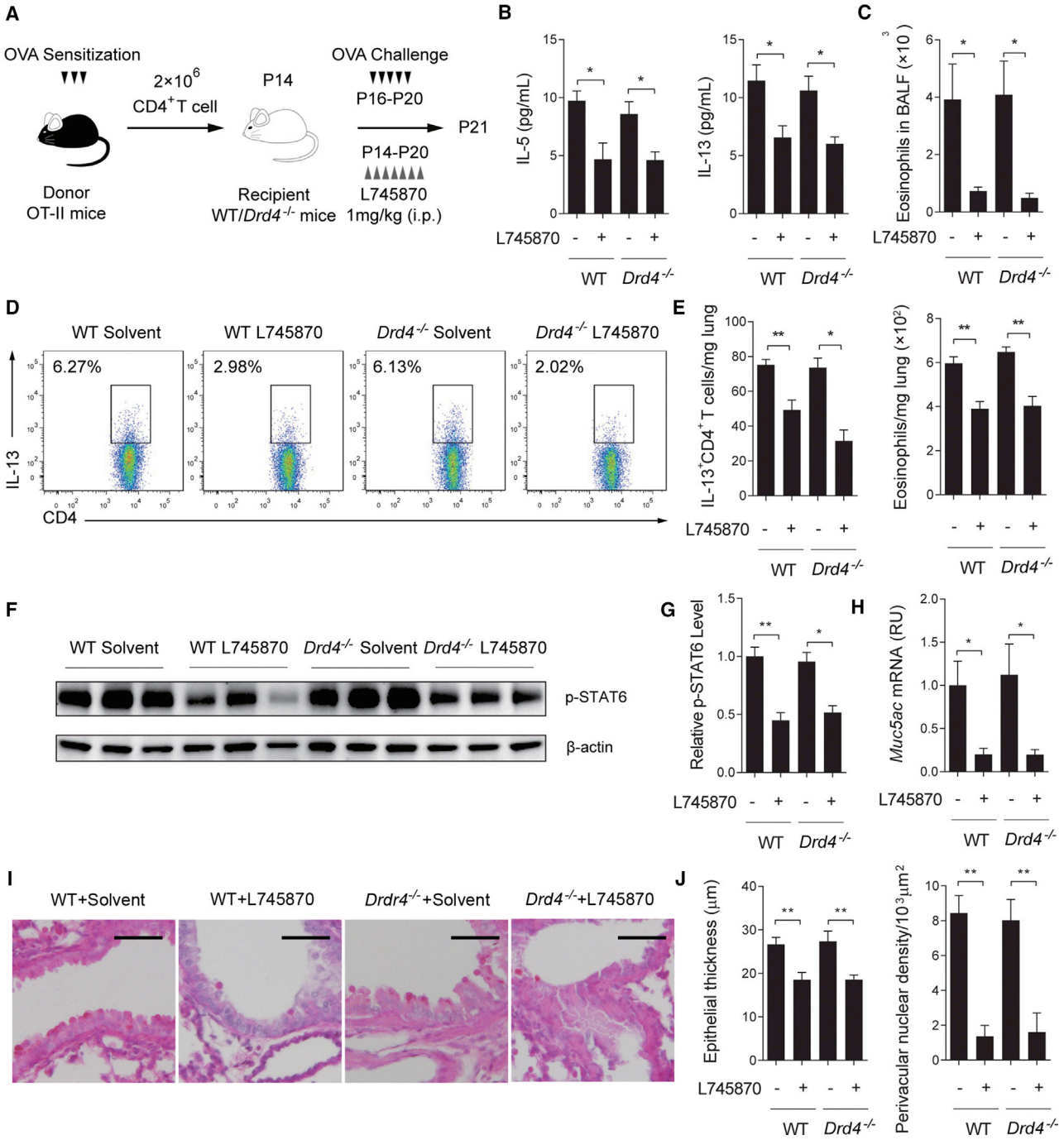

Figure 7. CD4+ T Cells Mediate Dopamine Signaling to Promote Th2 Inflammation in Neonatal Mice

(A) Scheme of adoptive transfer of CD4+ OT-II cells to recipient wild-type and *Drd4*$^{-/-}$ mice with and without L745870 treatment. CD4+ OT-II cells were isolated from OVA-sensitized donor mice at 5 weeks of age before adoptive transfer. The recipient mice were analyzed at P21.

(B) The amount of IL-5 and IL-13 in BALF of each group. N = 5–7 from 3 independent experiments.

(C) Quantification of eosinophils in BALF from each group. N = 5–7 in 3 independent experiments.

(D) Representative flow cytometry results of IL-13+CD4+ T cells in the lungs in each group. Similar results were obtained from 3 independent experiments.

(E) Relative abundance of IL-13+CD4+ T cells and eosinophils in the lungs. Data were normalized to the lung weight. N = 5–7 from 3 independent experiments.

(F and G) Western blot analysis of the amount of p-STAT6 in the lungs in each group. β-Actin was a loading control. Data were quantified in (G). N = 5–7 in 3 independent experiments.

(H and I) Mucus overproduction in the lung of each group assayed by PAS staining (H) and qPCR (I). N = 5–7 in 3 independent experiments. Scale bars, 100 μm.

(J) Pathological assays of epithelial thickness and perivascular nuclear density. Data represent mean ± SEM of 3 non-overlapping histological areas in each mouse; 5 mice in each group in 3 independent experiments.

*$p < 0.05$ and **$p < 0.01$ by two-tailed Student's t test.

are the critical mediator of dopamine signaling in the early lung to promote Th2 inflammation.

DISCUSSION

In this study, we discovered that the development of sympathetic innervation provides a critical mechanism underlying susceptibility to allergic asthma in early life. We show that sympathetic nerves are dopaminergic during post-natal development of the lung. By releasing dopamine, which induces Th2 cell differentiation, the immature sympathetic nervous system equips the early lung with a dopamine-enriched environment that fosters allergic inflammation. With age, sympathetic nerves mature into an adrenergic phenotype. Norepinephrine and epinephrine released from adrenergic nerves have no effect on Th2 cell differentiation activity, likely because of low adrenergic receptor expression, as shown by RNA-seq. Therefore, the dopaminergic-to-adrenergic transition of sympathetic innervation plays an age-related role in allergic inflammation. Our study identifies DRD4 as the functional receptor for dopamine in Th2 cell differentiation. DRD4 is selectively expressed by T cells but not ILCs. The differential expression of DRD4 in T cells and ILCs, together with previous findings showing that epinephrine negatively regulates ILC2 (Moriyama et al., 2018), highlights the complexity and specificity of neural regulation of type 2 inflammation.

We provide evidence that humans and mice exhibit a similar dopaminergic-to-adrenergic transition of sympathetic nerves during post-natal development of the airway. The conservation of this transition during evolution suggests that dopaminergic innervation may provide some advantage when the lung is immature and vulnerable to infection. One possibility is that, by facilitating type 2 inflammation, dopaminergic nerves endow the early lung with a mechanism of tissue repair following infection and eradication of parasitic worms. It is also possible that, in the context of the physiological role of norepinephrine in vasoconstriction of pulmonary vessels (Tuck, 1986), the dopaminergic phenotype in the early lung may support vascular development by preventing premature vascular constriction.

We show that the major source of dopamine is the nerves that innervate the airway and vasculature in the lung and lymphatic vessels in associated lymph nodes. Although the amount of dopamine released from the activated nerve is difficult to measure, the local concentration of dopamine can reach up to the range of hundreds of micromolar to millimolar upon firing of the nerve (Goto et al., 2007). Therefore, we speculate that the active, micromolar range of dopamine in Th2 cell differentiation may be physiologically relevant. In addition to direct communication between nerves and T cells, we cannot exclude the possibility that dopamine released by nerves may be transported through specific dopamine transporters or non-specifically taken up by immune cells, such as dendritic cells and macrophages. This possibility is supported by previous reports that dopamine can be detected in some immune cells by high-performance liquid chromatography (HPLC) without the evidence of tyrosine hydroxylase expression (Bergquist and Silberring, 1998; Cosentino et al., 2007; Josefsson et al., 1996; Nakano et al., 2009). In this scenario, dendritic cells may transport dopamine to T cells in the lymph node, where dendritic cells present allergen to initiate T cell differentiation, serving as an indirect means of neural regulation of Th2 cell differentiation through the dopamine-DRD4 pathway.

The expression and function of DRD4 in $CD4^+$ T cells is supported by previous studies of human samples (Kustrimovic et al., 2014; Sarkar et al., 2006). However, there are conflicting reports regarding dopamine receptor expression and signaling in T cells and mouse models. The conflict may be explained by the caveat of detection using non-qPCR assays of $CD4^+$ T cells (Contreras et al., 2016; Franz et al., 2015; Huang et al., 2010; Ilani et al., 2004). In addition, the inflammation defects in *Drd3*$^{-/-}$ mice may be unspecific to T cells (Contreras et al., 2016) because the cell type specificity of DRD3 expression is not well characterized. Furthermore, small-molecule dopamine receptor inhibitors may have off-target effects, which complicates the functional study of a specific dopamine receptor in inflammation. For example, a D1 receptor antagonist, SCH-23390, may also interfere with DRD4 (K_i = 1.1 μM; Bourne, 2001) at a concentration of 1 μM used in previous studies (Mori et al., 2013; Nakano et al., 2009).

Our results show that the dopamine-DRD4 pathway plays an augmenting role in Th2 cell differentiation by interacting with IL-2 and IL-4. We have provided evidence that the functional interaction between dopamine and IL-2 is mediated at least in part by the cAMP pathway. Considering a variety of signals in allergic inflammation that are known to upregulate cAMP production through commonly expressed receptors, the dopamine-DRD4 pathway uniquely represses cAMP production, thereby upregulating IL-2Rα expression. In addition, dopamine signaling is associated with reduced H3K27me3 in Th2 gene loci, an epigenetic mechanism that may facilitate Th2 gene transcription in synergy with IL-4. Based on the RNA-seq data, we speculate that the epigenetic mechanism may be mediated by the reduction in the expression of *Ezh2*, *Eed*, *Jarid2*, and *Aebp2*, the components of PRC2 that cause H3K27me3 to suppress gene transcription (Margueron and Reinberg, 2011). RNA-seq also showed that dopamine upregulated the expression of several transcriptional factors required for IL-4-induced Th2 cell differentiation, such as *c-Maf*, *Irf4*, *Xbp1*, and *Bhlhe40* (Henriksson et al., 2019), which may provide another mechanism underlying the synergic interaction between dopamine and IL-4. Whether changes in the expression of candidate epigenetic regulators and the transcriptional factors are regulated by the cAMP pathway warrants further investigation.

Previous clinical and basic studies showed that the immature immune system is poised toward type 2 inflammation (de Kleer et al., 2016; Hebel et al., 2014). Our study suggests that dopaminergic nerves in the early lung may potentiate an already type 2-poised immune system, contributing to the susceptibility to allergic asthma in early childhood (Stern et al., 2008). Importantly, our findings reveal the similarity of dopaminergic innervation of the early lung and the T cell response to dopamine between mice and humans. Identification of a dopamine-specific gene signature in Th2 cells will facilitate future study of dopamine regulation of allergic asthma in children. Based on RNA-seq data, several dopamine-regulated genes in mouse $CD4^+$ T cells have established disease relevance. For example, among the genes downregulated by dopamine, cAMP-responsive element modulator (CREM) has also been shown to exhibit reduced expression in $CD4^+$ T cells from children with recurrent

and persistent wheezing compared with healthy controls (Verjans et al., 2015). In addition, dopamine upregulates *Il2ra*, *Il7r*, and *Crlf2* (*Tlspr*), all of which have been identified to be associated with susceptibility to allergic asthma (Ferreira et al., 2017; Sherrill et al., 2010).

To understand the mechanism underlying the dopaminergic-to-adrenergic transition of sympathetic nerves in the developing lung, future studies are required to map the subset of sympathetic neurons that specifically supply the lung and to identify neurogenic signals required for development of these neurons. Neurons dynamically interact with target tissues during development. It is possible that the innervating sympathetic neurons may decrease the expression of tyrosine hydroxylase while upregulating DBH to fully differentiate into the adrenergic phenotype during post-natal maturation. Members of the neurotrophin family, such as nerve growth factor and brain-derived neurotrophic factor, have established roles in development of sympathetic neurons (Barbacid, 1994). We have shown that lung innervation requires neurotrophins (Aven et al., 2014; Patel et al., 2016; Radzikinas et al., 2011). Therefore, neurotrophins may regulate sympathetic innervation of the lung. Clinical studies have shown that the amounts of nerve growth factor and brain-derived neurotrophic factor are aberrantly regulated in infants following infection with respiratory syncytial virus (Tortorolo et al., 2005). In addition, brain-derived neurotrophic factor expression has been shown to be positively associated with the severity of allergic asthma (Watanabe et al., 2015). Identification of the neurotrophic factors that regulate the dopaminergic-to-adrenergic transition of sympathetic innervation may provide insights into the connection between respiratory viral infection in early life and allergic asthma.

In summary, our findings indicate that developing dopaminergic nerves in the airway contribute to susceptibility to allergic inflammation in early life. Targeting communication between sympathetic nerves and $CD4^+$ T cells via the dopamine-DRD4 pathway may be a strategy to battle the increasing prevalence of allergic asthma in children.

STAR★METHODS

Detailed methods are provided in the online version of this paper and include the following:

- KEY RESOURCES TABLE
- LEAD CONTACT AND MATERIALS AVAILABILITY
- EXPERIMENTAL MODELS AND SUBJECT DETAILS
  - Mice
  - Human donor lungs
- METHOD DETAILS
  - Neonatal and adult mouse models of allergic inflammation
  - Mouse primary lymphocyte preparation and culture
  - Primary human lymphocyte isolation and culture
  - Histology and antibody staining
  - Flow cytometry analysis of T cell cultures, BALF and lung samples
  - ILCs isolation and culture
  - Physiological measurements of airway reactivity
  - Cell proliferation assay
  - Quantitative Real Time PCR (qPCR)
  - Western Blot
  - ELISAs
  - RNA-seq analyses
  - Quantitative Chromatin precipitation (ChIP)-qPCR
- QUANTIFICATION AND STATISTICAL ANALYSIS
- DATA AND CODE AVAILABILITY

SUPPLEMENTAL INFORMATION

Supplemental Information can be found online at https://doi.org/10.1016/j.immuni.2019.10.002.

ACKNOWLEDGMENTS

We would like to thank Manuela Cernadas for technical guidance regarding flow cytometry analysis. For RNA-seq, library construction, sequencing, and differential expression analysis were performed at the Translational Genomics Core of Partners Personalized Medicine, a not-for-profit, fee-for-service core facility at Partners HealthCare (Boston, MA). This project was supported by NIH grants (R01HL132991 to X.A., K08HL135443 to Y.B., and F31HL126443 to J.B.).

AUTHOR CONTRIBUTIONS

W.W. and X.A. conceived the project. W.W., J.A.C., A.W., Y.B., and X.A. were involved in experimental design. W.W., J.A.C., A.W., F.S., and Y.B. performed most experiments and compiled data. K.G.T., J.B., N.K., M.R.J., V.K.K., and A.F. helped with experiments and data analysis. All authors participated in analyzing the data and writing or editing the paper.

DECLARATION OF INTERESTS

The authors declare no competing interests.

Received: May 7, 2019
Revised: August 28, 2019
Accepted: October 7, 2019
Published: November 19, 2019

REFERENCES

Aki, D., Li, H., Zhang, W., Zheng, M., Elly, C., Lee, J.H., Zou, W., and Liu, Y.C. (2018). The E3 ligases Itch and WWP2 cooperate to limit T_H2 differentiation by enhancing signaling through the TCR. Nat. Immunol. *19*, 766–775.

Anastassiou, E.D., Paliogianni, F., Balow, J.P., Yamada, H., and Boumpas, D.T. (1992). Prostaglandin E2 and other cyclic AMP-elevating agents modulate IL-2 and IL-2R alpha gene expression at multiple levels. J. Immunol. *148*, 2845–2852.

Anders, S., Pyl, P.T., and Huber, W. (2015). HTSeq–a Python framework to work with high-throughput sequencing data. Bioinformatics *31*, 166–169.

Angeletti, P.U., and Levi-Montalcini, R. (1972). Growth inhibition of sympathetic cells by some adrenergic blocking agents (6-hydroxydopamine-mice and rats-immunosympathectomy-chemical sympathectomy-superior cervical ganglion). Proc. Natl. Acad. Sci. USA *69*, 86–88.

Aven, L., and Ai, X. (2013). Mechanisms of respiratory innervation during embryonic development. Organogenesis *9*, 194–198.

Aven, L., Paez-Cortez, J., Achey, R., Krishnan, R., Ram-Mohan, S., Cruikshank, W.W., Fine, A., and Ai, X. (2014). An NT4/TrkB-dependent increase in innervation links early-life allergen exposure to persistent airway hyperreactivity. FASEB J. *28*, 897–907.

Barbacid, M. (1994). The Trk family of neurotrophin receptors. J. Neurobiol. *25*, 1386–1403.

Barrios, J., Patel, K.R., Aven, L., Achey, R., Minns, M.S., Lee, Y., Trinkaus-Randall, V.E., and Ai, X. (2017). Early life allergen-induced mucus overproduction requires augmented neural stimulation of pulmonary neuroendocrine cell secretion. FASEB J. *31*, 4117–4128.

Beaulieu, J.M., and Gainetdinov, R.R. (2011). The physiology, signaling, and pharmacology of dopamine receptors. Pharmacol. Rev. *63*, 182–217.

Becerra-Díaz, M., Wills-Karp, M., and Heller, N.M. (2017). New perspectives on the regulation of type II inflammation in asthma. F1000Res. *6*, 1014.

Bergquist, J., and Silberring, J. (1998). Identification of catecholamines in the immune system by electrospray ionization mass spectrometry. Rapid Commun. Mass Spectrom. *12*, 683–688.

Borovikova, L.V., Ivanova, S., Zhang, M., Yang, H., Botchkina, G.I., Watkins, L.R., Wang, H., Abumrad, N., Eaton, J.W., and Tracey, K.J. (2000). Vagus nerve stimulation attenuates the systemic inflammatory response to endotoxin. Nature *405*, 458–462.

Bourne, J.A. (2001). SCH 23390: the first selective dopamine D1-like receptor antagonist. CNS Drug Rev. *7*, 399–414.

Buttari, B., Profumo, E., Domenici, G., Tagliani, A., Ippoliti, F., Bonini, S., Businaro, R., Elenkov, I., and Riganò, R. (2014). Neuropeptide Y induces potent migration of human immature dendritic cells and promotes a Th2 polarization. FASEB J. *28*, 3038–3049.

Cardoso, V., Chesné, J., Ribeiro, H., García-Cassani, B., Carvalho, T., Bouchery, T., Shah, K., Barbosa-Morais, N.L., Harris, N., and Veiga-Fernandes, H. (2017). Neuronal regulation of type 2 innate lymphoid cells via neuromedin U. Nature *549*, 277–281.

Chavan, S.S., Pavlov, V.A., and Tracey, K.J. (2017). Mechanisms and Therapeutic Relevance of Neuro-immune Communication. Immunity *46*, 927–942.

Chen, T., Tibbitt, C.A., Feng, X., Stark, J.M., Rohrbeck, L., Rausch, L., Sedimbi, S.K., Karlsson, M.C.I., Lambrecht, B.N., Karlsson Hedestam, G.B., et al. (2017). PPAR-γ promotes type 2 immune responses in allergy and nematode infection. Sci. Immunol. *2*, eaal5196.

Church, R.J., Jania, L.A., and Koller, B.H. (2012). Prostaglandin E(2) produced by the lung augments the effector phase of allergic inflammation. J. Immunol. *188*, 4093–4102.

Cohen, L., e, X., Tarsi, J., Ramkumar, T., Horiuchi, T.K., Cochran, R., DeMartino, S., Schechtman, K.B., Hussain, I., Holtzman, M.J., and Castro, M.; NHLBI Severe Asthma Research Program (SARP) (2007). Epithelial cell proliferation contributes to airway remodeling in severe asthma. Am. J. Respir. Crit. Care Med. *176*, 138–145.

Contreras, F., Prado, C., González, H., Franz, D., Osorio-Barrios, F., Osorio, F., Ugalde, V., Lopez, E., Elgueta, D., Figueroa, A., et al. (2016). Dopamine Receptor D3 Signaling on CD4+ T Cells Favors Th1- and Th17-Mediated Immunity. J. Immunol. *196*, 4143–4149.

Cosentino, M., Fietta, A.M., Ferrari, M., Rasini, E., Bombelli, R., Carcano, E., Saporiti, F., Meloni, F., Marino, F., and Lecchini, S. (2007). Human CD4+CD25+ regulatory T cells selectively express tyrosine hydroxylase and contain endogenous catecholamines subserving an autocrine/paracrine inhibitory functional loop. Blood *109*, 632–642.

Cote-Sierra, J., Foucras, G., Guo, L., Chiodetti, L., Young, H.A., Hu-Li, J., Zhu, J., and Paul, W.E. (2004). Interleukin 2 plays a central role in Th2 differentiation. Proc. Natl. Acad. Sci. USA *101*, 3880–3885.

de Kleer, I.M., Kool, M., de Bruijn, M.J., Willart, M., van Moorleghem, J., Schuijs, M.J., Plantinga, M., Beyaert, R., Hams, E., Fallon, P.G., et al. (2016). Perinatal Activation of the Interleukin-33 Pathway Promotes Type 2 Immunity in the Developing Lung. Immunity *45*, 1285–1298.

Dettman, E.J., Simko, S.J., Ayanga, B., Carofino, B.L., Margolin, J.F., Morse, H.C., 3rd, and Justice, M.J. (2011). Prdm14 initiates lymphoblastic leukemia after expanding a population of cells resembling common lymphoid progenitors. Oncogene *30*, 2859–2873.

Fahy, J.V. (2015). Type 2 inflammation in asthma–present in most, absent in many. Nat. Rev. Immunol. *15*, 57–65.

Felten, D.L., Felten, S.Y., Carlson, S.L., Olschowka, J.A., and Livnat, S. (1985). Noradrenergic and peptidergic innervation of lymphoid tissue. J. Immunol. *135* (2, Suppl), 755s–765s.

Ferreira, M.A., Vonk, J.M., Baurecht, H., Marenholz, I., Tian, C., Hoffman, J.D., Helmer, Q., Tillander, A., Ullemar, V., van Dongen, J., et al.; 23andMe Research Team; AAGC collaborators; BIOS consortium; LifeLines Cohort Study (2017). Shared genetic origin of asthma, hay fever and eczema elucidates allergic disease biology. Nat. Genet. *49*, 1752–1757.

Flierl, M.A., Rittirsch, D., Nadeau, B.A., Chen, A.J., Sarma, J.V., Zetoune, F.S., McGuire, S.R., List, R.P., Day, D.E., Hoesel, L.M., et al. (2007). Phagocyte-derived catecholamines enhance acute inflammatory injury. Nature *449*, 721–725.

Franz, D., Contreras, F., González, H., Prado, C., Elgueta, D., Figueroa, C., and Pacheco, R. (2015). Dopamine receptors D3 and D5 regulate CD4(+)T-cell activation and differentiation by modulating ERK activation and cAMP production. J. Neuroimmunol. *284*, 18–29.

Goto, Y., Otani, S., and Grace, A.A. (2007). The Yin and Yang of dopamine release: a new perspective. Neuropharmacology *53*, 583–587.

Hebel, K., Weinert, S., Kuropka, B., Knolle, J., Kosak, B., Jorch, G., Arens, C., Krause, E., Braun-Dullaeus, R.C., and Brunner-Weinzierl, M.C. (2014). CD4+ T cells from human neonates and infants are poised spontaneously to run a nonclassical IL-4 program. J. Immunol. *192*, 5160–5170.

Henriksson, J., Chen, X., Gomes, T., Ullah, U., Meyer, K.B., Miragaia, R., Duddy, G., Pramanik, J., Yusa, K., Lahesmaa, R., and Teichmann, S.A. (2019). Genome-wide CRISPR Screens in T Helper Cells Reveal Pervasive Crosstalk between Activation and Differentiation. Cell *176*, 882–896.e18.

Ho, I.C., Lo, D., and Glimcher, L.H. (1998). c-maf promotes T helper cell type 2 (Th2) and attenuates Th1 differentiation by both interleukin 4-dependent and -independent mechanisms. J. Exp. Med. *188*, 1859–1866.

Huang, Y., Qiu, A.W., Peng, Y.P., Liu, Y., Huang, H.W., and Qiu, Y.H. (2010). Roles of dopamine receptor subtypes in mediating modulation of T lymphocyte function. Neuroendocrinol. Lett. *31*, 782–791.

Hyttel, J. (1983). SCH 23390 - the first selective dopamine D-1 antagonist. Eur. J. Pharmacol. *91*, 153–154.

Ilani, T., Strous, R.D., and Fuchs, S. (2004). Dopaminergic regulation of immune cells via D3 dopamine receptor: a pathway mediated by activated T cells. FASEB J. *18*, 1600–1602.

Josefsson, E., Bergquist, J., Ekman, R., and Tarkowski, A. (1996). Catecholamines are synthesized by mouse lymphocytes and regulate function of these cells by induction of apoptosis. Immunology *88*, 140–146.

Kim, M.N., Hong, J.Y., Shim, D.H., Sol, I.S., Kim, Y.S., Lee, J.H., Kim, K.W., Lee, J.M., and Sohn, M.H. (2018). Activated Leukocyte Cell Adhesion Molecule Stimulates the T-Cell Response in Allergic Asthma. Am. J. Respir. Crit. Care Med. *197*, 994–1008.

Klose, C.S.N., Mahlakõiv, T., Moeller, J.B., Rankin, L.C., Flamar, A.L., Kabata, H., Monticelli, L.A., Moriyama, S., Putzel, G.G., Rakhilin, N., et al. (2017). The neuropeptide neuromedin U stimulates innate lymphoid cells and type 2 inflammation. Nature *549*, 282–286.

Kustrimovic, N., Rasini, E., Legnaro, M., Marino, F., and Cosentino, M. (2014). Expression of dopaminergic receptors on human CD4+ T lymphocytes: flow cytometric analysis of naive and memory subsets and relevance for the neuroimmunology of neurodegenerative disease. J. Neuroimmune Pharmacol. *9*, 302–312.

Le Gros, G., Ben-Sasson, S.Z., Seder, R., Finkelman, F.D., and Paul, W.E. (1990). Generation of interleukin 4 (IL-4)-producing cells in vivo and in vitro: IL-2 and IL-4 are required for in vitro generation of IL-4-producing cells. J. Exp. Med. *172*, 921–929.

Margueron, R., and Reinberg, D. (2011). The Polycomb complex PRC2 and its mark in life. Nature *469*, 343–349.

Moreland, R.B., Patel, M., Hsieh, G.C., Wetter, J.M., Marsh, K., and Brioni, J.D. (2005). A-412997 is a selective dopamine D4 receptor agonist in rats. Pharmacol. Biochem. Behav. *82*, 140–147.

Mori, T., Kabashima, K., Fukamachi, S., Kuroda, E., Sakabe, J., Kobayashi, M., Nakajima, S., Nakano, K., Tanaka, Y., Matsushita, S., et al. (2013). D1-like dopamine receptors antagonist inhibits cutaneous immune reactions mediated by Th2 and mast cells. J. Dermatol. Sci. *71*, 37–44.

Moriyama, S., Brestoff, J.R., Flamar, A.L., Moeller, J.B., Klose, C.S.N., Rankin, L.C., Yudanin, N.A., Monticelli, L.A., Putzel, G.G., Rodewald, H.R., and Artis, D. (2018). β_2-adrenergic receptor-mediated negative regulation of group 2 innate lymphoid cell responses. Science *359*, 1056–1061.

Müller, J., Sperl, B., Reindl, W., Kiessling, A., and Berg, T. (2008). Discovery of chromone-based inhibitors of the transcription factor STAT5. ChemBioChem *9*, 723–727.

Nakano, K., Higashi, T., Takagi, R., Hashimoto, K., Tanaka, Y., and Matsushita, S. (2009). Dopamine released by dendritic cells polarizes Th2 differentiation. Int. Immunol. *21*, 645–654.

Ogren, S.O., Hall, H., Köhler, C., Magnusson, O., and Sjöstrand, S.E. (1986). The selective dopamine D2 receptor antagonist raclopride discriminates between dopamine-mediated motor functions. Psychopharmacology (Berl.) *90*, 287–294.

Ohtake, J., Kaneumi, S., Tanino, M., Kishikawa, T., Terada, S., Sumida, K., Masuko, K., Ohno, Y., Kita, T., Iwabuchi, S., et al. (2015). Neuropeptide signaling through neurokinin-1 and neurokinin-2 receptors augments antigen presentation by human dendritic cells. J. Allergy Clin. Immunol. *136*, 1690–1694.

Papa, I., Saliba, D., Ponzoni, M., Bustamante, S., Canete, P.F., Gonzalez-Figueroa, P., McNamara, H.A., Valvo, S., Grimbaldeston, M., Sweet, R.A., et al. (2017). T_{FH}-derived dopamine accelerates productive synapses in germinal centres. Nature *547*, 318–323.

Patel, K.R., Aven, L., Shao, F., Krishnamoorthy, N., Duvall, M.G., Levy, B.D., and Ai, X. (2016). Mast cell-derived neurotrophin 4 mediates allergen-induced airway hyperinnervation in early life. Mucosal Immunol. *9*, 1466–1476.

Patel, S., Freedman, S., Chapman, K.L., Emms, F., Fletcher, A.E., Knowles, M., Marwood, R., Mcallister, G., Myers, J., Curtis, N., et al. (1997). Biological profile of L-745,870, a selective antagonist with high affinity for the dopamine D4 receptor. J. Pharmacol. Exp. Ther. *283*, 636–647.

Radzikinas, K., Aven, L., Jiang, Z., Tran, T., Paez-Cortez, J., Boppidi, K., Lu, J., Fine, A., and Ai, X. (2011). A Shh/miR-206/BDNF cascade coordinates innervation and formation of airway smooth muscle. J. Neurosci. *31*, 15407–15415.

Rubinstein, M., Phillips, T.J., Bunzow, J.R., Falzone, T.L., Dziewczapolski, G., Zhang, G., Fang, Y., Larson, J.L., McDougall, J.A., Chester, J.A., et al. (1997). Mice lacking dopamine D4 receptors are supersensitive to ethanol, cocaine, and methamphetamine. Cell *90*, 991–1001.

Sarkar, C., Das, S., Chakroborty, D., Chowdhury, U.R., Basu, B., Dasgupta, P.S., and Basu, S. (2006). Cutting Edge: Stimulation of dopamine D4 receptors induce T cell quiescence by up-regulating Kruppel-like factor-2 expression through inhibition of ERK1/ERK2 phosphorylation. J. Immunol. *177*, 7525–7529.

Sherrill, J.D., Gao, P.S., Stucke, E.M., Blanchard, C., Collins, M.H., Putnam, P.E., Franciosi, J.P., Kushner, J.P., Abonia, J.P., Assa'ad, A.H., et al. (2010). Variants of thymic stromal lymphopoietin and its receptor associate with eosinophilic esophagitis. J. Allergy Clin. Immunol. *126*, 160–165.e3.

Stern, D.A., Morgan, W.J., Halonen, M., Wright, A.L., and Martinez, F.D. (2008). Wheezing and bronchial hyper-responsiveness in early childhood as predictors of newly diagnosed asthma in early adulthood: a longitudinal birth-cohort study. Lancet *372*, 1058–1064.

Talbot, S., Abdulnour, R.E., Burkett, P.R., Lee, S., Cronin, S.J., Pascal, M.A., Laedermann, C., Foster, S.L., Tran, J.V., Lai, N., et al. (2015). Silencing Nociceptor Neurons Reduces Allergic Airway Inflammation. Neuron *87*, 341–354.

Tortorolo, L., Langer, A., Polidori, G., Vento, G., Stampachiacchere, B., Aloe, L., and Piedimonte, G. (2005). Neurotrophin overexpression in lower airways of infants with respiratory syncytial virus infection. Am. J. Respir. Crit. Care Med. *172*, 233–237.

Tuck, M.L. (1986). The sympathetic nervous system in essential hypertension. Am. Heart J. *112*, 877–886.

Tumes, D.J., Onodera, A., Suzuki, A., Shinoda, K., Endo, Y., Iwamura, C., Hosokawa, H., Koseki, H., Tokoyoda, K., Suzuki, Y., et al. (2013). The polycomb protein Ezh2 regulates differentiation and plasticity of CD4(+) T helper type 1 and type 2 cells. Immunity *39*, 819–832.

Van Dyken, S.J., Nussbaum, J.C., Lee, J., Molofsky, A.B., Liang, H.E., Pollack, J.L., Gate, R.E., Haliburton, G.E., Ye, C.J., Marson, A., et al. (2016). A tissue checkpoint regulates type 2 immunity. Nat. Immunol. *17*, 1381–1387.

Verjans, E., Ohl, K., Reiss, L.K., van Wijk, F., Toncheva, A.A., Wiener, A., Yu, Y., Rieg, A.D., Gaertner, V.D., Roth, J., et al. (2015). The cAMP response element modulator (CREM) regulates TH2 mediated inflammation. Oncotarget *6*, 38538–38551.

Wang, H., Yu, M., Ochani, M., Amella, C.A., Tanovic, M., Susarla, S., Li, J.H., Wang, H., Yang, H., Ulloa, L., et al. (2003). Nicotinic acetylcholine receptor alpha7 subunit is an essential regulator of inflammation. Nature *421*, 384–388.

Watanabe, T., Fajt, M.L., Trudeau, J.B., Voraphani, N., Hu, H., Zhou, X., Holguin, F., and Wenzel, S.E. (2015). Brain-Derived Neurotrophic Factor Expression in Asthma. Association with Severity and Type 2 Inflammatory Processes. Am. J. Respir. Cell Mol. Biol. *53*, 844–852.

Zheng, W., and Flavell, R.A. (1997). The transcription factor GATA-3 is necessary and sufficient for Th2 cytokine gene expression in CD4 T cells. Cell *89*, 587–596.

Zhu, J., Cote-Sierra, J., Guo, L., and Paul, W.E. (2003). Stat5 activation plays a critical role in Th2 differentiation. Immunity *19*, 739–748.

STAR★METHODS

KEY RESOURCES TABLE

REAGENT or RESOURCE	SOURCE	IDENTIFIER
Antibodies		
Mouse monoclonal anti-Stat5 (Y694), FITC, clone SRBCZX	eBioscience	Cat#11-9010-41; RRID: AB_2572520
Rat monoclonal anti-MHC II, FITC, clone M5/114.15.2	eBioscience	Cat#11-5321-82; RRID: AB_465232
Armenian hamster monoclonal anti-CD3e, FITC, clone 145-2C11	eBioscience	Cat#11-0031-82; RRID: AB_464882
Rat monoclonal anti-CD62L, FITC, clone MEL-14	eBioscience	Cat#12-0621-81; RRID: AB_465720
Rat monoclonal anti-CD45, FITC, clone 30-F11	eBioscience	Cat#11-0451-82; RRID: AB_465050
Rat monoclonal anti-CD25, Alexa Fluor® 488, clone eBio3C7 (3C7)	eBioscience	Cat#53-0253-82; RRID: AB_763471
Rat monoclonal anti-CD8a, PE, clone 53-6.7	eBioscience	Cat#12-0081-83; RRID: AB_465531
Rat monoclonal anti-IL-5, PE, clone TRFK5	eBioscience	Cat#12-7052-81; RRID: AB_763588
Rat monoclonal anti-IL-13, PE, clone eBio13A	eBioscience	Cat#12-7133-41; RRID: AB_10852712
Mouse monoclonal anti-NK1.1, PE, clone PK136	eBioscience	Cat#12-5941-81; RRID: AB_466049
Rat monoclonal anti-MHC II, PE, clone M5/114.15.2	eBioscience	Cat#12-5321-81; RRID: AB_465927
Rat monoclonal anti-CD4, APC, clone RM4-5	eBioscience	Cat#17-0042-82; RRID: AB_469323
Rat monoclonal anti-CD44, APC, clone IM7	eBioscience	Cat#17-0441-81; RRID: AB_469389
Armenian hamster monoclonal anti-CD11c, APC, clone N418	eBioscience	Cat#17-0114-81; RRID: AB_469345
Rat monoclonal anti-CD11b, PE-Cy7, clone M1/70	eBioscience	Cat#25-0112-82; RRID: AB_469588
Mouse monoclonal anti-CD3, clone OKT3	eBioscience	Cat#16-0037-85; RRID:AB_468855
Armenian hamster monoclonal anti-FceR1α, PE-Cy7, clone MAR-1	eBioscience	Cat#25-5898-80; RRID: AB_2573492
Rat monoclonal anti-CD45, PE-Cy7, clone 30-F11	BioLegend	Cat#103114; RRID: AB_312979
Armenian hamster monoclonal anti-CD3e, APC-Cy7, clone 145-2C11	BioLegend	Cat#100329; RRID: AB_1877171
Rat monoclonal anti-CD19, APC, clone 6D5	BioLegend	Cat#115511; RRID: AB_313646
Rat monoclonal anti-Ly6G, APC, clone 1A8	BioLegend	Cat#127613; RRID: AB_1877163
Mouse monoclonal anti-CD45.2, APC-Cy7, clone 104	BioLegend	Cat#109823; RRID: AB_830788
Rat monoclonal anti-CD4, PE-Cy7, clone GK1.5	BioLegend	Cat#100421; RRID: AB_312706
Rat monoclonal anti-CD11b, APC, clone M1/70	Millipore	Cat# MABF520
Rat monoclonal anti-IFN-γ, FITC, clone XMG1.2	BD Biosciences	Cat#562019; RRID: AB_10893998
Mouse monoclonal anti-Siglec-F, PE, clone E50-2440	BD Biosciences	Cat#562068; RRID: AB_10896143
Rat monoclonal anti-Siglec-F, APC-Cy7, clone E50-2440	BD Biosciences	Cat#565527; RRID: AB_2732831
Rat monoclonal anti-c-Kit, PE, clone ACK45	BD Biosciences	Cat#553869; RRID: AB_395103
Armenian hamster monoclonal anti-CD3e, clone 145-2C11	BD Biosciences	Cat#553058; RRID:AB_394591
Armenian hamster monoclonal anti-CD28, clone 37.51	BD Biosciences	Cat#553295; RRID:AB_394764
Mouse monoclonal anti-CD28, clone CD28.2	BD Biosciences	Cat# 555725; RRID:AB_396068
Mouse monoclonal anti-Stat6 (pY641), clone J71-773.58.11	BD Biosciences	Cat#558241; RRID:AB_647299
Mouse monoclonal anti-DRD4, clone 2B9	Millipore	Cat#MABN125; RRID: AB_10917077
Rabbit polyclonal anti-tyrosine hydroxylase	Millipore	Cat#AB152; RRID: AB_390204
Rabbit polyclonal anti-dopamine beta hydroxylase	Millipore	Cat#AB1585; RRID: AB_90805
Rabbit polyclonal anti-trimethyl-Histone H3 (Lys27)	Millipore	Cat#07-449; RRID:AB_310624

(*Continued on next page*)

Continued

REAGENT or RESOURCE	SOURCE	IDENTIFIER
Mouse monoclonal anti-neural class III beta-tubulin, Clone Tuj1	R&D Systems	Cat#MAB1195; RRID: AB_357520
Rabbit polyclonal anti-CD4	Novus	Cat#NBP1-19371SS; RRID: AB_10011114
Rabbit polyclonal anti-vesicular acetylcholine transporter	Abcam	Cat#ab68986; RRID:AB_1143827
Rabbit polyclonal anti-DRD4	Sigma-Aldrich	Cat#SAB4500672; RRID: AB_10743979
Rabbit polyclonal anti-calcitonin gene related peptide	Sigma-Aldrich	Cat#C8198; RRID:AB_259091
Mouse monoclonal anti-β-actin	Sigma-Aldrich	Cat#A5441; RRID:AB_476744
Goat polyclonal anti-rabbit, HRP	Santa Cruz Biotechnology	Cat#sc-2004; RRID:AB_631746
Goat polyclonal anti-mouse, HRP	BD Biosciences	Cat#554002; RRID:AB_395198
Biological Samples		
Human donor lungs	International Institute for the Advancement of Medicine	https://www.iiam.org/
Chemicals, Peptides, and Recombinant Proteins		
OVA	Sigma-Aldrich	Cat#A5503
Dispase II	Sigma-Aldrich	Cat#4942078001
Red blood cell lysis buffer	Sigma-Aldrich	Cat#R7757
L-745,870 hydrochloride	Sigma-Aldrich	Cat#L131
Raclopride	Sigma-Aldrich	Cat#R121
SCH-23390 hydrochloride	Sigma-Aldrich	Cat#D054
A-412997 dihydrochloride	Sigma-Aldrich	Cat#SML0608
CAS285986-31-4	Sigma-Aldrich	Cat#573108
Epinephrine	Sigma-Aldrich	Cat#E4250
Norepinephrine	Sigma-Aldrich	Cat#A7257
Methacholine	Sigma-Aldrich	Cat#A2251
Imject alum	Thermo Fisher	Cat#77161
Dopamine	Thermo Fisher	Cat#35-485-0
RIPA buffer	Thermo Fisher	Cat#PI89900
Pierce Protein A/G Agarose	Thermo Fisher	Cat# 20421
Salmon sperm DNA	Thermo Fisher	Cat#15632011
DZNep	EMD Millipore	Cat# 252790-2MG
Forskolin	Tocris	Cat#1099
6-Hydroxydopamine hydrobromide	Tocris	Cat#2547
Collagenase Type 4	Worthington-Biochem	Cat#LS004188
DNase I	NEB	Cat#439807
cOmpleteproteinase inhibitor cocktail	Roche	Cat#11697498001
Proteinase K	Roche	Cat#14164600
RNase A	QIAGEN	Cat#1031301
Fixable Viability Dye eFluor 520	eBioscience	Cat#65-0867-18
Fixable Viability Dye eFluor 780	eBioscience	Cat#65-0865-14
Cell Stimulation Cocktail (plus protein transport inhibitors)	eBioscience	Cat#00-4975-03
Fixation/permeabilization solution	BD Biosciences	Cat#554722
Perm/Wash solution	BD Biosciences	Cat#554723
Murine IL-4	BioLegend	Cat#574302
Murine IL-2	R&D Systems	Cat#402-ML-010
Murine IL-12	R&D Systems	Cat#419-ML-010
Murine IL-6	R&D Systems	Cat#406-ML-005
Murine IL-23	R&D Systems	Cat#1887-ML-010
Human IL-4	R&D Systems	Cat#204-IL-010
Human IL-2	R&D Systems	Cat#202-IL-010

(*Continued on next page*)

Continued

REAGENT or RESOURCE	SOURCE	IDENTIFIER
Human TGF-β	R&D Systems	Cat#240-B-002
HDM	Greer Laboratories	Cat#XPB70D3A25
Critical Commercial Assays		
Naive $CD4^+$ T cells isolation kit, mouse	Miltenyi Biotec	Cat#130-104-453
Naive $CD4^+$ T cells isolation kit, human	Miltenyi Biotec	Cat#130-094-131
$CD4^+$ T cells isolation kit, mouse	Miltenyi Biotec	Cat#130-104-454
CD90.2 MicroBeads, mouse	Miltenyi Biotec	Cat#130-049-101
LS columns	Miltenyi Biotec	Cat#130-042-401
Lympholyte®-Mammal Cell Separation Media	Cedarlane®	Cat#CL5115
Mouse on Mouse Kit	Vector Laboratories	Cat#BMK-2202
Hematoxylin QS	Vector Laboratories	Cat#H-3404
Standard ABC kit	Vector Laboratories	Cat#PK-6100
DAB Peroxidase Substrate Kit	Vector Laboratories	Cat# SK-4100
PAS Staining Kit	Sigma-Aldrich	Cat#395B-1KT
IgE Ready-SET-Go! ELISA set	eBioscience	Cat#88-50460-88
IL-4 Ready-Set-Go! ELISA set	eBioscience	Cat#88-7044-86
IL-5 Ready-Set-Go! ELISA set	eBioscience	Cat#88-7054-88
IL-13 Ready-Set-Go! ELISA set	eBioscience	Cat#88-7137-76
Norepinephrine ELISA Kit	Abnova	Cat#89-028-610
Dopamine ELISA kit	Abnova	Cat#89-028-620
cAMP XP® Assay Kit	Cell signaling	Cat#4339S
Mouse OVA Specific IgE ELISA Kit	BioLegend	Cat#439807
CFSE Cell Division Tracker Kit	BioLegend	Cat#423801
RNeasy kit	QIAGEN	Cat#74106
Superscript III Reverse Transcriptase Kit	Thermo Fisher	Cat#18080-044
PicoPure RNA isolation kit	Thermo Fisher	Cat#KIT0204
SuperScript IV VILO Master Mix	Thermo Fisher	Cat#11756050
SuperSignal West Pico PLUS Chemiluminescent Substrate	Thermo Fisher	Cat#34577
Deposited Data		
Raw and analyzed data	This paper	GEO: GSE137968
Full genome sequences for *Mus musculus* (UCSC version mm10)	UCSC	https://genome.ucsc.edu/cgi-bin/hgGateway?db=mm10
Experimental Models: Organisms/Strains		
Mouse: *Drd4*$^{-/-}$: B6.129P2-Drd4 < tm1Dkg > /J	The Jackson Laboratory	JAX:008084
Mouse: OT-II: B6.Cg-Tg(TcraTcrb)425Cbn/J	The Jackson Laboratory	JAX:004194
Oligonucleotides		
Primers for ChIP PCR and qPCR	Dettman et al., 2011; Tumes et al., 2013	See the listed, previous publications for detail
Software and Algorithms		
FlowJo Software (version 10.5.3)	FlowJo	https://www.flowjo.com/
GraphPad Prism 6	GraphPad Software	https://www.graphpad.com
ImageJ 1.49v	ImageJ	https://imagej.nih.gov
R (version 3.2.5)	The R Foundation	https://www.r-project.org/
FastQC v.0.11.2	Babraham Institute	https://www.bioinformatics.babraham.ac.uk/projects/fastqc/
TopHat (version 2.0.13)	Johns Hopkins University	https://ccb.jhu.edu/software/tophat/index.shtml
HTSeq v.0.6	Anders et al., 2015	https://htseq.readthedocs.io

LEAD CONTACT AND MATERIALS AVAILABILITY

Further information and requests for resources and reagents should be directed to and will be fulfilled by the Lead Contact, Xingbin Ai (xai@partners.org). This study did not generate new unique reagents.

EXPERIMENTAL MODELS AND SUBJECT DETAILS

Mice

C57BL/6 (B6), *Drd4*$^{+/-}$ mice (stock number: 008084) and OT-II mice (stock number: 004194) were purchased from The Jackson Laboratories and were maintained in the SPF animal facility at Brigham and Women's Hospital, Harvard Medical School. All animal experiments were approved by the Institutional Animal Care and Use Committee. *Drd4*$^{+/-}$ mice were bred to produce *Drd4*$^{-/-}$ mice and control, wild-type littermates. Both male and female mice were used for experiments. Unless specified for the age of mice, adult mice at 3-4 months of age were used.

Human donor lungs

Lungs from de-identified male and female donors between 0-65 years of age were purchased from International Institute for the Advancement of Medicine (IIAM), a non-profit institute that provides non-transplantable human tissues for medical research. 4 adult lungs (1 female and 3 male donors of 40-65 years of age) and 4 lungs from children (1 female, 2 males and 1 unknown, 0-13 years of age) were used in this study. These donors were healthy volunteers, had no previous lung diseases, and mostly died of brain injuries and heart failure. All the information regarding the donor is anonymous. Because the experiment involves no intervention or interaction with the donors and relates to no living individuals, this project is deemed non-human subject research by the IRB committee at Brigham & Women's Hospital.

METHOD DETAILS

Neonatal and adult mouse models of allergic inflammation

For the neonatal model of OVA exposure (Aven et al., 2014), pups were sensitized by intraperitoneal injection of 10 μg OVA (Sigma Aldrich, A5503) in Imject alum (Thermo Scientific, 77161) at post-natal day 5 (P5) and P10. Mice were subjected to aerosolized challenges of 3% OVA solution between P18-P20, 20 min per day. For the neonatal model of HDM exposure (Barrios et al., 2017), pups were sensitized intra-nasally with 2 μg HDM (Greer Laboratories, XPB70D3A25) in PBS at P5 and P10. Mice were then intra-nasally challenged on 5 consecutive days between P16- P20, each day with 10 μg HDM. For both neonatal models of allergen exposure, mice were euthanized at P21. For the adult model of OVA exposure, adult mice were sensitized with 50 μg OVA in Imject alum on experimental day 0 (D0) and Day 5 followed by 3 aerosolized OVA challenges between D13-D15. For the adult model of HDM exposure, mice were sensitized intra-nasally with 10 μg HDM in PBS at D0 and D5. Mice were then intra-nasally challenged on 5 consecutive days between D11-D15, each day with 25 μg HDM. For both adult models of allergen exposure, mice were euthanized at D16. Non-allergic control mice of both age groups were challenged with saline. For the treatment with the DRD4 antagonist L745870 (Sigma Aldrich, L131), mice were injected intra-peritoneally L745870 at 1 mg/kg body weight (Patel et al., 1997) on a daily basis between P10-P20 for the neonatal model and experimental day 5-day 15 for the adult mouse model. For ablation of dopaminergic nerves, mice were injected subcutaneously 6OHDA (Tocris, 2547) at 100 mg/kg body weight once a day between P1-P7 and got another injection on P14 (Angeletti and Levi-Montalcini, 1972). For the treatment with the DRD4 agonist A412994, adult mice were injected intra-peritoneally with A412994 (Sigma Aldrich, SML0608) once per day between experimental day 12-day 15. A412994 was given at 0.1 μmol/kg body weight (Moreland et al., 2005). For adoptive transfer, donor OT-II mice at 5 weeks of age were sensitized twice and total CD4$^+$ T cells were purified from spleen using an isolation kit (Miltenyi Biotec, 130-104-454). 2×10^6 CD4$^+$ T cells were adoptively transferred to each WT or *Drd4*$^{-/-}$ mouse when the recipients were P14. The recipients were then injected intra-peritoneally L745870 at 1 mg/kg body weight once a day between P14-P20 and challenged with OVA daily between P18-P20. Bronchoalveolar lavage fluid (BALF), lungs and blood samples were collected 24 h after the last challenge in both neonatal and adult models (Aven et al., 2014).

Mouse primary lymphocyte preparation and culture

Mice were sacrificed by over-inhalation of isoflurane followed by cervical dislocation. Spleens were isolated, minced, and digested in RPMI-1640 (Life Technologies, 11875-119) with 10% FBS, 400 U/mL Collagenase Type 4 (Worthington-Biochem, LS004188), 0.1% Dispase II (Sigma, 4942078001) and 20 μg/mL DNase I (NEB, 439807) for 30 min at 37°C. For each sample, 12 mL of digestive solution was used. Digested spleens were mechanically disrupted by pushing through syringe with 18-gauze needle and passage through 100 μm and 40 μm wire meshes. Cells were pelleted by centrifugation and re-suspended in 2 mL red blood cell lysis buffer (Sigma Aldrich, R7757) to remove red blood cells. Naive CD4$^+$ T cells were enriched by negative selection using an isolation kit (Miltenyi Biotec, 130-104-453). CD4$^+$CD25$^-$CD44$^-$CD62L$^+$ cells were deemed naive CD4$^+$ T cells that accounted for ~95% of the purified cell population. Purified cells (2×10^6 per well) were cultured in a 12-well plate pre-coated with 1 μg/mL αCD3 (BD Biosciences, 553058). RPMI-1640 medium was supplemented with 10% FBS, 100 U/mL penicillin, 0.1 mg/mL streptomycin, 2 mM 2-mercaptoethanol. For Th0 condition, cells were cultured at the presence of 1 μg/mL αCD28 (BD Biosciences, 553295). For Th2 (Th0+IL-4)

condition, cells were cultured at the presence of 1 μg/mL αCD28, 5 ng/mL rmIL-2 (R&D Systems, 402-ML-010) and 10 ng/mL rmIL-4 (BioLegend, 574302). For Th1 condition, cells were cultured at the presence of 1 μg/mL αCD28, 5 ng/mL rmIL-2 (R&D Systems, 402-ML-010) and 10 ng/mL rmIL-12 (R&D Systems, 419-ML-010). For Th17 condition, cells were cultured at the presence of 1 μg/mL αCD28, 5 ng/mL rmIL-2 (R&D Systems, 402-ML-010), 2 ng/mL rhTGF-β (R&D Systems, 240-B-002) and 20 ng/mL rmIL-6 (R&D Systems, 406-ML-005) for 48h. And then 10 ng/mL rmIL-23 (R&D Systems, 1887-ML-010) was added to the culture. For treatment, individual neurotransmitter was added daily to T cell cultures on day 0 to day 2. These included dopamine (0.1- 25 μM, Fisher Scientific, 35-485-0), epinephrine (10 μM, Sigma Aldrich, E4250) and norepinephrine (10 μM, Sigma Aldrich, A7257). For most of cultures with dopamine, 10 μM dopamine was used. Other pharmaceutical reagents used in culture to modulate the dopamine pathway include: L-745,870 hydrochloride (300 nM, Sigma Aldrich, L131), raclopride (50 nM, Sigma Aldrich, R121), SCH-23390 hydrochloride (50 nM, Sigma Aldrich, D054), A-412997 dihydrochloride (100 nM, Sigma Aldrich, SML0608), forskolin (1 μM, Tocris, 1099), CAS285986-31-4 (20 μM, Sigma Aldrich, 573108), DZNep (7.5 nM, EMD Millipore, 252790-2MG). For treatment with CAS285986-31-4, cultures were analyzed on day 2. For all other cultures, cells and the conditioned media were harvested for gene and cytokine expression assays after 4 days in culture.

Primary human lymphocyte isolation and culture

Mediastinal lymph nodes associated with healthy donor lungs were dissected digested with 400 U/mL Collagenase Type 4, 0.1% Dispase II and 20 μg/mL DNase I for 30 min at 37°C. Digested samples were mechanically disrupted by pushing through syringe with 18-gauze needle and passage through 100 μm and 40 μm wire meshes. Naive $CD4^+$ T cells were enriched by negative selection using isolation kits (Miltenyi Biotec, 130-094-131). Purified cells (2×10^6 per well) were cultured in a 12-well plate pre-coated with 2 μg/mL αCD3 (eBioscience, 16-0037-85). RPMI-1640 medium was supplemented with 10% FBS, 100 U/mL penicillin, 0.1 mg/mL streptomycin, 2 mM 2-mercaptoethanol. For Th0 condition, cells were cultured at the presence of 2 μg/mL αCD28 (BD Biosciences, 555725). For Th2 (Th0+IL-4) condition, cells were cultured at the presence of 2 μg/mL αCD28, 5 ng/mL rhIL-2 (R&D Systems, 202-IL-010) and 10 ng/mL rhIL-4 (BioLegend, 204-IL-010).

Histology and antibody staining

Lungs and mediastinal lymph nodes associated with donor lungs were fixed in 4% paraformaldehyde in PBS overnight. After washing, tissues were processed for paraffin embedding and cryopreservation before paraffin sections (5 μm) and frozen sections (15 μm), respectively, were collected. Frozen sections were used for visualizing nerve fibers in Figure 1. For staining of cells in culture, cells were spun onto histological slides using a cytospin centrifuge before fixation. The procedure of antibody staining was previously described (Aven et al., 2014). Primary antibodies included: mouse anti-DRD4 (1:100; EMD Millipore, MABN125), rabbit anti-tyrosine hydroxylase (1:200; EMD Millipore, AB152), rabbit anti-DBH (1:100; EMD Millipore, AB1585), mouse anti–neural class III b-tubulin (TUBB3) antibody (1:200; R&D Systems, MAB1195) and rabbit anti-CD4 (1:400; Novus Biologicals, NBP1-19371SS). For staining of mouse tissue sections using mouse monoclonal primary antibodies, tissue sections were blocked using the Mouse on Mouse Kit (Vector Laboratories, BMK-2202). Biotinylated secondary antibodies and secondary antibodies conjugated with Alexa Fluor®488 and 546 were purchased from Thermo Fisher Scientific. For fluorescence staining, nuclei were stained with Hoechst dye (1:1000) and images were collected by confocal microscopy (Carl Zeiss, LSM 710). For DAB staining, sections were treated with standard ABC kit (Vector Labs, PK-6100) and DAB Peroxidase Substrate Kit (Vector Labs, SK-4100). After DAB staining, samples were counterstained with Hematoxylin QS (Vector Laboratories, H-3404). Mucus in lung sections was stained using periodic acid–Schiff (PAS) staining kit (Sigma-Aldrich, 395B-1KT). Bright field images were taken using a digital camera (Nikon DS-Fi2). To quantify sympathetic innervation, the immunoreactive areas of tyrosine hydroxylase and TUBB3 was quantified from non-overlapping images using ImageJ (National Institutes of Health, Bethesda, MD, USA) followed by the calculation of the ratio between tyrosine hydroxylase and TUBB3. To quantify pathological features of the lung (Cohen et al., 2007), 3 non-overlapping areas were quantified from one section, 3 sections for each mouse. The thickness of the airway epithelium was measured using ImageJ. The peri-vascular nuclear density was measured by quantifying the number of infiltrating cells in the peri-vascular area based on nuclear staining and then normalizing the number of nuclei to the size of the area measured by ImageJ.

Flow cytometry analysis of T cell cultures, BALF and lung samples

Mouse lungs were enzymatically dissociated into single cell preparation, as described in the preparation of mouse lymphocytes from the spleen. For cell surface marker staining, cells were first stained with eBioscience Fixable Viability Dye eFluor 520 or 780 (1:2000) in PBS at 4°C for 30 min. After washing twice, cells were subjected to cell surface markers staining in FACS buffer (5% BSA and 0.1% sodium azide in PBS) at 4°C for 30 min. For intracellular cytokine staining, cells were treated with eBioscience Cell Stimulation Cocktail (plus protein transport inhibitors) (eBioscience, 00-4975-03) for 4 hr before live/dead cell staining. Cells were then treated with fixation/permeabilization solution (BD Biosciences, 554722) before staining. For nuclear staining, cells were fixed in 4% paraformaldehyde for 30 min, permeabilized in 90% methanol at 4°C for 45 min and then stained with the antibody in FACS buffer at 4°C for 30 min. After staining, cells were first gated on CD45 and viability dye for live leukocytes. Doublets were excluded based on FSC-A versus FSC-H and SSC-W versus SSC-H. Among $CD3^+CD4^+$ T cells, the $CD62L^+CD44^-CD25^-$ population were deemed naive $CD4^+$ T cells. Eosinophils were the Siglec F^+CD11c^{low} population. Macrophages were $CD11c^+$Siglec F^+MHC II^{low}. Dendritic cells were $CD11c^+$Siglec F^+MHC II^{high}. Neutrophils were $CD11b^+Ly6G^+$Siglec F^-MHC II^-. Mast cells were FceR1α $^+$c-$Kit^+CD11b^-CD11c^-$. Lymphocytes include T cells ($CD3^+CD19^-$), B cells ($CD19^+CD3^-$) and NK cells ($NK1.1^+CD3^-$). For flow cytometry analyses of DRD4

expression, cells were treated with the Mouse on Mouse Kit before incubated with the mouse anti-DRD4 antibody (1:100; EMD Millipore, MABN125) and a fluorescent secondary antibody. Cells were then double labeled for surface markers of $CD4^+$ T cells, $CD8^+$ T cells, B cells, eosinophils, mast cells, macrophages, and dendritic cells. After staining, cells were analyzed on BD FACSCANTO II. Flowjo v.10.5.3 was used for data analysis. All the antibodies used for flow cytometry were listed in Key Resources Table.

ILCs isolation and culture

Cells from the dissociated adult mouse lungs were incubated with CD90.2 microbeads (Miltenyi Biotec, 130-049-101) for 17 min on ice and enriched for $CD90.2^+$ cells by positive selection using LS columns (Miltenyi Biotec, 130-042-401). $CD90.2^+$ cells were stained with antibodies for 20 min on ice, washed, and resuspended in complete medium. ILCs were defined as $CD45^+$ $CD90.2^+CD127^+ST2^+$ and negative for CD3, CD4, CD8, CD11b, CD11c, CD19, NK1.1, TCRβ, TCRγδ. ILCs were isolated by fluorescence activated cell sorting using a BD FACS Aria III. Cells were plated at a density of 6,000 cells per well in complete medium and cultured with IL-7, IL-7 + dopamine, IL-7 + IL-33 or IL-7 + IL-33 + dopamine. IL-7 was used at a final concentration of 20 ng/ml, IL-33 at 200 ng/ml and dopamine at 10 μM. After 3 days in culture, ILCs were subjected to gene expression analyses and the supernatant was analyzed by ELISA.

Physiological measurements of airway reactivity

For airway resistance assay, mice were injected with xylazine (10 mg/kg body weight), pentobarbital (100 mg/kg body weight) and pancuronium (0.5 mg/kg body weight), intubated and placed on a mechanical ventilator (Legacy flexiVent, SCIREQ). Ventilation was at 300 breaths/min (tidal volume 6–7 mL/kg body weight). Airway resistance was measured after airway delivery of nebulized methacholine in PBS (5 mg/mL, 15 mg/mL and 25 mg/mL). Data are presented as relative peak resistance to baseline within each experimental group. For airway contractility assay using lung slices, mouse lungs were infused with 1.5% low-melting agarose and sliced at 150 μm thickness using a tissue slicer (Precisionary Instruments Inc.). After overnight recovery in DMEM/F-12 (1:1; Life Technologies, 11320-033), lung slices were stimulated with increasing doses of methacholine (Sigma-Aldrich, A2251). Mid-sized airways with the diameter between 200-500 μm were imaged before stimulation and 5 min after stimulation with an inverted microscope (DMI6000B; Leica Microsystems, Buffalo Grove, IL, USA). The luminal area of the imaged airway was measured with ImageJ (National Institutes of Health, Bethesda, MD, USA). Airway contraction in response to methacholine was calculated as the percentage of reduction in the luminal area from the baseline.

Cell proliferation assay

Cell proliferation was analyzed with CFSE Cell Division Tracker Kit (BioLegend, 423801) following the manufacturer's protocol. Briefly, freshly isolated lymphocytes were incubated with 5 μM CFSE in PBS containing 5% FBS for 20 min at room temperature and protected from light. The staining was quenched by washing twice with RPMI-1640 with 10% FBS. The labeled lymphocytes were then cultured before flow cytometry analysis.

Quantitative Real Time PCR (qPCR)

Total RNA was extracted from cultured T cells and lungs using a RNeasy kit (QIAGEN, 74106) followed by reverse transcription using Superscript III Reverse Transcriptase (Thermo Fisher Scientific, 18080-044). For ILCs in culture, total RNA was extracted using PicoPure RNA isolation kit (Thermo Fisher Scientific, KIT0204) and reverse transcribed using SuperScript IV VILO Master Mix (Thermo Fisher Scientific, 11756050). Real time PCR was performed using CFX96 real-time system (Bio-Rad). TaqMan primers for mouse *Il13* (Mm00434204_m1), mouse *Il4* (Mm00445259_m1), mouse *Il5* (Mm00439646_m1), mouse *Areg* (Mm00437583_m1), mouse *Il2ra* (Mm01340213_m1), mouse *Muc5ac* (Mm01276704_m1), mouse *Ifng* (Mm01168134_m1), mouse *18S* rRNA (Mm03928990_g1), human *Il13* (Hs00174379_m1) and human *18S* rRNA (Hs99999901_s1) were purchased from Thermo Fisher Scientific. SYRB green primers for mouse *Th* gene (Mm.PY.58.33106186), mouse *Drd1* (Mm.PT.58.43576955.g), *Drd2* (Mm.PT.58.7811767), *Drd3* (Mm.PT.58.12468013), *Drd4* (Mm.PT.58.10440082) and *Drd5* (Mm.PT.58.43058779.g) were purchased from Integrated DNA Technologies. Relative gene expression was measured by normalizing to *18S* rRNA using ΔΔCt (cycle threshold difference). Expression of *Il4*, *Il5*, *Il13* and *Areg* in ILCs was normalized to the housekeeping gene *Actb* (Thermo Fisher Scientific, 4352341E).

Western Blot

Lungs and cells were homogenized in RIPA buffer with cOmpleteproteinase inhibitor cocktail (Roche, 11697498001) followed by standard western blot assays. Primary antibodies include rabbit anti-tyrosine hydroxylase (1:1000; EMD Millipore, AB152), rabbit anti-DBH (1:1000; EMD Millipore, AB1585), rabbit anti-VAChT (1:1000; Abcam, AB68986), rabbit anti-CGRP (1:1000; Sigma Aldrich, C8198), mouse anti-p-STAT6 (pY641) (1:1000; BD Biosciences, 558241), rabbit anti-DRD4 (1:1000; Sigma Aldrich, SAB4500672-100UG), mouse anti-DRD4 (1:1000; EMD Millipore, MABN125) and mouse anti-β-actin (1:3000; Sigma Aldrich, A5441). HRP–conjugated secondary antibodies include: goat anti-rabbit (1:3000; Santa Cruz Biotechnology, sc-2004) and goat anti-mouse (1:3000; BD Biosciences, 554002). The antigen-antibody complex was detected by SuperSignal West Pico PLUS Chemiluminescent Substrate (Thermo Fisher, 34577).

ELISAs

Serum was collected from blood samples of mice and the amount of OVA-specific IgE and total IgE were analyzed using ELISA Kits (BioLegend, 439807 and eBioscience, 88-50460-88). BALF was collected and the amount of IL-4, IL-5 and IL-13 were analyzed using Ready-Set-Go! ELISA sets (eBioscience, 88-7044-86, 88-7054-88 and 88-7137-76). For dopamine and norepinephrine assays, the lung was homogenized in cold RIPA buffer (Thermo Scientific, PI89900) and the amount of dopamine and norepinephrine in the supernatant were analyzed by ELISA kits (Abnova, 89-028-620 and 89-028-610). For the measurement of intracellular cAMP, naive $CD4^+$ T cells were cultured under Th0 condition overnight followed by the treatment with dopamine (10 μM) and forskolin (1 μM) for 1 hr. Cells were lysed with 100 μL RIPA buffer with 1 mM phenylmethylsulfonyl fluoride. The supernatant was collected before assays using the cAMP XP® Assay Kit (Cell signaling, 4339S).

RNA-seq analyses

Naive mouse $CD4^+$ T cells in Th0 culture with and without dopamine treatment were harvested on day 4. Total RNA was purified with a RNeasy kit (QIAGEN) followed with DNase I treatment. RNA-seq libraries were prepared with the TruSeq Stranded Total RNA with Ribo-Zero Globin kit (Illumina) following the manufacturer's instructions. Quality of the libraries was validated by quantitation with picogreen, size analysis on an Agilent Bioanalyzer or Tapestation 2200 and qPCR quantitation against a standard curve. Bar-coded cDNA libraries were pooled together in equal concentrations in one pool per biological triplicates and were sequenced on a HiSeq2500 (Illumina) at the Translational Genomics Core of Partners HealthCare Personalized Medicine (Cambridge, MA, USA). Briefly, raw reads were pre-processed using FastQC v.0.11.2, and then mapped to the mouse genome (*Mus musculus* UCSC version mm10) using the TopHat version 2.0.13. The read count table was produced using HTSeq v.0.6. Differentially expressed gene transcripts were selected based on an adjusted p value less than 0.05. Heatmap and volcano plot were performed using R-3.2.5. For pathway analysis, a list of all genes detected in the samples was ranked on the t-statistic. This list was analyzed with the fGSEA package in R using the complete Molecular Signatures Database MSigDB v6.1 gene set (http://software.broadinstitute.org/gsea/index.jsp). We only showed those pathways that had an FDR < 0.05.

Quantitative Chromatin precipitation (ChIP)-qPCR

Cultures of naive $CD4^+$ T cells were harvested on day 4. Histone was cross-linked to DNA with 1% paraformaldehyde in PBS for 10 min at 37°C. After washing with cold PBS, cells were re-suspended in 100 μL SDS lysis buffer per 1 million cells that contained 1% SDS, 10mM EDTA, 50mM Tris-HCl (pH 8.1) and cOmpleteproteinase inhibitor cocktail. Cells in suspension were sonicated using QSONICA Model Q125(50A with 14 cycles of 30 s on and 30 s off) to break genomic DNA into fragments between 200-500 bp in length. 100 μL of each sample was used as template for measurement of input DNA. Another 100 μL of each sample was diluted with 900 μL of ChIP dilution buffer (0.01% SDS, 1.1% Triton X-100, 1.2 mM EDTA, 16.7 mM Tris-HCl (pH 8.1), 150mM NaCl) and pre-cleared with 60 μL salmon sperm DNA (Invitrogen, 15632011) /protein-A agarose slurry (Thermo Fisher, 20421) for 1 h at 4°C with rotation. After centrifugation, pre-cleared samples were incubated with 5 μg of anti-trimethyl-Histone H3 (Lys27) antibody (Millipore, 07-449) overnight at 4°C with rotation followed by 2 hr incubation with protein A agarose slurry pretreated with salmon sperm DNA. The beads were then pelleted and washed extensively using buffers with increasing concentrations of NaCl. Immune complexes were eluted twice by addition of 250 μL of elution buffer (1% SDS, 0.1M $NaHCO_3$) and incubation for 15 min with rotation at room temperature. Cross-linking was reversed by adding 20 μL NaCl (5 M) and incubating at 65°C overnight. The samples were then treated with 1 μL RNase A (QIAGEN, 1031301) at 37°C for 1 hr and 2 μL Proteinase K (Roche, 14164600) at 45°C for 2 hr before DNA extraction using phenol/chloroform and purified using ethanol. The primers used for ChIP q-PCR were previously described (Tumes et al., 2013) and purchased from Integrated DNA Technologies. The relative H3K27me3 binding to the target loci was measured by normalizing to the input material using ΔCt.

QUANTIFICATION AND STATISTICAL ANALYSIS

Quantification and statistical analyzed were described in the Method Details section above and Figure legends associated with each experiment. GraphPad Prism 6 was used for data analysis. Data in all bar graphs represent mean ± SEM from at least 3 independent experiments. For comparisons between two conditions, statistical significance was analyzed using the unpaired Student's t test. For multiple comparisons between treatment and methacholine concentration or genotype (Figures 5H, S5K, and S6J), statistical analysis was performed with one-way ANOVA followed by Tukey's post-hoc test for multiple comparisons. The difference between experimental groups was considered statistically significant if *P value* was less than 0.05.

DATA AND CODE AVAILABILITY

The RNA-seq datasets of Th0 cultures with and without dopamine treatment are generated during this study and are available at the GEO repository with the accession number GEO: GSE137968.

Immunity, Volume *51*

Supplemental Information

Age-Related Dopaminergic Innervation Augments T Helper 2-Type Allergic Inflammation in the Postnatal Lung

Wei Wang, Jonathan A. Cohen, Antonia Wallrapp, Kenneth G. Trieu, Juliana Barrios, Fengzhi Shao, Nandini Krishnamoorthy, Vijay K. Kuchroo, Matthew R. Jones, Alan Fine, Yan Bai, and Xingbin Ai

Figure S1

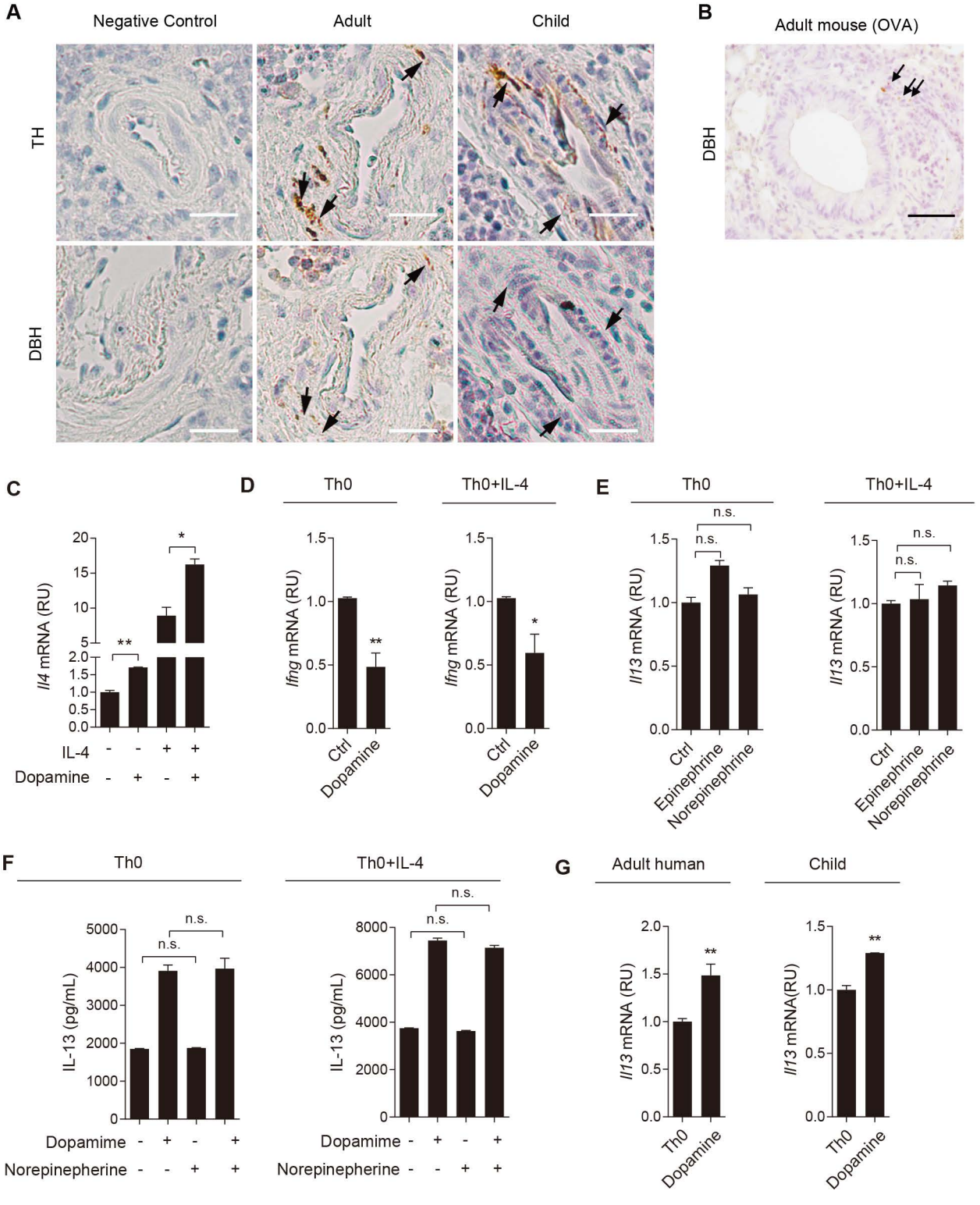
A
Negative Control
Adult
Child
TH
DBH
B
Adult mouse (OVA)
DBH
C
Il4 mRNA (RU)
IL-4
Dopamine
D
Th0
Th0+IL-4
Ifng mRNA (RU)
Ctrl
Dopamine
E
Th0
Th0+IL-4
Il13 mRNA (RU)
Ctrl
Epinephrine
Norepinephrine
n.s.
F
Th0
Th0+IL-4
IL-13 (pg/mL)
Dopamime
Norepinepherine
G
Adult human
Child
Il13 mRNA (RU)
Il13 mRNA(RU)
Th0
Dopamine

Figure S1. DBH is selectively expressed by nerves innervating human lymph nodes and mouse lungs; dopamine, but not norepinephrine and epinephrine, promotes a Th2 phenotype in CD4+ T cells.

Related to Figures 1 and 2. **(A)** Representative images of TH and DBH staining of adjacent tissue sections of lymph nodes associated with donor lungs from adults (40-65 years of age) and children (0-13 years of age). Arrows point to TH+ and DBH+ nerves. Scale bars, 50 μm. Similar results were found in 3 individuals in each age group. (**B**) Representative DBH staining in the adult mouse lung following OVA exposure. Arrows mark DBH+ labelled nerves. Scale bars, 50 μm. For (**C-G**), cultures were treated with neurotransmitters at a concentration of 10 μM and analyzed at day 4 for gene expression by qPCR and for IL-13 production by ELISA. (**C, D**) The expression of *Il4* and *Ifng* genes in mouse Th0 and Th0+IL-4 cultures with and without dopamine treatment. (**E**) *Il13* gene expression in mouse Th0 and Th0+IL-4 cultures with and without the treatment of epinephrine and norepinephrine. (**F)** IL-13 production in mouse Th0 and Th0+IL-4 cultures treated with dopamine and norepinephrine, alone and in combination. (**G**) *Il13* gene expression in human CD4+ T cells in Th0 cultures with and without the treatment of dopamine. Naïve CD4+ T cells were purified from the lymph nodes associated with donor lungs in adults (40-65 years of age) and children (0-13 years of age). For all the bar graphs, data present mean ± SEM of the results in triplicates in each experiment and from at least 3 independent experiments. *$p<0.05$; **$p<0.01$ by two-tailed student's t test. n.s., not significant.

Figure S2

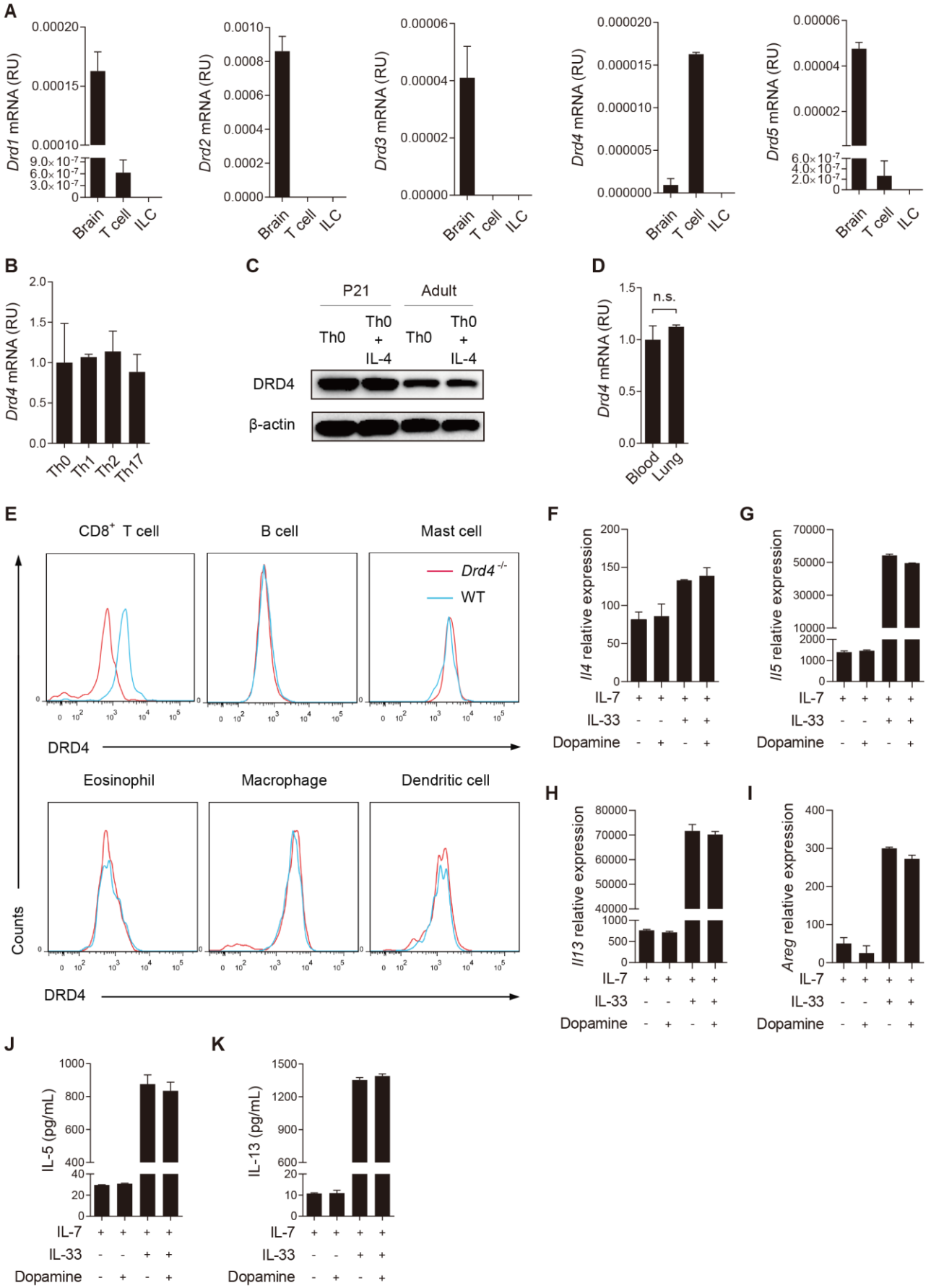
A
Drd1 mRNA (RU)
Drd2 mRNA (RU)
Drd3 mRNA (RU)
Drd4 mRNA (RU)
Drd5 mRNA (RU)
Brain
T cell
ILC
B
Drd4 mRNA (RU)
Th0
Th1
Th2
Th17
C
P21
Adult
Th0
Th0 + IL-4
DRD4
β-actin
D
Drd4 mRNA (RU)
n.s.
Blood
Lung
E
CD8+ T cell
B cell
Mast cell
Drd4 -/-
WT
DRD4
Eosinophil
Macrophage
Dendritic cell
Counts
F
Il4 relative expression
G
Il5 relative expression
H
Il13 relative expression
I
Areg relative expression
IL-7
IL-33
Dopamine
J
IL-5 (pg/mL)
K
IL-13 (pg/mL)

Figure S2. CD4$^+$ T cells and a subset of CD8$^+$ T cells, but no ILCs, express DRD4. Related to Figures 3 and 7. (**A**) qPCR analyses of *Drd1-Drd5* gene expression in purified naïve CD4$^+$ T cells from mouse spleen and ILCs from mouse lung. Mouse brain was positive control. For the analyses in T cells, the results represent mean ± SEM of 3 independent experiments. For the analyses of ILCs, the results represent mean ± SEM of 2 independent experiments. (**B**) *Drd4* gene expression in Th0, Th1, Th2 and Th17 cultures at day 4. Data represent mean ± SEM of 3 independent experiments. (**C**) DRD4 expression in Th0 and Th0+IL-4 cultures prepared from P21 and adult mice by Western blot. β-actin is loading control. Each lane represents one sample. Data represent the results in 3 independent experiments. (**D**) *Drd4* gene expression in CD4$^+$ T cells isolated from blood and lung-associated lymph nodes. Cells were isolated from samples pooled from 5 mice for each experiment. Data represent mean ± SEM of 2 independent experiments. (**E**) Flow cytometry analyses of DRD4 expression in CD8$^+$ T cells, B cells, mast cells, eosinophils, macrophages, dendritic cells. B cells were isolated from mouse spleens and all other immune cells were isolated from mouse lungs. Samples prepared from *Drd4*$^{-/-}$ mice were negative control for the specificity of the DRD4 antibody. Similar results were obtained from 3 independent experiments. (**F-K**) ILCs were isolated from 5 mouse lungs by cell sorting before cells were maintained in media with IL-7 (20 ng/mL), IL-7 + dopamine (10 μM), IL-7 + IL-33 (200 ng/mL) or IL-7 + IL-33 + dopamine. The expression of type 2 cytokine and *amphiregulin* (*Areg*) genes was analyzed at day 3 in culture. Data represent mean ± SEM of cultures in duplicates.

Figure S3

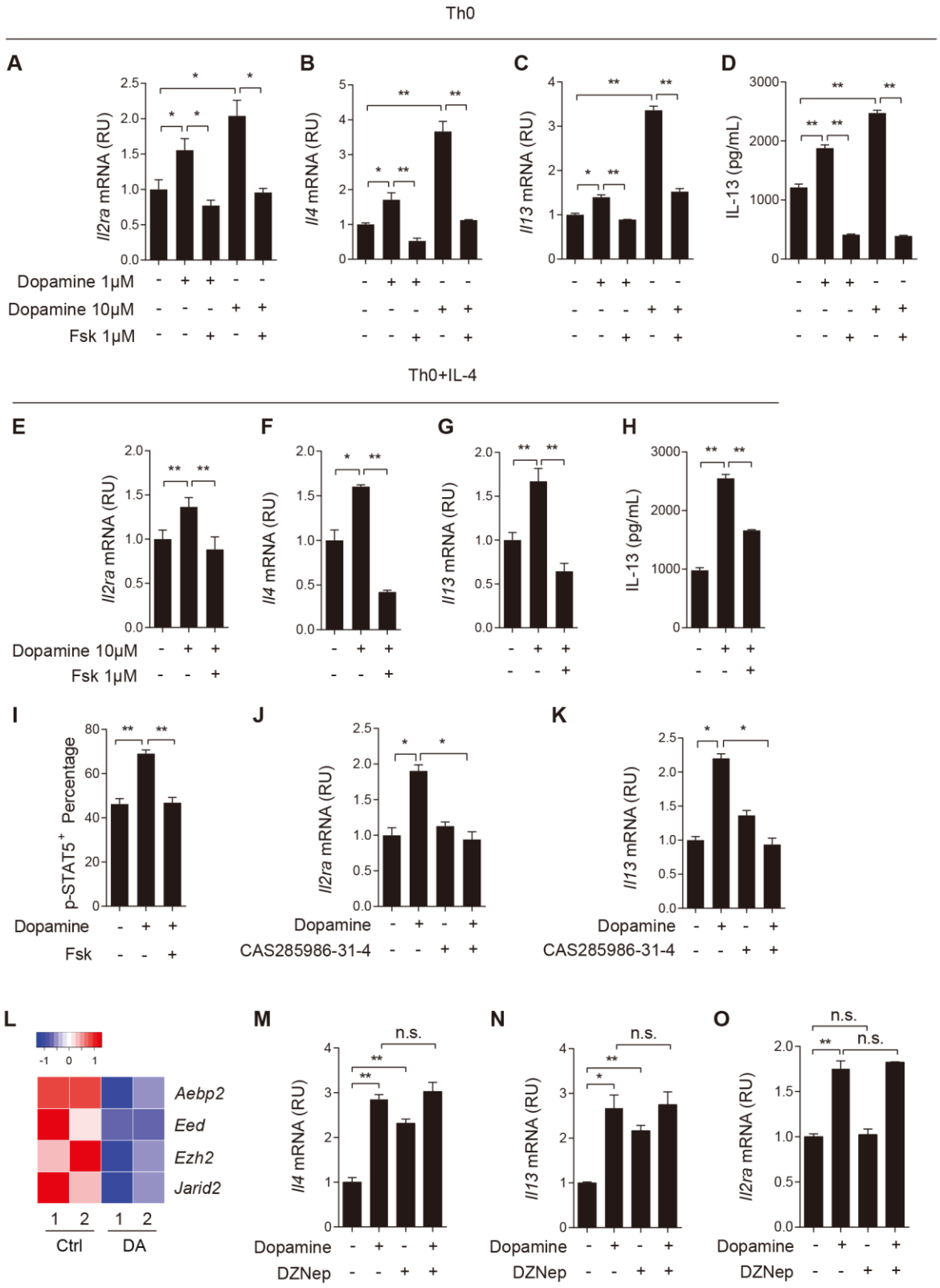

Figure S3. Dopamine signaling downregulates the cAMP and EZH2 pathways. Related to Figures 3 and 4. (**A-C**) Relative expression of *Il2ra, Il4 and Il13* genes in mouse Th0 cultures with and without dopamine and Fsk (1μM) treatment. (**D**) The production of IL-13 in each group was measured by ELISA. (**E-H**) *Il2ra,*

Il4 and Il13 gene expression and IL-13 production in Th0+IL-4 cultures with and without dopamine and Fsk treatment. (**I**) Quantification of the abundance of p-STAT5^{+} cells in Th0+IL-4 cultures treated with dopamine alone and a combination of dopamine and Fsk. Cultures were analyzed by flow cytometry. (**J**, **K**) Relative expression of *Il2ra* and *Il13* genes in Th0 cultures treated with dopamine and CAS285986-31-4 (20 µM), alone and together. (**L**) Heat map of differential gene expression of *Ezh2* and other PRC2 component genes in Th0 cultures treated with dopamine (DA). Data are from the results of RNA-seq. (**M-O**) Relative expression of *Il4, Il13 and Il2ra* genes in mouse Th0 cultures treated with dopamine and DZNep (7.5 nM), alone and in combination. Data were normalized to untreated baseline. All bar graphs represent mean ± SEM of 3 independent experiments. *$p<0.05$; **$p<0.01$ by two-tailed student's t test. n.s., not significant.

Figure S4

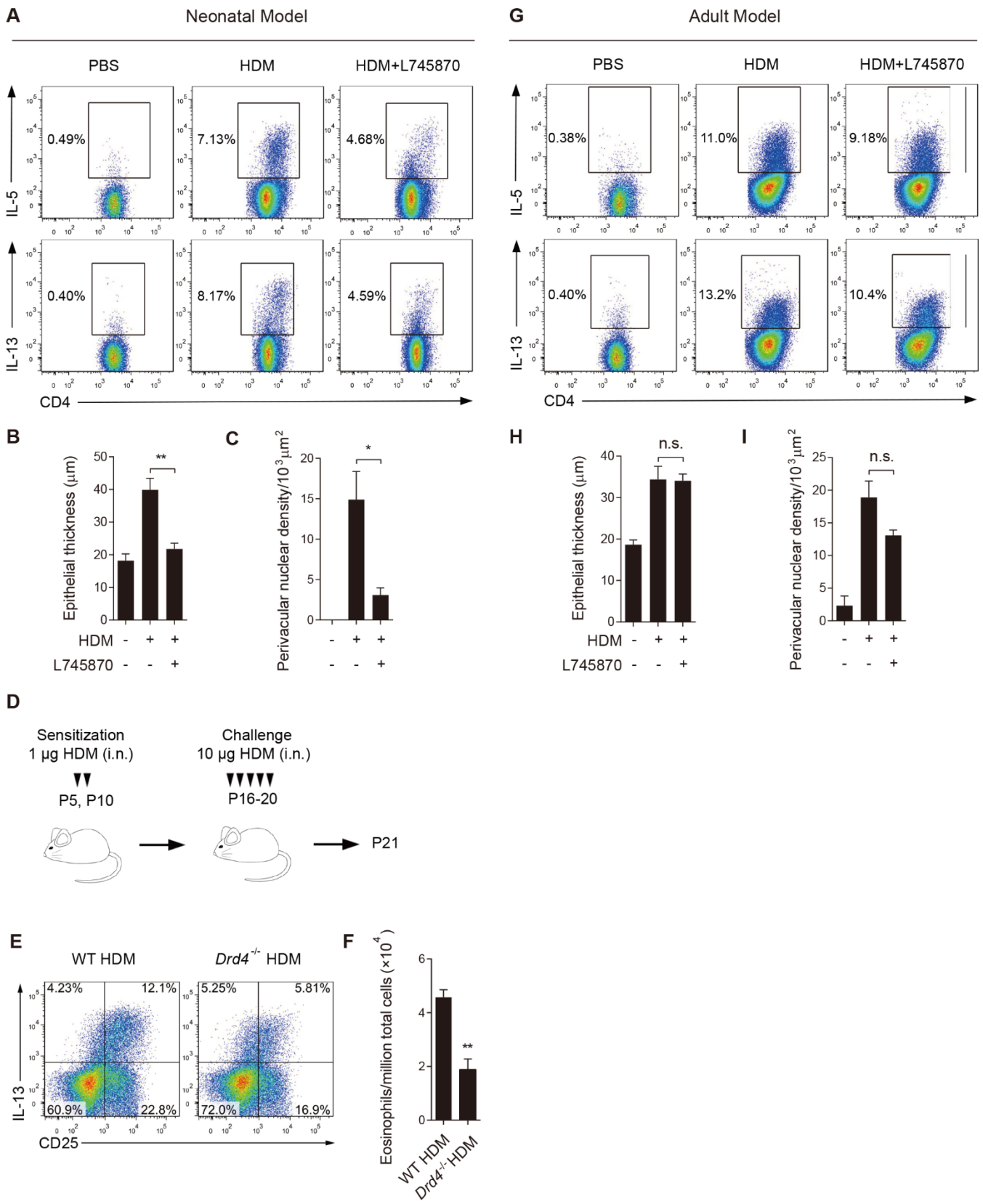

Figure S4. Functional disruption of DRD4 by L745870 and genetic deficiency ameliorates Th2 inflammation in neonatal mice following HDM exposure. Related to Figure 5. (**A**) Flow cytometry

analyses of IL-5^{+}CD4^{+} and IL-13^{+}CD4^{+} T cells in the lung following HDM exposure with and without L745870 treatment in neonates. Results were representative of 3 independent experiments. (**B**, **C**) Pathological measurements of epithelial thickness and peri-vascular nuclear density in each group. Data represent mean ± SEM of 3 non-overlapping histological areas in each mouse, 6 mice in each group from 3 independent experiments. (**D**) Experimental scheme of HDM exposure in WT and *Drd4*$^{-/-}$ neonatal mice. Mice were sacrificed 1 day after the last challenge. (**E**) Representative flow cytometry analyses of IL-13^{+}CD25^{+}CD4^{+} T cells in WT and *Drd4*$^{-/-}$ mice at P21. Similar results were obtained in 3 independent experiments. (**F**) The abundance of eosinophils in the lung of WT and *Drd4*$^{-/-}$ mice following HDM exposure at P21. Data represent mean ± SEM of 6 mice of each genotype in 3 independent experiment. (**G-I**) Assessment of Th2 inflammation in adult mice following HDM exposure by flow cytometry and pathological measurements as described in (**A-C**) for neonatal mice. N=5 adult mice from 2 independent experiments. *$p<0.05$; **$p<0.01$ by two-tailed student's t test. n.s., not significant.

Figure S5

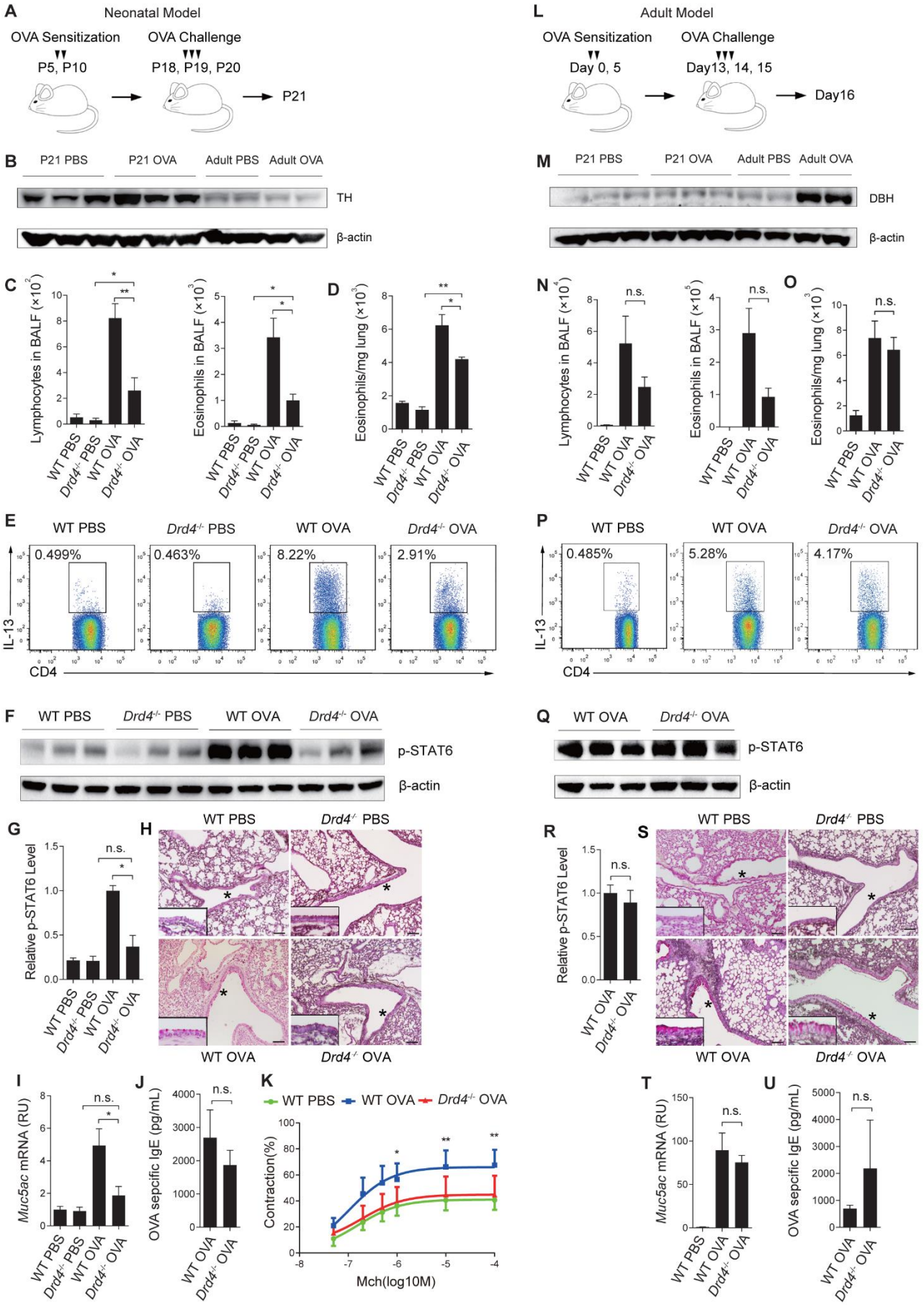
A
Neonatal Model
OVA Sensitization
P5, P10
OVA Challenge
P18, P19, P20
P21
L
Adult Model
OVA Sensitization
Day 0, 5
OVA Challenge
Day13, 14, 15
Day16
B
P21 PBS
P21 OVA
Adult PBS
Adult OVA
TH
β-actin
M
DBH
β-actin
C
Lymphocytes in BALF (×10^2)
Eosinophils in BALF (×10^3)
D
Eosinophils/mg lung (×10^3)
WT PBS
Drd4-/- PBS
WT OVA
Drd4-/- OVA
N
Lymphocytes in BALF (×10^4)
Eosinophils in BALF (×10^5)
O
Eosinophils/mg lung (×10^3)
n.s.
E
0.499%
0.463%
8.22%
2.91%
IL-13
CD4
P
0.485%
5.28%
4.17%
F
p-STAT6
β-actin
Q
G
Relative p-STAT6 Level
H
R
S
I
Muc5ac mRNA (RU)
J
OVA sepcific IgE (pg/mL)
K
Contraction(%)
Mch(log10M)
T
U

Figure S5. DRD4 deficiency ameliorates Th2 inflammation in neonatal mice, but not in adult mice, following OVA exposure. Related to Figure 5. (**A** and **L)** Experimental scheme of OVA sensitization and challenge in neonatal mice (**A**) and adult mice (**L**). Mice were sacrificed 1 day after the last challenge. **(B** and **M)** The amount of tyrosine hydroxylase and DBH in saline and OVA-exposed lungs of WT neonatal and adult mice. β-actin was loading control. Each lane represents one sample. Similar results were obtained in 3 independent experiments. (**C**) Flow cytometry analyses of lymphocytes and eosinophils in BALF of WT and *DRD4*$^{-/-}$ mice following OVA exposure at P21. N=6 in 3 independent experiments. (**D**) The abundance of eosinophils in the lung of WT and *Drd4*$^{-/-}$ mice at P21. Results were normalized to lung weight. N=5 in 3 independent experiments. (**E**) Representative cytometry results of IL-13^{+}CD4^{+} T cells in P21 lungs of each group. Similar results were obtained from 3 independent experiments. (**F**) Western blot analyses of p-STAT6 in the lung of WT and *Drd4*$^{-/-}$ mice at P21. β-actin was loading control. Each lane represents one sample. Similar results were obtained in 3 independent experiments. Data were quantified in **(G**). (**H**) Representative images of PAS staining of tissue sections in P21 lungs from each group. The area of the airway epithelium marked by * is enlarged and shown by the insert. Similar results were obtained in 3 independent experiments. Scale bars, 100 µm. (**I**) Mucus production in WT and *Drd4*$^{-/-}$ P21 lungs assayed by *Muc5ac* qPCR. N=5 for P21 *Drd4*$^{-/-}$ PBS group and N=10-12 for other groups in 3 independent experiments. (**J**) The amount of OVA-specific IgE in serum of WT and *Drd4*$^{-/-}$ mice at P21. N=12 in 3 independent experiments. (**K**) Assessment of airway hypercontractility following OVA exposure in WT and *Drd4*$^{-/-}$ mice at P21 using precision cut lung slices. Airway contractility in response to methacholine was measured by the percentage of reduction in the luminal size from the baseline. N=15-20 airways from 3 mice of each group in 2 independent experiments. (**N**-**U**) Assessment of Th2 inflammation in adult, WT and *Drd4*$^{-/-}$ mice following OVA exposure using flow cytometry, immunological and pathological assays as described for neonatal mice in (**C**-**J)**. N=5-7 for adult WT groups and N=5 for *Drd4*$^{-/-}$ group in 3 independent experiments. For the results in (**K**), data were analyzed by one-way ANOVA for multiple comparisons between treatment and methacholine dosage. For all other panels, data were analyzed by two-tailed student's t test. *$p<0.05$; **$p<0.01$; n.s., not significant.

We noted significant variations in OVA-specific IgE in the neonatal OVA models in (**J**). The variation may contribute to the statistically insignificant difference in OVA-specific IgE between WT and *Drd4*$^{-/-}$ mice.

Figure S6

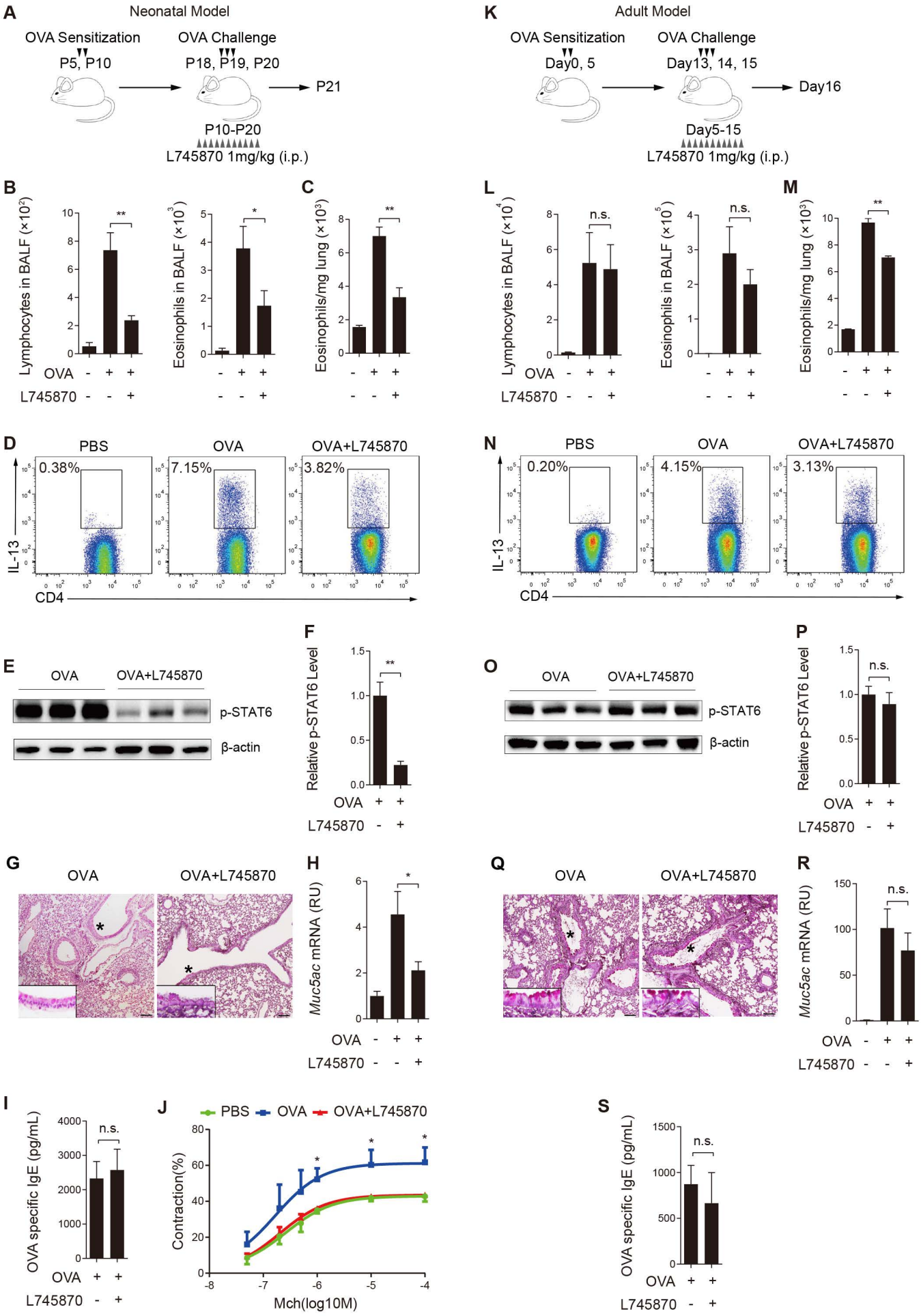
A
Neonatal Model
OVA Sensitization
P5, P10
OVA Challenge
P18, P19, P20
P21
P10-P20
L745870 1mg/kg (i.p.)
K
Adult Model
OVA Sensitization
Day0, 5
OVA Challenge
Day13, 14, 15
Day16
Day5-15
L745870 1mg/kg (i.p.)
B
Lymphocytes in BALF (×10²)
Eosinophils in BALF (×10³)
C
Eosinophils/mg lung (×10³)
OVA
L745870
L
Lymphocytes in BALF (×10⁴)
Eosinophils in BALF (×10⁵)
n.s.
M
Eosinophils/mg lung (×10³)
D
PBS
OVA
OVA+L745870
0.38%
7.15%
3.82%
IL-13
CD4
N
0.20%
4.15%
3.13%
E
p-STAT6
β-actin
F
Relative p-STAT6 Level
O
P
G
H
Muc5ac mRNA (RU)
Q
R
I
OVA specific IgE (pg/mL)
J
Contraction(%)
Mch(log10M)
S

Figure S6. Pharmaceutical blockade of DRD4 signaling ameliorates Th2 inflammation in neonatal mice, but not adult mice, following OVA exposure. Related to Figure 5. (**A**) Experimental scheme of L745870 treatment during OVA sensitization and challenge in neonatal mice. L745870 was given intra-peritoneally at 1 mg/kg body weight daily between P10-P20. Mice were analyzed one day after the last challenge at P21. (**B**) Flow cytometry analyses of lymphocytes and eosinophils in BALF of each group at P21. N=5 for P21 PBS group, N=7 for P21 OVA group and N=7 for P21 OVA+L745870 group in 3 independent experiments. (**C**) The abundance of eosinophils in the lung of each group at P21. Results were normalized to lung weight. N=5 for P21 PBS group, N=7 for P21 OVA group and N=7 for P21 OVA+L745870 group in 3 independent experiments. (**D**) Representative flow cytometry analyses of IL-$13^{+}CD4^{+}$ T cells in P21 lungs of each group. Similar results were obtained from 3 independent experiments. (**E**, **F**) Quantification of p-STAT6 in P21 mouse lungs with and without L745870 treatment by Western blot. β-actin was loading control. Each lane represents one sample. Similar results were obtained from 5-7 mice in 3 independent experiments. (**G**, **H**) Mucus production in different experimental groups assayed by PAS staining and *Muc5ac* qPCR. The area of the airway epithelium marked by * is enlarged and shown in the insert in (**G**). N=9 in 3 independent experiments. Scale bars, 100 µm. (**I**) The amount of OVA-specific IgE in serum from mice at P21 in each group. N=17 in the OVA group and N=12 in OVA+L745870 group from 3 independent experiments. (**J**) Assessment of airway hypercontractility in OVA-exposed mice with and without L745870 treatment at P21 using precision cut lung slices. Airway contractility in response to methacholine was measured by the percentage of reduction in the luminal size from the baseline. N=15-20 airways from 3 mice in 2 independent experiments for each group. (**K**) Experimental scheme of L745870 (1 mg/kg body weight) treatment during OVA sensitization and challenge in adult mice. Adult lungs were analyzed one day after the last challenge at experimental day 16. (**L-S**) Assessment of Th2 inflammation in adult mice with and without L745870 treatment following OVA exposure using similar assays as described in (**B-I**) for neonatal mice. For BALF assays in (**L**), N=7 for each group in 3 independent experiments. For assays in (**M**, **N**), N=5-6 mice in 3 independent experiments. For results in (**O**, **P**), N=3 in 2 independent experiments. For results in (**Q**, **R**), N=8 in 3 independent experiments. For results in (**S**), N=6 in 3 independent experiments. For airway contractility measurement in (**J**), data were analyzed by one-way ANOVA for multiple comparisons between treatment and methacholine dosage. For all other results, data were analyzed by two-tailed student's t test. *$p<0.05$; **$p<0.01$; n.s., not significant.

We noted significant variations in OVA-specific IgE in the neonatal OVA models in (**I**). The variation may explain why the amount of OVA-specific IgE was not statistically significant between WT and *Drd4*$^{-/-}$ mice at P21, although Th2 inflammation was diminished. For panel (**M**), the reduction in eosinophilic infiltrates in the adult lung reached statistical significance in L745870-treated model. However, in other adult exposure

experiments (Figures 5**K** and S5**O**), there was a consistent trend of mild reduction in the number of eosinophils by DRD4 deficiency without reaching statistical significance. The discrepancy may be contributed by technical variations among multiple repeats of the experiment. It is important to note that comparing neonatal and adult mice (Figures S6**C** and S6**M**), L745870 treatment caused a greater reduction in the number of eosinophils in neonates than adults. These findings support our conclusion that the dopamine-DRD4 pathway contributes significantly to the Th2 inflammation in the early lung.

Figure S7

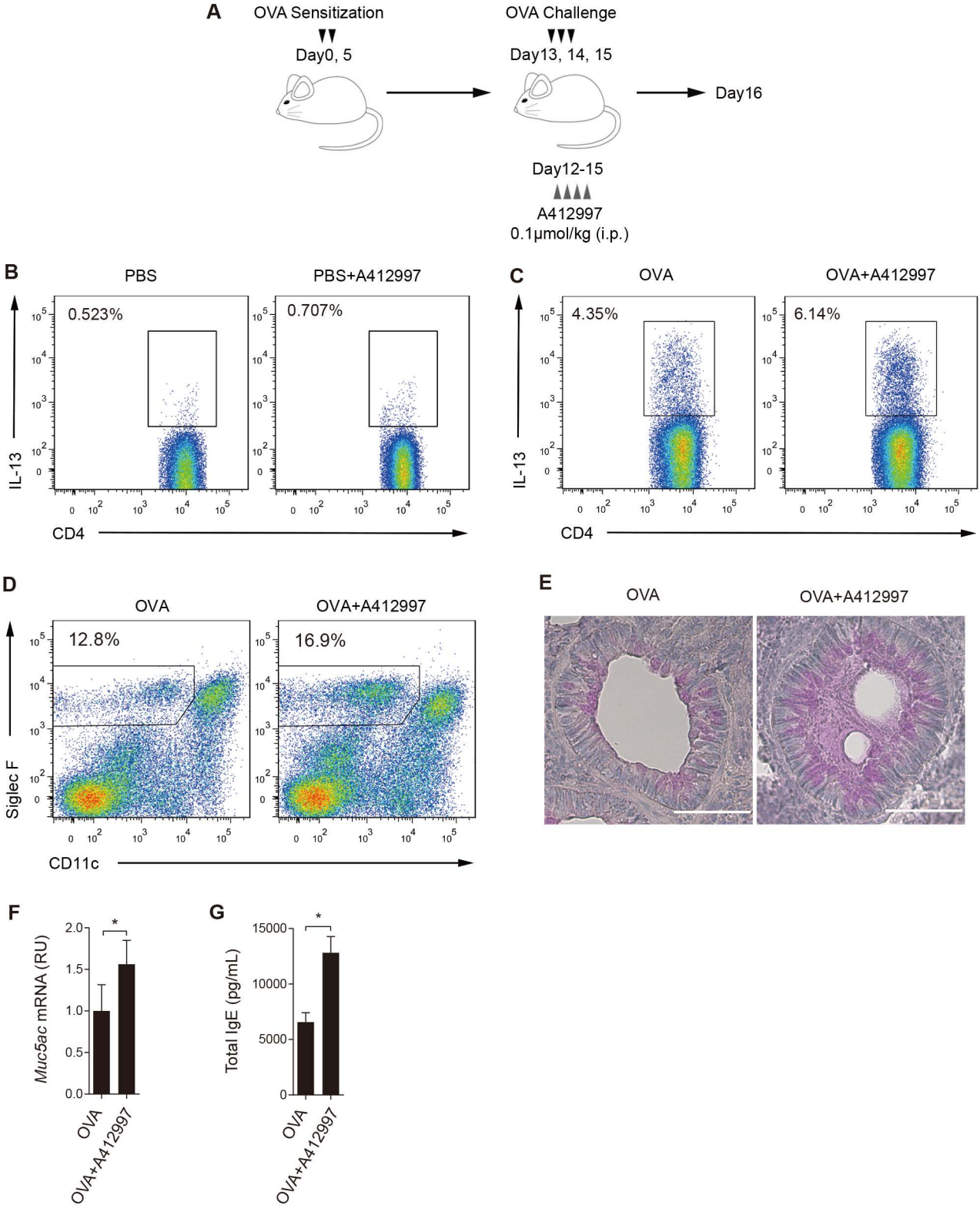
A
OVA Sensitization
Day0, 5
OVA Challenge
Day13, 14, 15
Day16
Day12-15
A412997
0.1μmol/kg (i.p.)
B
PBS
PBS+A412997
0.523%
0.707%
IL-13
CD4
C
OVA
OVA+A412997
4.35%
6.14%
IL-13
CD4
D
OVA
OVA+A412997
12.8%
16.9%
Siglec F
CD11c
E
OVA
OVA+A412997
F
Muc5ac mRNA (RU)
OVA
OVA+A412997
G
Total IgE (pg/mL)
OVA
OVA+A412997

Figure S7. Activation of DRD4 in adult mice by an agonist A412997 worsens Th2 inflammation following OVA exposure. Related to Figure 6.
(**A**) Experimental scheme of A412997 treatment during OVA sensitization and challenge in adult mice. A412997 was given intraperitoneally to adult mice between experimental day 12 -15. A412997 was given once per day at a dose of 1 μmol/kg body weight. Mice were analyzed one day after the last challenge on experimental day 16. (**B-D**) Representative flow cytometry analyses of IL-13^{+}CD4^{+} T cells and eosinophils in the lung of saline- and OVA-exposed mice with and without A412997 treatment. Similar results were obtained from 3 independent experiments. (**E, F**) Mucus overproduction assayed by PAS staining and *Muc5ac* gene expression in OVA-exposed mice with and without A412997 treatment. N=6 in 3 independent experiments. Scale bars, 50 μm. (**G**) The amount of total IgE in serum of OVA-exposed mice with and without A412997 treatment. N=6 in 3 independent experiments. *$p<0.05$ by two-tailed student's t test.

Article

Immunity

Age-Related Dopaminergic Innervation Augments T Helper 2-Type Allergic Inflammation in the Postnatal Lung

Graphical Abstract

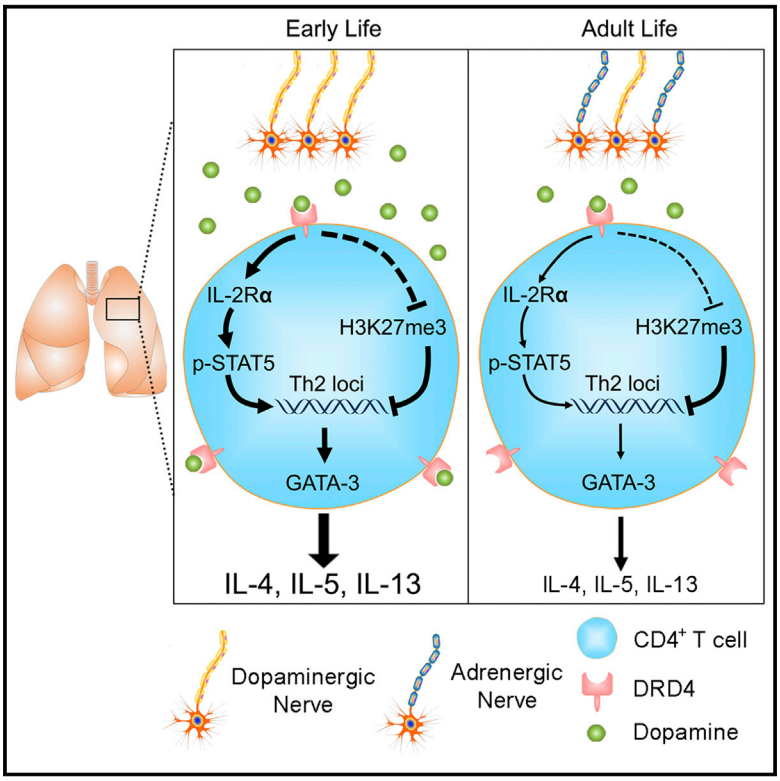

Authors

Wei Wang, Jonathan A. Cohen, Antonia Wallrapp, ..., Alan Fine, Yan Bai, Xingbin Ai

Correspondence

xai@partners.org

In Brief

Children are more prone to developing allergic asthma than adults. Wang et al. find that sympathetic nerves undergo a dopaminergic-to-adrenergic transition during post-natal development of the lung. Dopamine signaling in CD4$^+$ T cells promotes a Th2 phenotype, which makes young mice more susceptible to allergy. These findings provide an age-related mechanism underlying the susceptibility of the young to allergic inflammation.

Highlights

- Sympathetic innervation in the lung undergoes a dopaminergic-to-adrenergic transition
- Dopamine signals through DRD4 in CD4$^+$ T cells to induce a Th2 phenotype
- Dopaminergic nerves in the early lung foster susceptibility to allergic inflammation

Wang et al., 2019, Immunity *51*, 1102–1118
December 17, 2019 © 2019 Elsevier Inc.
https://doi.org/10.1016/j.immuni.2019.10.002

CellPress

CellPress

Immunity
Article

Age-Related Dopaminergic Innervation Augments T Helper 2-Type Allergic Inflammation in the Postnatal Lung

Wei Wang,[1] Jonathan A. Cohen,[1] Antonia Wallrapp,[2] Kenneth G. Trieu,[1] Juliana Barrios,[3] Fengzhi Shao,[3] Nandini Krishnamoorthy,[1] Vijay K. Kuchroo,[2] Matthew R. Jones,[3] Alan Fine,[3,4] Yan Bai,[1] and Xingbin Ai[1,5,6,*]
[1]Division of Pulmonary and Critical Care Medicine, Department of Medicine, Brigham and Women's Hospital, Boston, MA, USA
[2]Evergrande Center for Immunologic Diseases, Harvard Medical School and Brigham and Women's Hospital, Boston, MA, USA
[3]The Pulmonary Center, Department of Medicine, Boston University School of Medicine, Boston, MA, USA
[4]The West Roxbury Veteran's Hospital, West Roxbury, MA, USA
[5]Present address: Division of Newborn Medicine, Department of Pediatrics, Massachusetts General Hospital for Children, Boston, MA, USA
[6]Lead Contact
*Correspondence: xai@partners.org
https://doi.org/10.1016/j.immuni.2019.10.002

SUMMARY

Young children are more susceptible to developing allergic asthma than adults. As neural innervation of the peripheral tissue continues to develop after birth, neurons may modulate tissue inflammation in an age-related manner. Here we showed that sympathetic nerves underwent a dopaminergic-to-adrenergic transition during post-natal development of the lung in mice and humans. Dopamine signaled through a specific dopamine receptor (DRD4) to promote T helper 2 (Th2) cell differentiation. The dopamine-DRD4 pathway acted synergistically with the cytokine IL-4 by upregulating IL-2-STAT5 signaling and reducing inhibitory histone trimethylation at Th2 gene loci. In murine models of allergen exposure, the dopamine-DRD4 pathway augmented Th2 inflammation in the lungs of young mice. However, this pathway operated marginally after sympathetic nerves became adrenergic in the adult lung. Taken together, the communication between dopaminergic nerves and CD4$^+$ T cells provides an age-related mechanism underlying the susceptibility to allergic inflammation in the early lung.

INTRODUCTION

The nervous system communicates with the immune system to regulate inflammation. Pathogen exposure and tissue injury stimulate immune cells and trigger a neural reflex (Chavan et al., 2017). Activation of the neural reflex causes release of neurotransmitters from the innervating afferent and efferent neurons. These neurotransmitters can signal to immune cells, thereby modulating innate and adaptive immune responses. For example, the cholinergic vagal system is activated in sepsis and, by releasing acetylcholine, represses tumor necrosis factor production in spleen macrophages (Borovikova et al., 2000; Wang et al., 2003). In other organs, such as the gut, cholinergic and sympathetic nerves play opposing roles in modulating innate lymphoid type 2 cell (ILC2)-mediated type 2 inflammation by secreting neuromedin U and epinephrine, respectively (Cardoso et al., 2017; Klose et al., 2017; Moriyama et al., 2018).

Allergic asthma is a common airway disease characterized by eosinophilia, mucus overproduction, airway hyperreactivity, and tissue remodeling (Becerra-Díaz et al., 2017; Fahy, 2015). These hallmarks are driven by type 2 cytokines, including interleukin-4 (IL-4), IL-5, and IL-13. Major effector cells in asthma are T helper 2 (Th2) cells. These cells are differentiated from naive CD4$^+$ T cells through a well-orchestrated process that involves priming in the lymph nodes and maturation in the lungs (Van Dyken et al., 2016). Th2 cell differentiation requires IL-4 and IL-2. IL-4 induces differentiation and maintains the Th2 phenotype (Le Gros et al., 1990), whereas IL-2, which is expressed by T cells upon activation, promotes proliferation and Th2 differentiation by transcriptionally activating expression of the *Il2ra*, *Il4*, and *Il4ra* genes via STAT5 (Cote-Sierra et al., 2004; Zhu et al., 2003). Apart from cytokines, neurotransmitters modulate type 2 inflammation. Neuropeptides are known to enhance the antigen-presenting activity of dendritic cells in adult murine models of allergic asthma (Buttari et al., 2014; Ohtake et al., 2015; Talbot et al., 2015). Dopamine has also been shown to induce a Th2 phenotype in CD4$^+$ T cells in culture (Huang et al., 2010; Nakano et al., 2009). However, the intracellular signaling mechanism of dopamine driving Th2 cell differentiation is unknown. In addition, there are conflicting reports regarding the identity of the dopamine receptors involved and the role of dopamine in disease models (Contreras et al., 2016; Franz et al., 2015; Huang et al., 2010; Ilani et al., 2004; Mori et al., 2013; Nakano et al., 2009).

To date, studies related to neural regulation of type 2 inflammation have been limited to mature tissues in adult disease models. As neurons undergo dynamic changes in the abundance and phenotype during post-natal maturation, neuron-immune cell communication may differ with age, contributing to disease susceptibility in a tissue-specific and age-related manner. This age-related communication may be particularly important in asthma because young children are more susceptible to developing allergic asthma than adults (Stern et al., 2008).

 © 2019 Elsevier Inc.

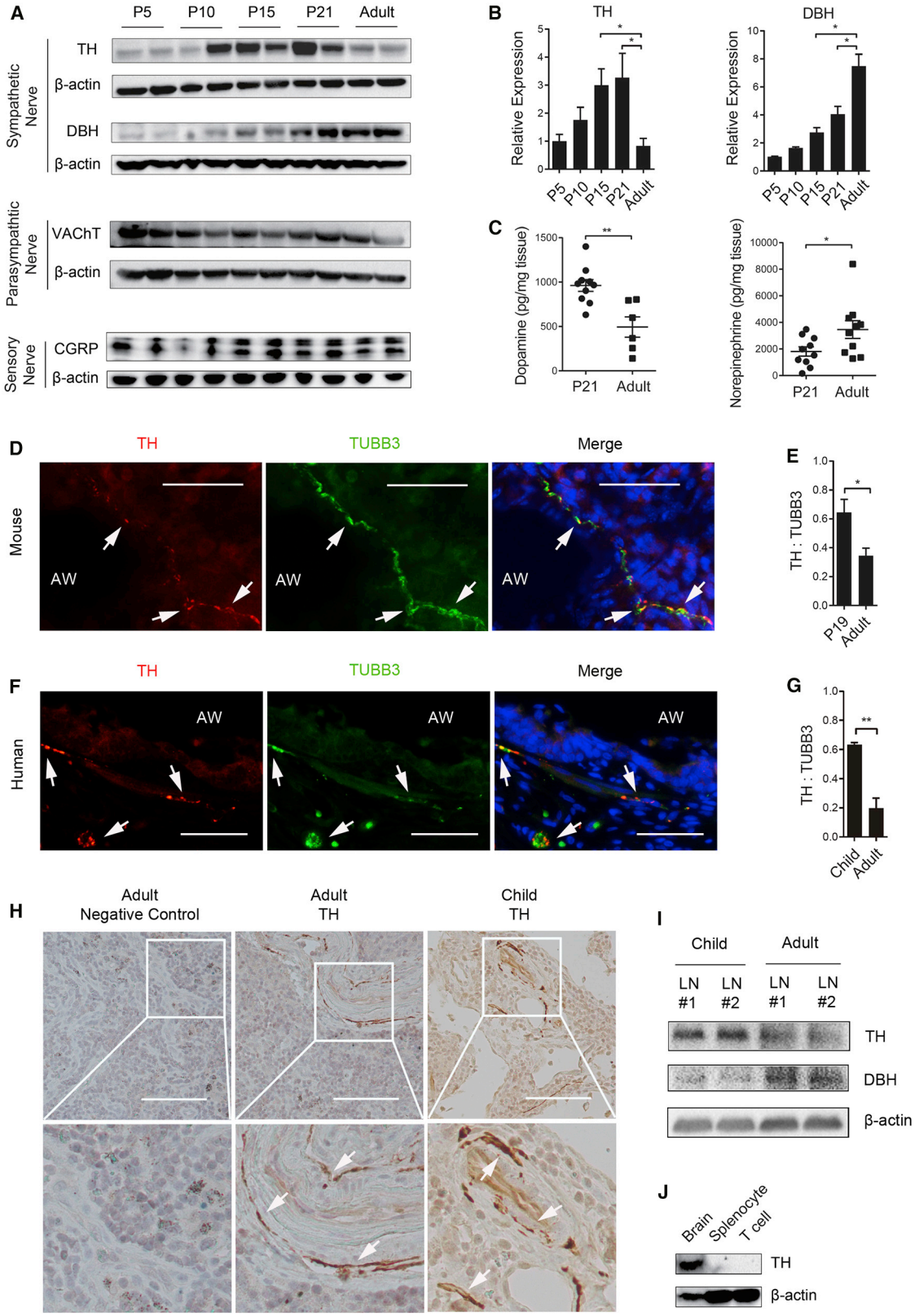

(legend on next page)

In the lungs, nerves innervate the smooth muscle compartment in the airway and vasculature. These nerves are mostly derived from neurons whose cell bodies are located outside of the pulmonary tract in the nodose ganglion, sympathetic ganglion, and brain stem. Nodose sensory afferents and cholinergic and sympathetic efferents are connected through brain stem neurons to form a neurocircuitry that controls fundamental respiratory functions, such as breathing and coughing (Aven and Ai, 2013). Development of the neurocircuitry requires locally produced neurotrophins, such as brain-derived neurotrophic factor and neurotrophin 4 (Aven et al., 2014; Patel et al., 2016; Radzikinas et al., 2011). Temporal expression of these neurotrophins dynamically regulates the process of airway innervation during embryogenesis and post-natal maturation. In the murine lung, neural innervation peaks around post-natal day 14 (P14), followed by a decline in the third post-natal week before it reaches the mature configuration in adults (Aven et al., 2014).

In this study, we characterized the post-natal development of the 3 major types of nerves in the murine lung and discovered that sympathetic nerves transitioned from a predominantly dopamine-producing (dopaminergic) phenotype in early post-natal life to a norepinephrine-producing (adrenergic) phenotype in adult life. We investigated dopamine signaling in T cells and in murine models of allergic inflammation. We found that dopaminergic nerves in the early lung augmented Th2 inflammation by communicating with $CD4^+$ T cells via the dopamine-DRD4 pathway, whereas adrenergic nerves in the adult lung had no Th2-inducing activities. Our findings provide evidence of the development of sympathetic innervation as an age-related modulatory mechanism in Th2 inflammation in the lung, which has implications for the susceptibility and etiology of allergic asthma in young children.

RESULTS

Sympathetic Nerves in the Lung Undergo a Dopaminergic-to-Adrenergic Transition during Post-natal Development

We characterized the developmental dynamics of the 3 major types of nerves in the murine lung after birth. Western blot analysis showed that the relative abundance of sensory and cholinergic nerves, identified by calcitonin gene-related peptide (CGRP) and vesicular acetylcholine transporter (VAChT), respectively, remained mostly unchanged by age (Figure 1A). For sympathetic nerves, however, tyrosine hydroxylase (TH), a specific marker and the rate-limiting enzyme for the biosynthesis of dopamine, peaked around P15–P21, followed by a decline in the adult lung, whereas the amount of dopamine β-hydroxylase (DBH), an enzyme that converts dopamine to norepinephrine, increased with age (Figures 1A and 1B). These changes in tyrosine hydroxylase and DBH were associated with a 50% reduction in the amount of dopamine from P21 (961.9 ± 66.72 pg/mg lung weight) to adults (494.0 ± 114.7 pg/mg lung weight), with a reciprocal increase in norepinephrine (1,815 ± 349 pg/mg lung weight at P21 versus 3,469 ± 669 pg/mg lung weight in adults) (Figure 1C).

Previous studies detected tyrosine hydroxylase in a subset of immune cells, mostly by gene expression assays (Cosentino et al., 2007; Flierl et al., 2007; Papa et al., 2017). To address whether the age-related reduction in tyrosine hydroxylase expression in the post-natal lung was caused by a change in sympathetic innervation, we investigated the source of tyrosine hydroxylase in both mouse and human lungs. Because the lung samples in western blot and dopamine measurement assays likely included lymph nodes associated with bronchi, we separately examined the lung and associated lymph nodes. Because of technical difficulties of dissecting lymph nodes associated with mouse lungs, especially in neonates, we resorted to lymph nodes associated with human donor lungs for the assay. Double-staining for tyrosine hydroxylase and a pan-neural marker, neuron-specific class III β-tubulin (TUBB3), detected tyrosine hydroxylase exclusively in $TUBB3^+$ structures along the airway and blood vessel in mice and humans (Figures 1D and 1F). In addition, tyrosine hydroxylase and DBH were found selectively in nerves along the lymphatic vessel in lymph nodes associated with adult donor lungs (Figures 1H and S1A). DBH was also found only in nerves in the mouse lung (Figure S1B). Furthermore, tyrosine hydroxylase in isolated mouse splenocytes and purified $CD4^+$ T cells was below detection compared with robust expression in neurons (Figure 1J).

After validating the nerve as the major source of tyrosine hydroxylase, we quantified the abundance of sympathetic nerves

Figure 1. Sympathetic Nerves in the Lung Transition from Dopaminergic to Adrenergic Phenotypes from Early Life to Adult Life

(A and B) Western blot analyses (A) of the markers of sympathetic nerves (tyrosine hydroxylase [TH] and dopamine β-hydroxylase [DBH]), parasympathetic nerves (vesicular acetylcholine transporter [VAChT]), and sensory nerves (calcitonin gene-related peptide [CGRP]) in mouse lungs at different post-natal ages. β-Actin was a loading control. Each lane represents one sample. The expression of TH and DBH is presented as fold change relative to post-natal day 5 (P5) in (B). N = 6 from 2 independent experiments.

(C) The amount of dopamine and norepinephrine in the lungs of P21 and adult mice. Results were normalized to the lung weight. Each mark represents one sample.

(D and F) Double-fluorescent staining for TH and neuron-specific class III β-tubulin (TUBB3) in the lungs of mice (D) and humans (F). To visualize nerves, frozen sections (15 μm in thickness) were used for double staining. Nuclei were labeled with Hoechst dye. Arrows mark TH^+TUBB3^+ nerves. AW, airway. Scale bars, 30 μm.

(E and G) Relative abundance of TH^+ nerves in the lungs of mice (E) and humans (G) of two age groups. For quantification, the immunoreactivity of TH was normalized to TUBB3 in double-stained tissue sections. Airways with a diameter of 0.2–0.5 mm in P19 and adult mice and human mid-sized airways with a diameter of 1–2 mm in children (0–13 years of age) and adults (40–65 years of age) were quantified. Data represent mean ± SEM from 5 non-overlapping images from each sample and a total of 3 mouse samples and 4 human samples of each age group.

(H) Representative images of TH staining of lymph nodes associated with donor lungs. Bottom panels: enlarged images outlined in the top panels. Arrows point to TH^+ nerves. Similar results were obtained from 3 donors for each age group.

(I) The expression of TH and DBH in human lymph nodes of each age group, assayed by western blot (see also Figure S1).

(J) The amount of TH in mouse brain, splenocytes, and purified $CD4^+$ T cells, assayed by western blot. Data represent the results from 3 independent experiments. $^*p < 0.05$ and $^{**}p < 0.01$ by two-tailed Student's t test.

See also Figure S1.

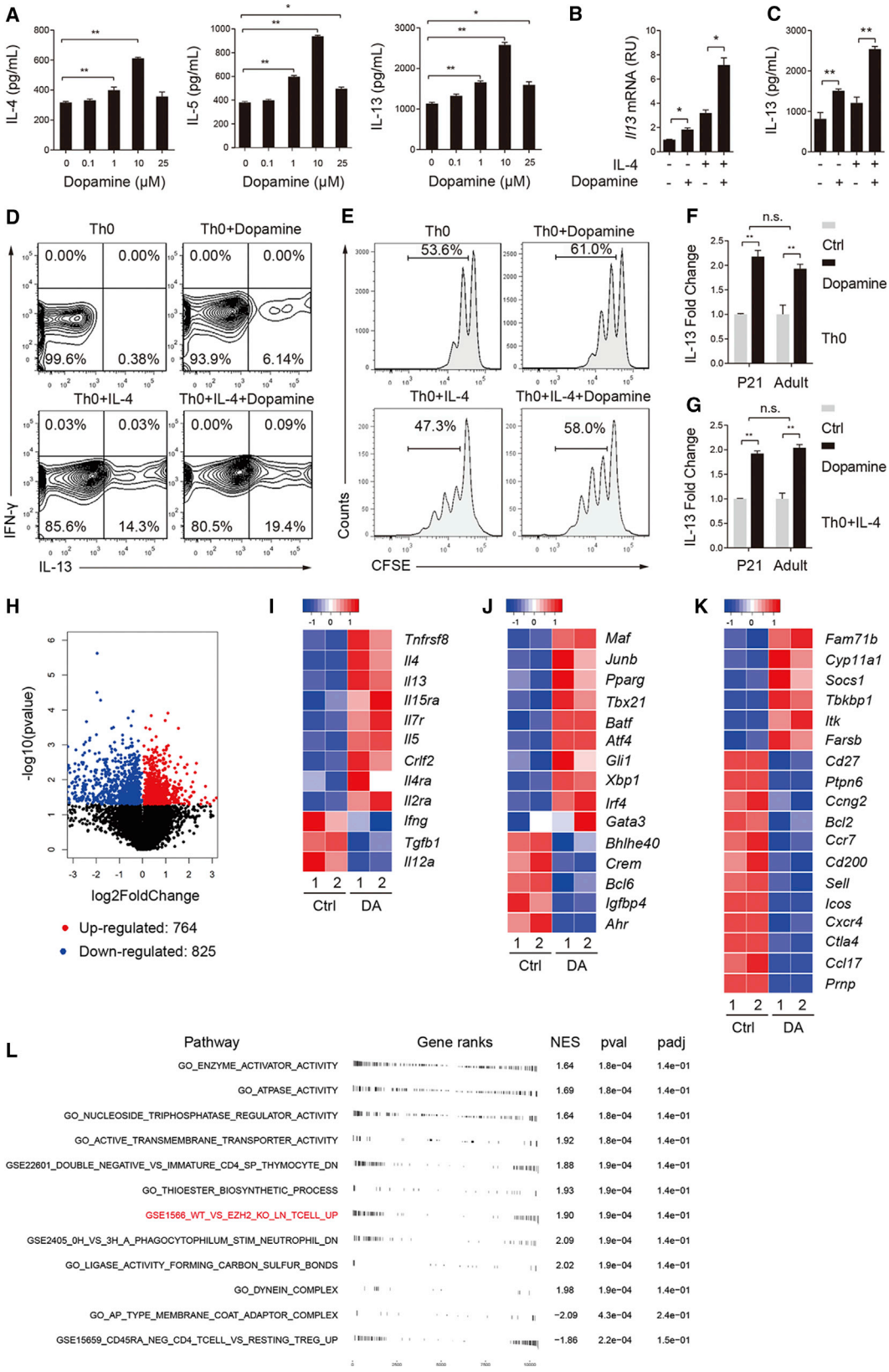

(legend on next page)

in immature and adult lungs. To control for variations caused by the size of the airway, we normalized the immunoreactivity of tyrosine hydroxylase to TUBB3. We found that the extent of tyrosine hydroxylase$^+$ innervation was a fold higher in P19 mice and children (0–13 years of age) compared with the adult counterparts (3–4 months of age in mice and 40–65 years of age in humans) (Figures 1E and 1G). In addition, lymph nodes associated with donor lungs had more abundant tyrosine hydroxylase but less DBH in children compared with adults, as shown by western blot and antibody staining (Figures 1I and S1A). Taken together, sympathetic nerves that innervate the lung and associated lymph nodes transition from a predominantly dopaminergic phenotype in early post-natal life to an adrenergic phenotype in adulthood. In accordance, the sympathetic nervous system in the adult lung is known to be mostly adrenergic (Felten et al., 1985).

Dopamine Promotes a Th2 Phenotype of Naive CD4$^+$ T Cells

We tested whether sympathetic nerves played an age-related role in inflammation by releasing dopamine in the early lung. Dopamine has been shown previously to induce Th2 cytokine expression *in vitro* (Huang et al., 2010; Nakano et al., 2009). To investigate the mechanism of dopamine signaling in Th2 cell differentiation, we isolated naive CD4$^+$ T cells from mouse spleen using a negative selection kit. Cells were stimulated with αCD3 and αCD28 alone (Th0) and in the presence of IL-4 (Th0+IL-4). Dopamine dose-dependently elevated the expression of IL-4, IL-5, and IL-13 in Th0 cultures (Figure 2A). In contrast, norepinephrine and epinephrine, two neurotransmitters that are enzymatically converted from dopamine, had no Th2-inducing activities (Figures S1E and S1F). The activity of dopamine peaked at 10 μM by doubling the amount of Th2 cytokines in Th0 and Th0+IL-4 cultures on day 4 (Figures 2A–2C and S1C) while repressing Th1 cytokines such as *Ifng* (Figure S1D). We thus used 10 μM dopamine for all *in vitro* studies. We noted that the extent of increase in *Il4* and IL-13 expression by dopamine+IL-4 was greater than single treatments combined (Figures 2B and 2C and S1C). In addition, dopamine induced the appearance of IL-13$^+$ cells in Th0 cultures (6.14%) and increased the percentage of IL-13$^+$ cells in Th0+IL-4 cultures from 14.3% to 19.4% (Figure 2D). Furthermore, dopamine promoted T cell proliferation by ~20% in both Th0 and Th0+IL-4 cultures (Figure 2E). Because of the effect of dopamine on cell proliferation, the total number of IL-13$^+$ cells in dopamine-treated Th0+IL-4 culture was slightly higher than the combined effect of single treatments. Taken together, dopamine promotes Th2 cell differentiation in synergy with IL-4.

To evaluate whether age affected T cell responses to dopamine, we compared IL-13 expression in dopamine-treated CD4$^+$ T cells isolated from neonatal and adult mice. We found no difference in the extent of IL-13 induction by dopamine between neonatal and adult cultures (Figures 2F and 2G). In addition, dopamine similarly elevated *Il13* expression in human CD4$^+$ T cells isolated from lymph nodes associated with donor lungs from children and adults (Figure S1G). Furthermore, after identifying DRD4 as the functional dopamine receptor on CD4$^+$ T cells (Figure 3), we showed that age had no effect on DRD4 expression (Figure S2C). Therefore, dopamine promotes Th2 cell differentiation independent of age.

Dopamine Promotes Th2 Cell Differentiation through a Global Transcriptional Program

To gain insights into the mechanism of dopamine signaling in Th2 cell differentiation, we performed RNA sequencing (RNA-seq) of day 4 Th0 cultures. Among a total of 1,589 differentially expressed genes with an adjusted $p < 0.05$ (Figure 2H), dopamine elevated the expression of Th2 cytokine genes such as *Il4*, *Il5*, and *Il13* while repressing Th1 cytokine genes such as *Ifng* and *Il12a* (Figure 2I). These findings were consistent with the results of qPCR and ELISA in culture (Figures 2A–2C, S1C, and S1D). Dopamine also increased the expression of receptor genes for IL-2 and IL-4 (Figure 2I), suggesting a feedforward mechanism for these two essential cytokines in Th2 differentiation. Furthermore, dopamine upregulated expression of the Th2-specifying gene *Gata3* as well as other transcriptional factors known to play a role in Th2 differentiation, including *Maf* and *Pparg* (Chen et al., 2017; Henriksson et al., 2019; Ho et al., 1998; Zheng and Flavell, 1997; Figure 2J). Genes involved in T cell activation during Th2 differentiation (Aki et al., 2018; Henriksson et al.,

Figure 2. Dopamine Promotes a Th2 Phenotype in Naive CD4$^+$ T Cell Cultures

Naive CD4$^+$ T cells isolated from mouse spleens were stimulated with αCD3 and αCD28 (Th0) and IL-4 (Th0+IL-4). Cultures were analyzed on day 4. Except for (A), all other cultures were treated with 10 μM dopamine.

(A) Production of IL-4, IL-5, and IL-13 by Th0 cultures treated with increasing concentrations of dopamine. Data represent mean ± SEM of 3 independent experiments.

(B and C) *Il13* mRNA (B) and protein expression (C) in cultures with and without dopamine and IL-4 (10 ng/mL). Data are representative of at least 5 independent experiments.

(D) Flow cytometry analyses of CD4$^+$ T cell cultures for IL-13 and IFN-γ expression. Data are representative of 2 independent experiments.

(E) Flow cytometry analyses of cell proliferation under each culture condition. Data are representative of 3 independent experiments.

(F and G) IL-13 production in dopamine-treated neonatal and adult cultures relative to the untreated baseline control. Data represent mean ± SEM from 3 independent experiments.

(H) Volcano plot of transcripts with fragments per kilobase (FPKM) > 1 in RNA-seq of Th0 cultures with and without dopamine. Red dots represent significantly upregulated genes, and blue dots represent significantly downregulated genes.

(I–K) Heatmaps of differential gene expression of cytokines and receptors (I), transcriptional factors (J), and other genes involved in T cell activation and Th2 differentiation (K). Each column represents one sample. Genes were ranked by fold change. All listed genes have an adjusted $p < 0.05$. DA, dopamine.

(L) Pathway analyses of gene set enrichment in dopamine-treated Th0 cultures. Pathways that had a false discovery rate (FDR) < 0.05 are shown. NES, normalized enrichment score (a positive score indicates gene set enrichment at the top of the ranked list or those that were upregulated by dopamine); pval, enriched p value; padj, Benjamini-Hochberg-adjusted p value set to < 0.25.

*$p < 0.05$ and **$p < 0.01$ by two-tailed Student's t test.

See also Figure S1.

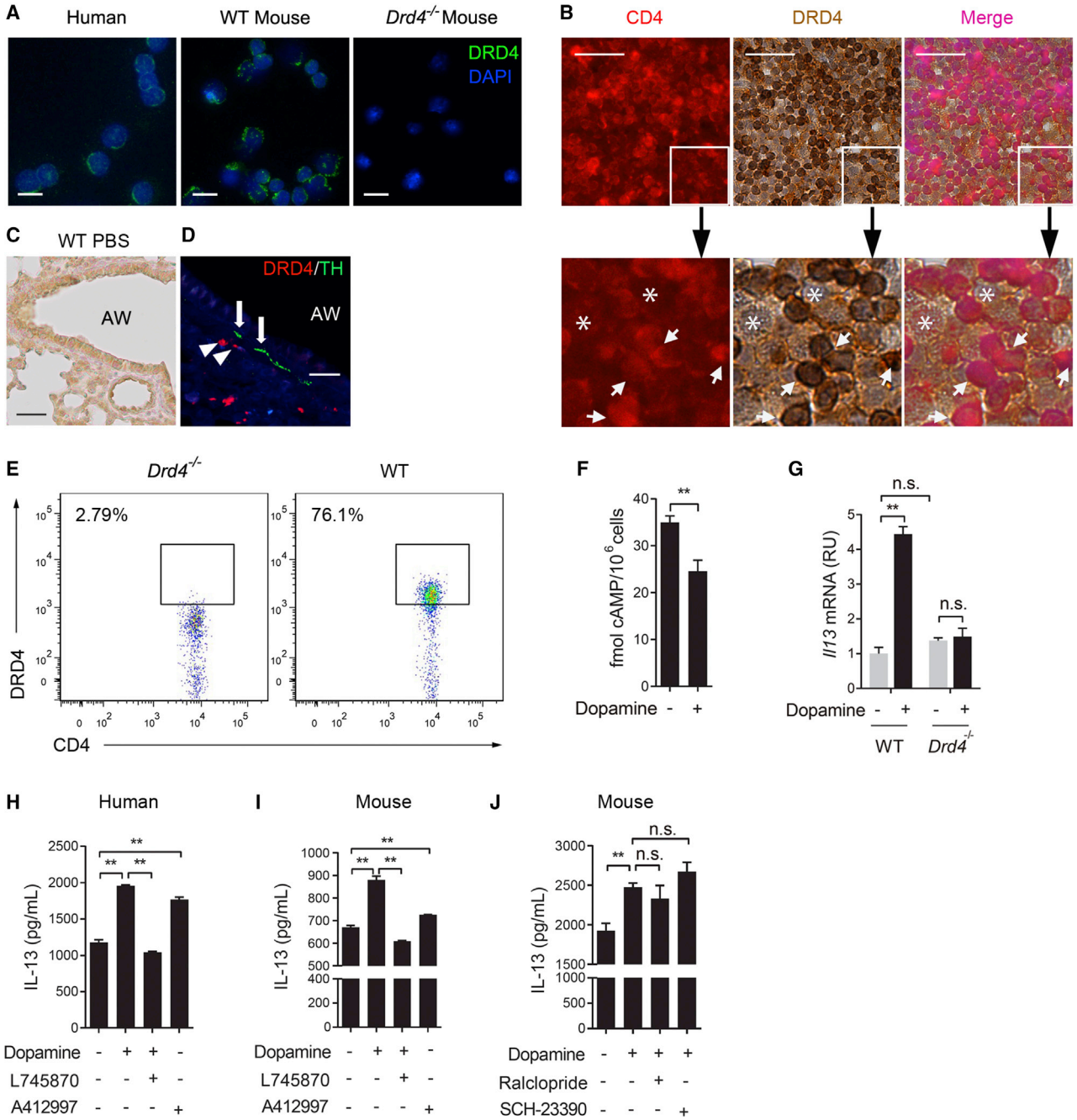

Figure 3. Dopamine Signals through a Major DRD4 Receptor on CD4$^+$ T Cells to Promote the Th2 Phenotype

(A) Staining for DRD4 in mouse and human CD4$^+$ T cell cultures. Nuclei were labeled with Hoechst dye.

(B) Double staining for CD4 and DRD4 using histological sections of lymph nodes associated with adult human donor lungs. The outlined area is enlarged in the bottom panel. Arrows mark CD4$^+$DRD4$^+$ cells. Asterisks mark cells that are double negative. Images show representative results of 3 donors.

(C) DRD4 staining of lung sections of P21 mice at baseline.

(D) Double staining for DRD4 and TH in P21 mouse lungs following OVA exposure. Arrowheads mark DRD4$^+$ cells, and arrows mark TH$^+$ nerves.

(A–D) Images are representative of the results of 3 independent experiments.

(E) Flow cytometry analyses of DRD4 expression in CD4$^+$ T cells in mouse lungs following allergen exposure at P21. Similar results were obtained in 2 independent experiments.

(F) The amount of intracellular cAMP in control and dopamine-treated Th0 cultures. Data represent mean ± SEM of 3 independent experiments.

(G) *Il13* mRNA expression in wild-type and *Drd4*$^{-/-}$ CD4$^+$ T cells with or without dopamine treatment. Data represent fold change relative to WT cultures at baseline of 3 independent experiments.

(H–J) IL-13 production by CD4$^+$ T cells of mouse (H) and human (I) in each treatment group (the DRD4 antagonist L-745870 [300 nM], the DRD4 agonist A412997 [100 nM], the DRD2/3 antagonist raclopride [50 nM], and the DRD1/5 antagonist SCH-23390 [50 nM]). (J) IL-13 production by mouse CD4$^+$ T cells in each

(legend continued on next page)

2019) were also changed by dopamine (Figure 2K). Notably, dopamine had no effect on expression of the *Il6*, *Il9*, *Il10*, and *Il17* genes. Therefore, dopamine signaling selectively promotes Th2 cytokine expression in naive CD4$^+$ T cells by activating a transcriptional program.

We generated a list of all genes detected in the samples ranked on the t-statistic followed by pathway analyses. We found that dopamine regulated energy consumption, ion channel activity, and cell cycle pathways (Figure 2L). These findings are consistent with the positive effect of dopamine on T cell proliferation (Figure 2E). We also found a significant overlap of differentially expressed genes between dopamine treatment and EZH2 deficiency in CD4$^+$ T cells (Figure 2L). EZH2 is a histone methyltransferase within Polycomb Repressive Complex 2 (PRC2). EZH2 enzymatically catalyzes histone 3 trimethylation at lysine 27 (H3K27me3) to induce epigenetic silencing of gene expression (Margueron and Reinberg, 2011). These findings suggest that epigenetic mechanisms may be involved in dopamine-induced Th2 cell differentiation.

DRD4 Is the Functional Dopamine Receptor on CD4$^+$ T Cells

Among the 5 dopamine receptor genes (*Drd1–Drd5*), qPCR of naive mouse CD4$^+$ T cells and RNA-seq of T cell cultures detected mRNA expression of *Drd1*, *Drd4*, and *Drd5*, and *Drd4* gene expression was the highest (Figure S2A). To confirm DRD4 expression by CD4$^+$ T cells, we stained the Th0 culture with a DRD4 antibody. The specificity of this DRD4 antibody was confirmed by negative staining of *Drd4*$^{-/-}$ CD4$^+$ T cells (Figures 3A and 3E). DRD4 was detected on the surface of CD4$^+$ T cells in culture from mice and humans (Figure 3A), and its expression was unchanged by T cell differentiation, age, and the location of CD4$^+$ T cells (in circulation or in tissue) (Figures S2B–S2D). A majority of CD4$^+$ T cells (97%) in human lymph nodes were DRD4$^+$ (Figure 3B).

DRD4 was not detected in the normal mouse lung by antibody staining, likely because of a low abundance of CD4$^+$ T cells at baseline (Figure 3C). However, following allergen exposure of neonatal mice, DRD4$^+$ cells appeared in close proximity to tyrosine hydroxylase$^+$ nerves around airways and blood vessels where immune cells were recruited into the lung (Figure 3D). To extensively characterize DRD4 expression in immune cells, we employed flow cytometry analyses. Because there is no commercially available flow antibody for DRD4, we used the DRD4 antibody for immunohistochemistry and included *Drd4*$^{-/-}$ cells as a negative control. CD4$^+$ T cells accounted for ~18% of all immune cell recruits following allergen exposure. DRD4 was expressed by a majority of the recruited CD4$^+$ T cells (76%) (Figure 3E). In contrast, other immune cells involved in type 2 inflammation, such as ILCs, B cells, mast cells, eosinophils, and antigen-presenting cells (macrophages and dendritic cells), had no detectable DRD4 expression (Figures S2A and S2E). Given a significant role of ILCs in type 2 inflammation, we evaluated the other four dopamine receptor genes and found no expression of any dopamine receptor genes in ILCs (Figure S2A). In accordance, dopamine had no effect on type 2 cytokine expression by ILCs or differentiated ILC2 cells in culture (Figures S2F–S2K). Last, ~20% of DRD4$^+$ cells were CD4$^-$, and these DRD4$^+$ CD4$^-$ cells likely included CD8$^+$ T cells (Figure S2E).

DRD4 belongs to the D2 receptor subfamily that blocks adenylate cyclase, whereas DRD1 and DRD5 are D1 receptors that activate adenylate cyclase (Beaulieu and Gainetdinov, 2011). Dopamine reduced the amount of intracellular cyclic AMP (cAMP) from 35 fmol to 23 fmol per one million CD4$^+$ T cells (Figure 3F), further supporting DRD4 being the major dopamine receptor.

To test whether DRD4 was required for dopamine-induced Th2 differentiation, we first compared the effect of dopamine on *Il13* mRNA expression in cultures from wild-type and *Drd4*$^{-/-}$ mice. Dopamine increased *Il13* gene expression in wild-type cells; however, it had no effect in *Drd4*$^{-/-}$ cells (Figure 3G). Notably, we found no baseline difference in *Il13* mRNA between wild-type and *Drd4*$^{-/-}$ cultures (Figure 3G). This finding is consistent with a lack of tyrosine hydroxylase expression by T cells (Figure 1J) and, hence, no baseline dopamine signaling. Second, a specific DRD4 antagonist, L745870 (300 nM; Patel et al., 1997), completely blocked the effect of dopamine on IL-13 expression in mouse and human CD4$^+$ T cells, whereas a DRD4-specific agonist, A412997 (100 nM; Moreland et al., 2005), increased IL-13 expression (Figures 3H and 3I). Third, SCH-23390 (50 nM, an inhibitor of DRD1/5; Hyttel, 1983), and raclopride (50 nM, an inhibitor of DRD2/3; Ogren et al., 1986), had no effect on dopamine-induced IL-13 expression (Figure 3J). These findings demonstrate that DRD4 is the functional receptor on CD4$^+$ T cells that mediates dopamine signaling in Th2 differentiation.

The Dopamine-DRD4 Pathway Promotes Th2 Cell Differentiation by Enhancing IL-2-STAT5 Signaling

Among the key regulators of Th2 cell differentiation, the expression of *Il2ra* is known to be repressed by cAMP (Anastassiou et al., 1992). Therefore, the dopamine-DRD4 pathway may increase the expression of IL-2Rα (also called CD25) by repressing cAMP production, promoting IL-2 signaling and Th2 differentiation. In support of this hypothesis, dopamine elevated *Il2ra* gene expression, as shown by RNA-seq (Figure 2I). Dopamine also increased CD4$^+$ T cell proliferation (Figure 2E), consistent with an enhanced, proliferative role of IL-2.

To test whether dopamine upregulated IL-2Rα expression and signaling by reducing cAMP production, we compared CD4$^+$ T cell cultures treated with dopamine alone and in combination with forskolin (Fsk, 1 μM), an agonist of adenylate cyclase. Fsk completely prevented dopamine-induced increases in *Il2ra* gene expression and the percentage of CD25$^+$CD4$^+$ T cells in both Th0 and Th0+IL-4 cultures (Figures 4A, 4B, S3A, and S3E). Consistent with increased IL-2Rα expression, dopamine significantly elevated the signaling activity of IL-2, as shown by increased STAT5 phosphorylation (p-STAT5) in Th0+IL-4

treatment group (the DRD2/3 antagonist raclopride [50 nM] and the DRD1/5 antagonist SCH-23390 [50 nM]). Data represent mean ± SEM of 3 independent experiments.

**$p < 0.01$ by two-tailed Student's t test. n.s., not significant. Scale bars, 10 μm in (A) and 50 μm in (B)–(D).

See also Figures S2 and S3.

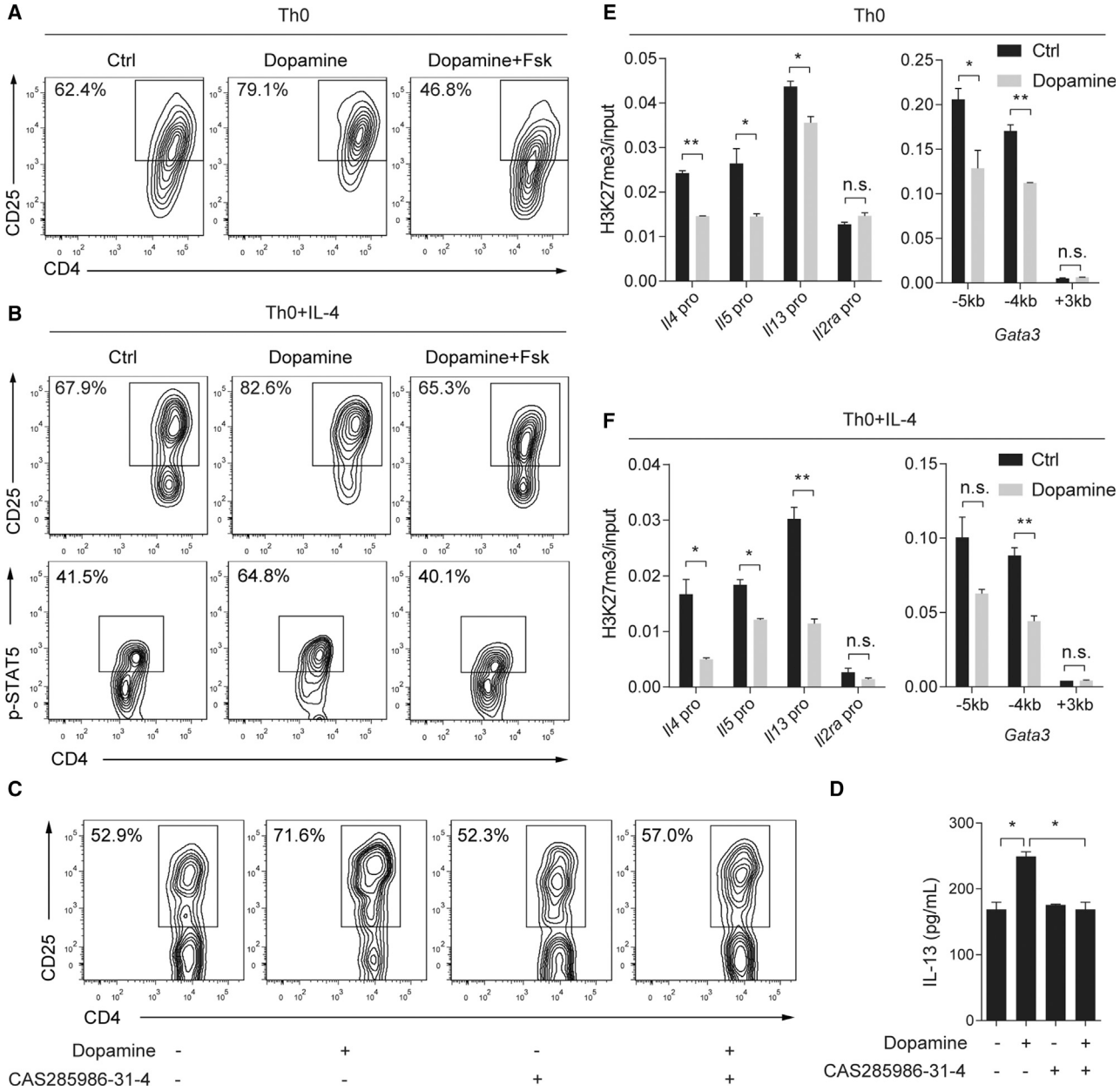

Figure 4. Dopamine Promotes Th2 Differentiation by Upregulating IL-2 Signaling and Reducing H3K27me3 at Th2 Gene Loci

(A) Flow cytometry analyses of IL-2Rα (also called CD25) in Th0 cultures treated with dopamine alone and in combination with forskolin (Fsk; 1 μM). Similar results were obtained in 3 independent experiments.

(B) Flow cytometry analyses of CD25 and p-STAT5 in Th0+IL-4 cultures of each treatment group. Similar results were obtained in 5 independent experiments.

(C) Flow cytometry analyses of CD25 expression in day 2 Th0 cultures following treatment with dopamine and a STAT5-specific inhibitor, CAS285986-31-4 (20 μM). Data are representative of 3 independent experiments.

(D) IL-13 production in day 2 Th0 cultures in each treatment group, measured by ELISA.

(E and F) The relative amount of H3K27me3 at the promoters of *Il4*, *Il5*, *Il13*, *Il2ra*, and *Gata3* genes in Th0 and Th0+IL-4 cultures by quantitative ChIP analyses. Bar graphs (D–F) represent mean ± SEM of three independent experiments. *$p < 0.05$, **$p < 0.01$ by two-tailed Student's t test.

See also Figure S3.

cultures (Figures 4B and S3I). However, the amount of p-STAT5 was reduced almost to baseline by Fsk (Figures 4B and S3I). We then tested whether elevated IL-2 signaling by dopamine was required for the increase in Th2 cytokine expression. For this assay, we treated Th0 cultures with a specific STAT5 inhibitor, CAS285986-31-4 (Müller et al., 2008). To diminish the side effect of the inhibitor on cell survival, we tested different concentrations of the inhibitor and the duration of treatment. The STAT5 inhibitor at 20 μM had no detectable effect on cell growth and baseline expression of CD25 and IL-13 in day 2 cultures (Figures 4C,

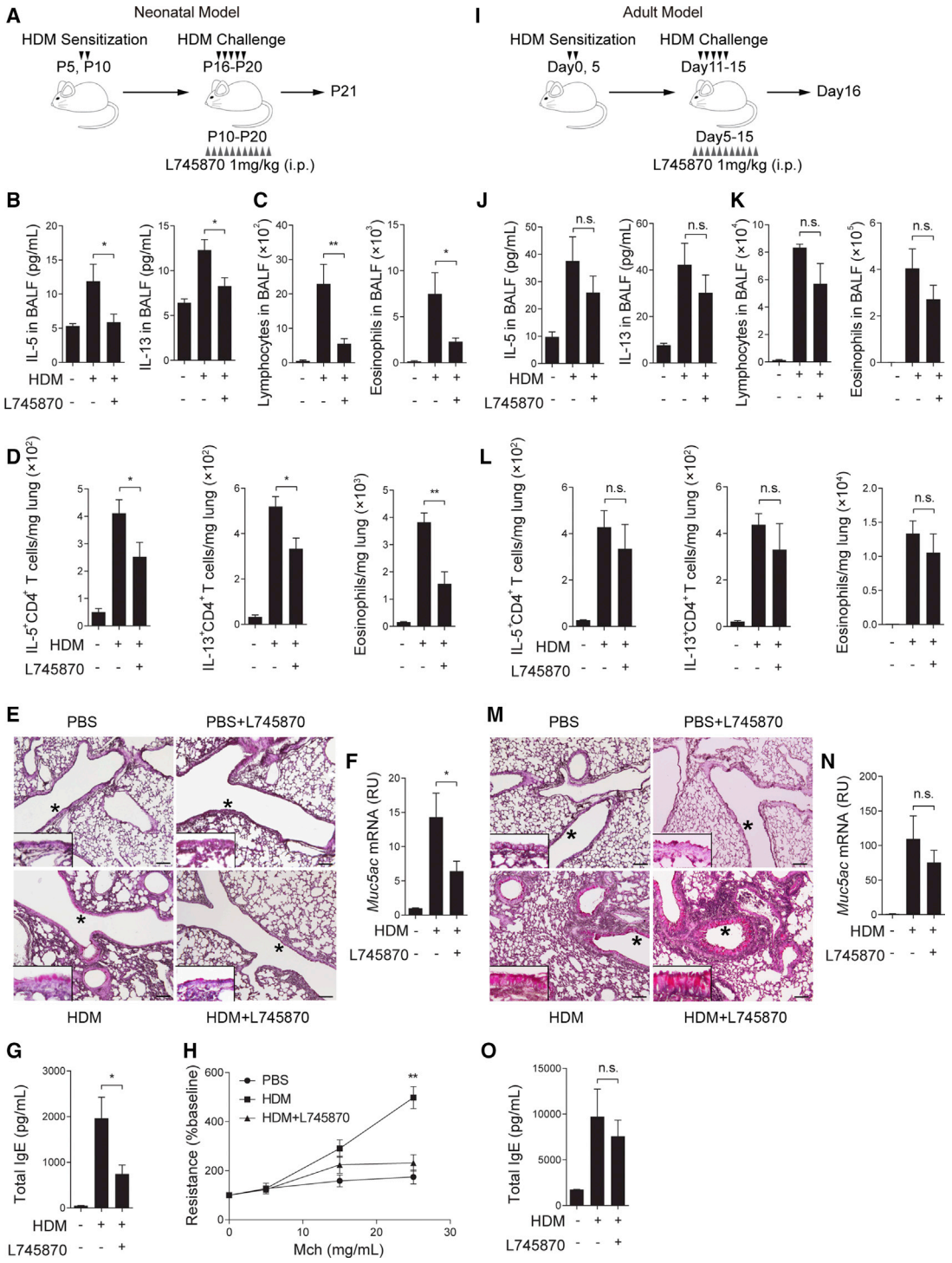

Figure 5. The Dopamine-DRD4 Pathway Plays a Significant Role in Th2 Inflammation in Neonatal Mice

(A and I) Schemes of HDM allergen sensitization and challenge with L745870 treatment in neonatal mice (A) and adult mice (I). Mice were analyzed 1 day after the last challenge.

(B and J) The amounts of IL-5 and IL-13 in BALF of neonatal and adult mice in each group. N = 12 from 3 independent experiments in (B) and N = 5 from 2 independent experiments in (J).

(C and K) The abundance of lymphocytes and eosinophils in BALF of neonatal and adult mice. N = 12 from 3 independent experiments in (C) and N = 5 from 2 independent experiments in (K).

(D and L) The abundance of IL-5$^+$ and IL-13$^+$ CD4$^+$ T cells and eosinophils in the lungs of neonatal and adult mice. Data were normalized to the lung weight. N = 8 from 2 independent experiments in (D) and N = 5 from 2 independent experiments in (L).

(legend continued on next page)

4D, S3J, and S3K); however, the STAT5 inhibitor abolished induction of CD25 and IL-13 expression by dopamine (Figures 4C, 4D, S3J, and S3K). Last, to link cAMP production and Th2 cytokine gene regulation in the dopamine-DRD4 pathway, we analyzed IL-13 and *Il4* expression in Th0 and Th0+IL-4 cultures that were treated with dopamine alone or dopamine+Fsk. The combined treatment diminished the increase in IL-13 and *Il4* expression in dopamine-treated cultures (Figures S3B–S3D and S3F–S3H). Therefore, the dopamine-DRD4 pathway blocks cAMP production to upregulate IL-2Rα expression, elevating IL-2 signaling activities to promote Th2 differentiation.

Dopamine Transcriptionally Upregulates Th2 Genes with an Associated Reduction in H3K27me3 at These Th2 Gene Loci

Pathway analysis of RNA-seq data suggested that dopamine signaling in $CD4^+$ T cells may involve epigenetic mechanisms by counteracting the activity of EZH2 (Figure 2L). EZH2 is known to bind directly to the promoters of Th2 genes such as *Gata3*, *Il4*, *Il5*, and *Il13* and repress gene transcription by causing H3K27me3 (Tumes et al., 2013). To test whether dopamine reduced H3K27me3 at the Th2 gene loci, we performed chromatin immunoprecipitation (ChIP) with a specific H3K27me3 antibody, followed by qPCR using primers flanking the established EZH2-binding sites within the promoter of the Th2 genes (Tumes et al., 2013). Compared with the untreated control, dopamine reduced H3K27me3 at the promoters of the *Il4*, *Il5*, and *Il13* genes in Th0 and Th0+IL-4 cultures (Figures 4E and 4F). For the *Gata3* promoter, dopamine decreased H3K27me3 at the −5 kb and −4 kb sites but not at the +3 kb site (Figures 4E and 4F). In contrast, dopamine had no effect on H3K27me3 in the promoter of *Il2ra*, a gene that exhibited little EZH2 binding (Tumes et al., 2013; Figures 4E and 4F). Taken together, dopamine signaling decreases epigenetic silencing of selected Th2 genes, which may facilitate Th2 cell differentiation.

To test whether dopamine opposed EZH2 to mediate epigenetic modification, we showed that dopamine reduced the expression of *Ezh2* and 3 regulatory subunit genes within PRC2, *Eed*, *Jarid2*, and *Aebp2* (Figure S3L). In addition, blockade of EZH2 activity with a specific inhibitor, 3-deazaneplanocin A (DZNep), promoted Th2 cytokine expression similarly as dopamine (Figures S3M and S3N; Tumes et al., 2013). Importantly, DZNep blunted the effect of dopamine on *Il4* and *Il13* gene expression in culture (Figures S3M and S3N). As a control for the functional specificity of DZNep, we showed that DZNep had no effect on the *Il2ra* gene with or without dopamine (Figure S3O). These findings support that dopamine-induced Th2 differentiation involves epigenetic regulation at key Th2 gene loci by repressing EZH2 and other components within PRC2.

The Dopamine-DRD4 Pathway Plays a Critical, Augmenting Role in Th2 Inflammation Following Allergen Exposure in Neonatal Mice but Not in Adult Mice

The dopaminergic-to-adrenergic transition of the sympathetic nervous system during post-natal development was associated with more dopamine in the early lung than the adult lung (Figure 1). We reasoned that, if dopamine served as an age-related neural signal to augment Th2 cell differentiation, then blockade of dopamine-DRD4 signaling would preferentially ameliorate Th2 inflammation in early life. To test this hypothesis, we assessed the effect of DRD4 inhibition on Th2 inflammation in neonatal and adult mice following exposure to house dust mites (HDMs) or ovalbumin (OVA) (Figures 5 and S4–S6). To block DRD4, we employed a specific DRD4 inhibitor (L745870) and *Drd4*$^{-/-}$ mice. Notably, *Drd4*$^{-/-}$ mice have no previously reported phenotypes except for addictive behavior (Rubinstein et al., 1997). Consistently, no baseline lung phenotype was found in L745870-treated mice and *Drd4*$^{-/-}$ mice without allergen exposure (PBS condition) (Figures 5E, 5M, S5C–S5I, and S5S).

Neonatal mice were sensitized and challenged intranasally with HDMs and treated with L745870 between P10 and P20 (Figure 5A), a time period when tyrosine hydroxylase expression increased sharply in the lung (Figure 1A). Because of technical issues with neonatal intranasal delivery that often causes variations in efficacy, we chose to deliver L745870 by intraperitoneal injection. At P21, compared with solvent, L745870 reduced the amount of IL-5 and IL-13 (Figure 5B) and diminished the abundance of lymphocytes and eosinophils in bronchoalveolar lavage fluid (BALF) (Figure 5C). L745870 also significantly decreased the number of IL-5- and IL-13-expressing $CD4^+$ T cells and eosinophils in the lung (Figures 5D and S4A). In addition, L745870 decreased HDM-induced mucus overproduction and the amount of total immunoglobulin E (IgE) in serum and ameliorated airway hyperresponsiveness to methacholine (Figures 5E–5H). Furthermore, L745870 improved pathological scores in the HDM-exposed lungs, as assayed by the thickness of airway epithelium and peri-vascular nuclear density (Figures S4B and S4C). Last, similar to L745870 treatment, genetic disruption of DRD4 reduced Th2 inflammation in neonatal mice following HDM exposure (Figures S4D–S4F).

We assessed the effect of L745870 in the adult HDM mouse model (Figure 5I). The dosage of HDMs was adjusted to the body weight of adult mice. Adult mice that were treated with L745870 for the same duration as neonates exhibited no significant difference in Th2 inflammation compared with solvent treatment (Figures 5J–5O and S4G–S4I).

As a complementary model of allergic inflammation, we subjected neonatal and adult mice to OVA sensitization and

(E and M) Representative image of periodic acid–Schiff (PAS) staining in lung sections of neonatal and adult mice. The epithelial areas marked by asterisks are enlarged and shown in the insets. Scale bars, 100 μm.

(F and N) Mucus production in neonatal and adult lungs, assayed by *Muc5ac* qPCR. N = 12 from 3 independent experiments in (F) and N = 5 in 2 independent experiments in (N).

(G and O) The amount of total IgE in serum from neonatal and adult mice. N = 12 from 3 independent experiments in (G) and N = 5 from 2 independent experiments in (O).

(H) Airway resistance in neonatal mice of each group relative to the baseline. N = 4–5 in 2 independent experiments.

**$p < 0.01$ by one-way ANOVA followed by Tukey's post-hoc test in (H). For all other panels, *$p < 0.05$, **$p < 0.01$ by two-tailed Student's t test.

See also Figures S4–S6.

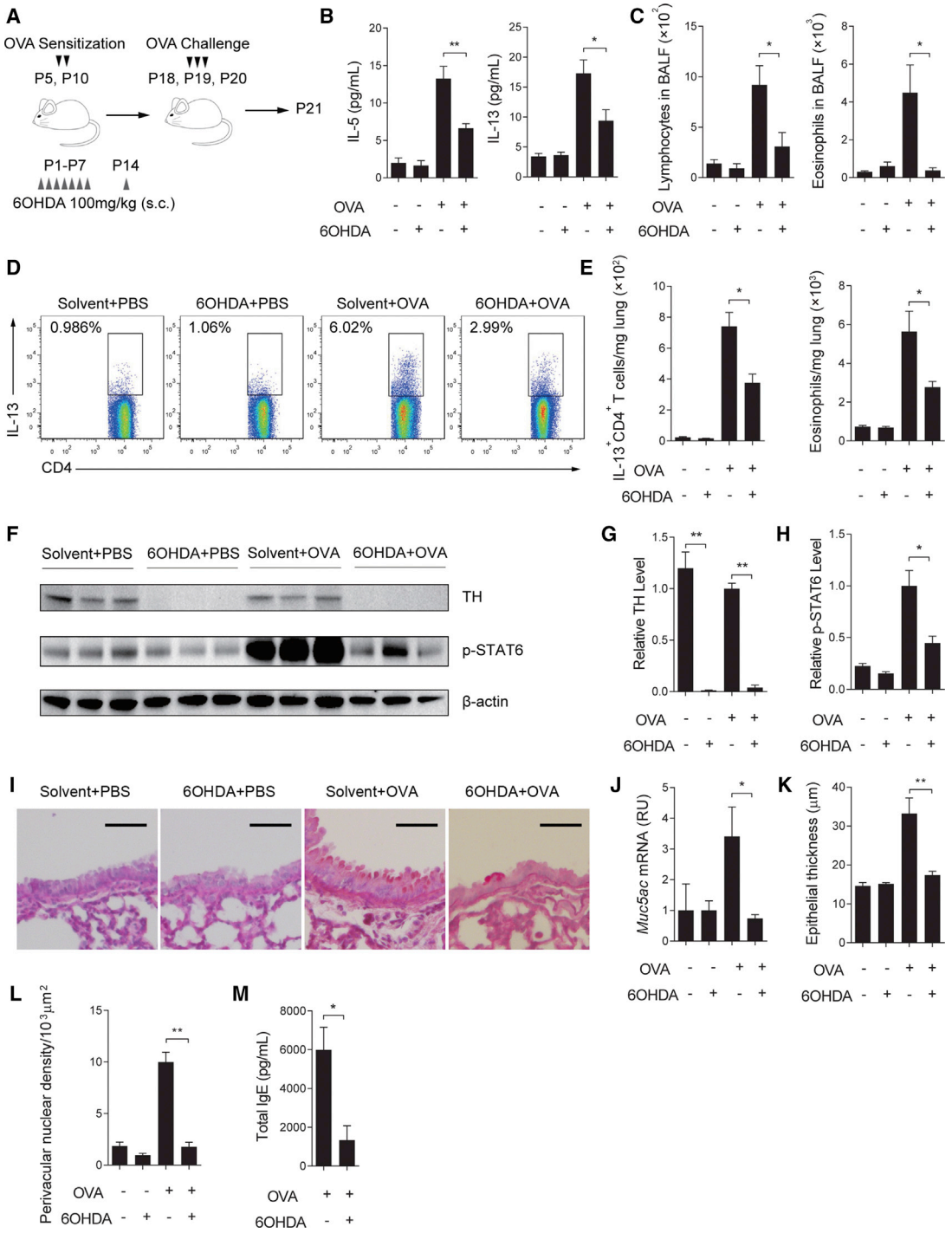

Figure 6. Ablation of Dopaminergic Nerves Ameliorates Allergic Inflammation in Young Mice

(A) Scheme of 6OHDA treatment during OVA sensitization and challenge in neonatal mice. Mice were analyzed 1 day after the last challenge at P21.

(B) The amount of IL-5 and IL-13 in BALF in each group. N = 5–7 from 2 independent experiments.

(C) Quantification of lymphocytes and eosinophils in BALF at P21. N = 5–7 from 2 independent experiments.

(D) Flow cytometry analyses of IL-13$^+$CD4$^+$ T cells in the lungs in each group. Similar results were obtained from 2 independent experiments.

(E) The abundance of IL-13$^+$CD4$^+$ T cells and eosinophils in the lungs in each group. Data were normalized to the lung weight. N = 5–7 in 2 independent experiments.

(F) Western blot analyses of relative expression of tyrosine hydroxylase (TH) and phosphorylated STAT6 (p-STAT6) in the lung of each group. β-actin was loading control. Each lane represents one sample.

(G and H) Quantification of the relative level of TH (G) and p-STAT6 (H) based on western blot. N = 5–7 in 2 independent experiments.

(legend continued on next page)

challenge (Figures S5 and S6). We showed that L745870 treatment and DRD4 deficiency profoundly reduced Th2 inflammation, airway hypercontractility, and mucus overproduction following OVA exposure in neonates while having a marginal effect in adult mice (Figures S5 and S6). Taken together, the dopamine-DRD4 pathway plays an age-related role in augmenting Th2 inflammation in early life.

Allergen exposure had no effect on the age-related reduction in expression of tyrosine hydroxylase (Figure S5B) and neonatal DBH expression (Figure S5M). In accordance, the amount of dopamine remained unchanged in allergen-exposed mouse lungs at P21 (898.2 ± 95.57 pg/mg lung weight [OVA] versus 961.9 ± 66.72 pg/mg lung weight [PBS]). However, DBH expression in the adult lung was elevated by allergen exposure (Figure S5M). This was associated with a decrease in the already lower amount of dopamine (229.4 ± 73.08 pg/mg lung weight [OVA] versus 494.0 ± 114.7 pg/mg lung weight [PBS]). Therefore, allergen exposure potentiates the age-related difference in dopamine.

Dopamine in the Lungs Is a Critical, Age-Related Regulator of Th2 Inflammation

To provide further evidence that the age-related role of dopamine-DRD4 signaling in allergic inflammation was determined by the amount of dopamine, we assessed the effect of dopaminergic neuron ablation on Th2 inflammation in neonates following allergen exposure. For this assay, mice were treated with 6-hydroxydopamine (6OHDA), a specific neurotoxin for dopaminergic neurons during the first 2 weeks after birth (Angeletti and Levi-Montalcini, 1972; Figure 6A). 6OHDA diminished tyrosine hydroxylase$^+$ nerves in the lung at P21 (Figures 6F and 6G). 6OHDA treatment had no detectable effect on inflammation at baseline (Figures 6B–6L). However, following OVA exposure, mice treated with 6OHDA exhibited a significant reduction in IL-5 and IL-13 (Figure 6B) and the abundance of lymphocytes and eosinophils in the BALF (Figure 6C). 6OHDA also reduced the abundance of IL-13$^+$CD4$^+$ T cells and eosinophils in the lungs (Figures 6D and 6E), the amount of p-STAT6 (Figures 6F and 6H), mucus overproduction (Figures 6I and 6J), and the amount of total IgE in serum (Figures 6M). Furthermore, 6OHDA improved pathological scores in OVA-exposed lungs, as measured by airway epithelial thickness and perivascular nuclear density (Figures 6K and 6L).

6OHDA has a broad effect on the sympathetic nervous system. To alleviate the concern of side effects of 6OHDA, we took a complementary gain-of-function approach by treating adult mice with a specific DRD4 agonist, A412997 (Moreland et al., 2005), to offset the low dopamine activity in the adult lung (Figure S7A). DRD4 activation alone was insufficient to induce inflammation (Figure S7B). Following OVA exposure, the DRD4 agonist substantially worsened Th2 inflammation and mucus overproduction in adult mice (Figures S7C–S7G). Taken together, the amount of dopamine is a critical regulator of Th2 inflammation in the lung.

CD4$^+$ T Cells Mediate Dopamine-DRD4 Signaling in Early Life to Augment Th2 Inflammation

To establish that CD4$^+$ T cells were the critical mediator of dopamine-DRD4 signaling in the early lung, we performed an adoptive transfer assay using CD4$^+$ T cells isolated from OT-II mice. OT-II mice express a transgenic T cell receptor for OVA. OVA sensitization of OT-II mice stimulated T cell activation and proliferation (Church et al., 2012; Kim et al., 2018), as evident by a 3-fold increase in the number of splenic CD4$^+$ T cells with a significant, activated CD44^{high}CD62L^{low} subpopulation (~25%). Because age had no effect on the T cell response to dopamine (Figures 2F, 2G, S1G), we isolated CD4$^+$ T cells from 5-week-old OT-II mice for the adoptive transfer assay because the spleen at this age is fully grown and contains more CD4$^+$ T cells than the neonatal spleen. Purified splenic CD4$^+$ T cells from OVA-sensitized OT-II mice were intratracheally transferred into wild-type and *Drd4*$^{-/-}$ recipients at P14, followed by OVA challenge (Figure 7A). Because the recipients were not sensitized, OVA challenge induced allergic inflammation only through the transferred OT-II cells. At P21, wild-type and *Drd4*$^{-/-}$ recipients exhibited comparable Th2 inflammation, as assayed by the amount of IL-5 and IL-13 and the number of eosinophils in BALF (Figures 7B and 7C), infiltrating IL-13$^+$CD4$^+$ T cells and eosinophils in the lungs (Figures 7D and 7E), the amount of p-STAT6 (Figures 7F and 7G), mucus overproduction (Figures 7H and 7I), and pathological scores (Figure 7J). These findings indicate that adoptively transferred CD4$^+$ T cells from OVA-sensitized OT-II mice are sufficient to induce allergic inflammation in neonates independent of the genotype of the recipient.

After validating the adoptive transfer approach in neonatal allergic inflammation, we went on to evaluate the contribution of the transferred OT-II cells and the recipient to dopamine-augmented allergic inflammation. For this assay, we treated wild-type and *Drd4*$^{-/-}$ recipient mice with the DRD4 inhibitor L745870 immediately after adoptive transfer at P14 (Figure 7A). We reasoned if cells from recipient mice played a role in DRD4 regulation of allergic inflammation, then L745870 treatment would have a greater inhibitory effect on wild-type littermates than on *Drd4*$^{-/-}$ mice. However, we found that L745870 treatment similarly reduced Th2 inflammation regardless of the recipient genotype, as shown by immunological assays of Th2 inflammation, mucus overproduction, and pathological scores (Figures 7B–7J). Therefore, transferred CD4$^+$ T cells from OVA-sensitized OT-II mice primarily mediate dopamine-DRD4 signaling in the early lung to augment Th2 inflammation. These findings, together with selective expression of DRD4 in CD4$^+$ T cells, but not ILCs and other immune cells involved in type 2 inflammation (Figures 3A, 3B, S2A, and S2E), provide strong evidence that CD4$^+$ T cells

(I and J) Mucus overproduction in the lung of each group assayed by PAS staining (I) and qPCR (J). N = 5 from 2 independent experiments. Scale bars, 100 μm.
(K and L) Pathological assays of epithelial thickness (K) and perivascular nuclear density (L). Data represent mean ± SEM of 3 non-overlapping histological areas in each mouse; 3–5 mice in each group from 2 independent experiments.
(M) The amount of total IgE in serum from each group. N = 5–7 in 2 independent experiments.
*$p < 0.05$ and **$p < 0.01$ by two-tailed Student's t test.
See also Figure S7.

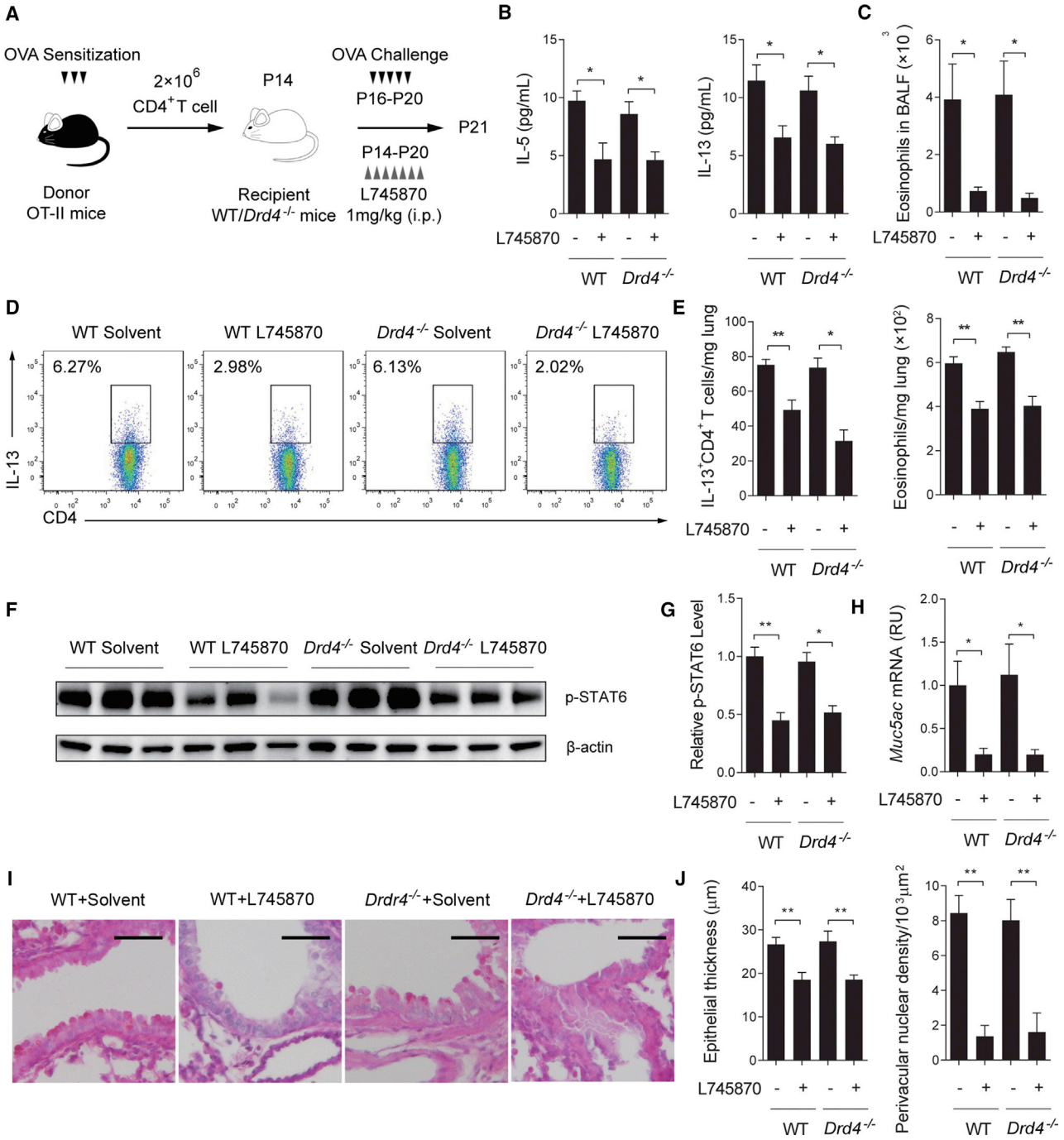

Figure 7. CD4+ T Cells Mediate Dopamine Signaling to Promote Th2 Inflammation in Neonatal Mice

(A) Scheme of adoptive transfer of CD4+ OT-II cells to recipient wild-type and *Drd4*$^{-/-}$ mice with and without L745870 treatment. CD4+ OT-II cells were isolated from OVA-sensitized donor mice at 5 weeks of age before adoptive transfer. The recipient mice were analyzed at P21.

(B) The amount of IL-5 and IL-13 in BALF of each group. N = 5–7 from 3 independent experiments.

(C) Quantification of eosinophils in BALF from each group. N = 5–7 in 3 independent experiments.

(D) Representative flow cytometry results of IL-13+CD4+ T cells in the lungs in each group. Similar results were obtained from 3 independent experiments.

(E) Relative abundance of IL-13+CD4+ T cells and eosinophils in the lungs. Data were normalized to the lung weight. N = 5–7 from 3 independent experiments.

(F and G) Western blot analysis of the amount of p-STAT6 in the lungs in each group. β-Actin was a loading control. Data were quantified in (G). N = 5–7 in 3 independent experiments.

(H and I) Mucus overproduction in the lung of each group assayed by PAS staining (H) and qPCR (I). N = 5–7 in 3 independent experiments. Scale bars, 100 μm.

(J) Pathological assays of epithelial thickness and perivascular nuclear density. Data represent mean ± SEM of 3 non-overlapping histological areas in each mouse; 5 mice in each group in 3 independent experiments.

*$p < 0.05$ and **$p < 0.01$ by two-tailed Student's t test.

are the critical mediator of dopamine signaling in the early lung to promote Th2 inflammation.

DISCUSSION

In this study, we discovered that the development of sympathetic innervation provides a critical mechanism underlying susceptibility to allergic asthma in early life. We show that sympathetic nerves are dopaminergic during post-natal development of the lung. By releasing dopamine, which induces Th2 cell differentiation, the immature sympathetic nervous system equips the early lung with a dopamine-enriched environment that fosters allergic inflammation. With age, sympathetic nerves mature into an adrenergic phenotype. Norepinephrine and epinephrine released from adrenergic nerves have no effect on Th2 cell differentiation activity, likely because of low adrenergic receptor expression, as shown by RNA-seq. Therefore, the dopaminergic-to-adrenergic transition of sympathetic innervation plays an age-related role in allergic inflammation. Our study identifies DRD4 as the functional receptor for dopamine in Th2 cell differentiation. DRD4 is selectively expressed by T cells but not ILCs. The differential expression of DRD4 in T cells and ILCs, together with previous findings showing that epinephrine negatively regulates ILC2 (Moriyama et al., 2018), highlights the complexity and specificity of neural regulation of type 2 inflammation.

We provide evidence that humans and mice exhibit a similar dopaminergic-to-adrenergic transition of sympathetic nerves during post-natal development of the airway. The conservation of this transition during evolution suggests that dopaminergic innervation may provide some advantage when the lung is immature and vulnerable to infection. One possibility is that, by facilitating type 2 inflammation, dopaminergic nerves endow the early lung with a mechanism of tissue repair following infection and eradication of parasitic worms. It is also possible that, in the context of the physiological role of norepinephrine in vasoconstriction of pulmonary vessels (Tuck, 1986), the dopaminergic phenotype in the early lung may support vascular development by preventing premature vascular constriction.

We show that the major source of dopamine is the nerves that innervate the airway and vasculature in the lung and lymphatic vessels in associated lymph nodes. Although the amount of dopamine released from the activated nerve is difficult to measure, the local concentration of dopamine can reach up to the range of hundreds of micromolar to millimolar upon firing of the nerve (Goto et al., 2007). Therefore, we speculate that the active, micromolar range of dopamine in Th2 cell differentiation may be physiologically relevant. In addition to direct communication between nerves and T cells, we cannot exclude the possibility that dopamine released by nerves may be transported through specific dopamine transporters or non-specifically taken up by immune cells, such as dendritic cells and macrophages. This possibility is supported by previous reports that dopamine can be detected in some immune cells by high-performance liquid chromatography (HPLC) without the evidence of tyrosine hydroxylase expression (Bergquist and Silberring, 1998; Cosentino et al., 2007; Josefsson et al., 1996; Nakano et al., 2009). In this scenario, dendritic cells may transport dopamine to T cells in the lymph node, where dendritic cells present allergen to initiate T cell differentiation, serving as an indirect means of neural regulation of Th2 cell differentiation through the dopamine-DRD4 pathway.

The expression and function of DRD4 in $CD4^+$ T cells is supported by previous studies of human samples (Kustrimovic et al., 2014; Sarkar et al., 2006). However, there are conflicting reports regarding dopamine receptor expression and signaling in T cells and mouse models. The conflict may be explained by the caveat of detection using non-qPCR assays of $CD4^+$ T cells (Contreras et al., 2016; Franz et al., 2015; Huang et al., 2010; Ilani et al., 2004). In addition, the inflammation defects in *Drd3*$^{-/-}$ mice may be unspecific to T cells (Contreras et al., 2016) because the cell type specificity of DRD3 expression is not well characterized. Furthermore, small-molecule dopamine receptor inhibitors may have off-target effects, which complicates the functional study of a specific dopamine receptor in inflammation. For example, a D1 receptor antagonist, SCH-23390, may also interfere with DRD4 (K_i = 1.1 μM; Bourne, 2001) at a concentration of 1 μM used in previous studies (Mori et al., 2013; Nakano et al., 2009).

Our results show that the dopamine-DRD4 pathway plays an augmenting role in Th2 cell differentiation by interacting with IL-2 and IL-4. We have provided evidence that the functional interaction between dopamine and IL-2 is mediated at least in part by the cAMP pathway. Considering a variety of signals in allergic inflammation that are known to upregulate cAMP production through commonly expressed receptors, the dopamine-DRD4 pathway uniquely represses cAMP production, thereby upregulating IL-2Rα expression. In addition, dopamine signaling is associated with reduced H3K27me3 in Th2 gene loci, an epigenetic mechanism that may facilitate Th2 gene transcription in synergy with IL-4. Based on the RNA-seq data, we speculate that the epigenetic mechanism may be mediated by the reduction in the expression of *Ezh2*, *Eed*, *Jarid2*, and *Aebp2*, the components of PRC2 that cause H3K27me3 to suppress gene transcription (Margueron and Reinberg, 2011). RNA-seq also showed that dopamine upregulated the expression of several transcriptional factors required for IL-4-induced Th2 cell differentiation, such as *c-Maf*, *Irf4*, *Xbp1*, and *Bhlhe40* (Henriksson et al., 2019), which may provide another mechanism underlying the synergic interaction between dopamine and IL-4. Whether changes in the expression of candidate epigenetic regulators and the transcriptional factors are regulated by the cAMP pathway warrants further investigation.

Previous clinical and basic studies showed that the immature immune system is poised toward type 2 inflammation (de Kleer et al., 2016; Hebel et al., 2014). Our study suggests that dopaminergic nerves in the early lung may potentiate an already type 2-poised immune system, contributing to the susceptibility to allergic asthma in early childhood (Stern et al., 2008). Importantly, our findings reveal the similarity of dopaminergic innervation of the early lung and the T cell response to dopamine between mice and humans. Identification of a dopamine-specific gene signature in Th2 cells will facilitate future study of dopamine regulation of allergic asthma in children. Based on RNA-seq data, several dopamine-regulated genes in mouse $CD4^+$ T cells have established disease relevance. For example, among the genes downregulated by dopamine, cAMP-responsive element modulator (CREM) has also been shown to exhibit reduced expression in $CD4^+$ T cells from children with recurrent

and persistent wheezing compared with healthy controls (Verjans et al., 2015). In addition, dopamine upregulates *Il2ra*, *Il7r*, and *Crlf2* (*Tlspr*), all of which have been identified to be associated with susceptibility to allergic asthma (Ferreira et al., 2017; Sherrill et al., 2010).

To understand the mechanism underlying the dopaminergic-to-adrenergic transition of sympathetic nerves in the developing lung, future studies are required to map the subset of sympathetic neurons that specifically supply the lung and to identify neurogenic signals required for development of these neurons. Neurons dynamically interact with target tissues during development. It is possible that the innervating sympathetic neurons may decrease the expression of tyrosine hydroxylase while upregulating DBH to fully differentiate into the adrenergic phenotype during post-natal maturation. Members of the neurotrophin family, such as nerve growth factor and brain-derived neurotrophic factor, have established roles in development of sympathetic neurons (Barbacid, 1994). We have shown that lung innervation requires neurotrophins (Aven et al., 2014; Patel et al., 2016; Radzikinas et al., 2011). Therefore, neurotrophins may regulate sympathetic innervation of the lung. Clinical studies have shown that the amounts of nerve growth factor and brain-derived neurotrophic factor are aberrantly regulated in infants following infection with respiratory syncytial virus (Tortorolo et al., 2005). In addition, brain-derived neurotrophic factor expression has been shown to be positively associated with the severity of allergic asthma (Watanabe et al., 2015). Identification of the neurotrophic factors that regulate the dopaminergic-to-adrenergic transition of sympathetic innervation may provide insights into the connection between respiratory viral infection in early life and allergic asthma.

In summary, our findings indicate that developing dopaminergic nerves in the airway contribute to susceptibility to allergic inflammation in early life. Targeting communication between sympathetic nerves and $CD4^+$ T cells via the dopamine-DRD4 pathway may be a strategy to battle the increasing prevalence of allergic asthma in children.

STAR★METHODS

Detailed methods are provided in the online version of this paper and include the following:

- KEY RESOURCES TABLE
- LEAD CONTACT AND MATERIALS AVAILABILITY
- EXPERIMENTAL MODELS AND SUBJECT DETAILS
  - Mice
  - Human donor lungs
- METHOD DETAILS
  - Neonatal and adult mouse models of allergic inflammation
  - Mouse primary lymphocyte preparation and culture
  - Primary human lymphocyte isolation and culture
  - Histology and antibody staining
  - Flow cytometry analysis of T cell cultures, BALF and lung samples
  - ILCs isolation and culture
  - Physiological measurements of airway reactivity
  - Cell proliferation assay
  - Quantitative Real Time PCR (qPCR)
  - Western Blot
  - ELISAs
  - RNA-seq analyses
  - Quantitative Chromatin precipitation (ChIP)-qPCR
- QUANTIFICATION AND STATISTICAL ANALYSIS
- DATA AND CODE AVAILABILITY

SUPPLEMENTAL INFORMATION

Supplemental Information can be found online at https://doi.org/10.1016/j.immuni.2019.10.002.

ACKNOWLEDGMENTS

We would like to thank Manuela Cernadas for technical guidance regarding flow cytometry analysis. For RNA-seq, library construction, sequencing, and differential expression analysis were performed at the Translational Genomics Core of Partners Personalized Medicine, a not-for-profit, fee-for-service core facility at Partners HealthCare (Boston, MA). This project was supported by NIH grants (R01HL132991 to X.A., K08HL135443 to Y.B., and F31HL126443 to J.B.).

AUTHOR CONTRIBUTIONS

W.W. and X.A. conceived the project. W.W., J.A.C., A.W., Y.B., and X.A. were involved in experimental design. W.W., J.A.C., A.W., F.S., and Y.B. performed most experiments and compiled data. K.G.T., J.B., N.K., M.R.J., V.K.K., and A.F. helped with experiments and data analysis. All authors participated in analyzing the data and writing or editing the paper.

DECLARATION OF INTERESTS

The authors declare no competing interests.

Received: May 7, 2019
Revised: August 28, 2019
Accepted: October 7, 2019
Published: November 19, 2019

REFERENCES

Aki, D., Li, H., Zhang, W., Zheng, M., Elly, C., Lee, J.H., Zou, W., and Liu, Y.C. (2018). The E3 ligases Itch and WWP2 cooperate to limit T_H2 differentiation by enhancing signaling through the TCR. Nat. Immunol. *19*, 766–775.

Anastassiou, E.D., Paliogianni, F., Balow, J.P., Yamada, H., and Boumpas, D.T. (1992). Prostaglandin E2 and other cyclic AMP-elevating agents modulate IL-2 and IL-2R alpha gene expression at multiple levels. J. Immunol. *148*, 2845–2852.

Anders, S., Pyl, P.T., and Huber, W. (2015). HTSeq–a Python framework to work with high-throughput sequencing data. Bioinformatics *31*, 166–169.

Angeletti, P.U., and Levi-Montalcini, R. (1972). Growth inhibition of sympathetic cells by some adrenergic blocking agents (6-hydroxydopamine-mice and rats-immunosympathectomy-chemical sympathectomy-superior cervical ganglion). Proc. Natl. Acad. Sci. USA *69*, 86–88.

Aven, L., and Ai, X. (2013). Mechanisms of respiratory innervation during embryonic development. Organogenesis *9*, 194–198.

Aven, L., Paez-Cortez, J., Achey, R., Krishnan, R., Ram-Mohan, S., Cruikshank, W.W., Fine, A., and Ai, X. (2014). An NT4/TrkB-dependent increase in innervation links early-life allergen exposure to persistent airway hyperreactivity. FASEB J. *28*, 897–907.

Barbacid, M. (1994). The Trk family of neurotrophin receptors. J. Neurobiol. *25*, 1386–1403.

Barrios, J., Patel, K.R., Aven, L., Achey, R., Minns, M.S., Lee, Y., Trinkaus-Randall, V.E., and Ai, X. (2017). Early life allergen-induced mucus overproduction requires augmented neural stimulation of pulmonary neuroendocrine cell secretion. FASEB J. *31*, 4117–4128.

Beaulieu, J.M., and Gainetdinov, R.R. (2011). The physiology, signaling, and pharmacology of dopamine receptors. Pharmacol. Rev. *63*, 182–217.

Becerra-Díaz, M., Wills-Karp, M., and Heller, N.M. (2017). New perspectives on the regulation of type II inflammation in asthma. F1000Res. *6*, 1014.

Bergquist, J., and Silberring, J. (1998). Identification of catecholamines in the immune system by electrospray ionization mass spectrometry. Rapid Commun. Mass Spectrom. *12*, 683–688.

Borovikova, L.V., Ivanova, S., Zhang, M., Yang, H., Botchkina, G.I., Watkins, L.R., Wang, H., Abumrad, N., Eaton, J.W., and Tracey, K.J. (2000). Vagus nerve stimulation attenuates the systemic inflammatory response to endotoxin. Nature *405*, 458–462.

Bourne, J.A. (2001). SCH 23390: the first selective dopamine D1-like receptor antagonist. CNS Drug Rev. *7*, 399–414.

Buttari, B., Profumo, E., Domenici, G., Tagliani, A., Ippoliti, F., Bonini, S., Businaro, R., Elenkov, I., and Riganò, R. (2014). Neuropeptide Y induces potent migration of human immature dendritic cells and promotes a Th2 polarization. FASEB J. *28*, 3038–3049.

Cardoso, V., Chesné, J., Ribeiro, H., García-Cassani, B., Carvalho, T., Bouchery, T., Shah, K., Barbosa-Morais, N.L., Harris, N., and Veiga-Fernandes, H. (2017). Neuronal regulation of type 2 innate lymphoid cells via neuromedin U. Nature *549*, 277–281.

Chavan, S.S., Pavlov, V.A., and Tracey, K.J. (2017). Mechanisms and Therapeutic Relevance of Neuro-immune Communication. Immunity *46*, 927–942.

Chen, T., Tibbitt, C.A., Feng, X., Stark, J.M., Rohrbeck, L., Rausch, L., Sedimbi, S.K., Karlsson, M.C.I., Lambrecht, B.N., Karlsson Hedestam, G.B., et al. (2017). PPAR-γ promotes type 2 immune responses in allergy and nematode infection. Sci. Immunol. *2*, eaal5196.

Church, R.J., Jania, L.A., and Koller, B.H. (2012). Prostaglandin E(2) produced by the lung augments the effector phase of allergic inflammation. J. Immunol. *188*, 4093–4102.

Cohen, L., e, X., Tarsi, J., Ramkumar, T., Horiuchi, T.K., Cochran, R., DeMartino, S., Schechtman, K.B., Hussain, I., Holtzman, M.J., and Castro, M.; NHLBI Severe Asthma Research Program (SARP) (2007). Epithelial cell proliferation contributes to airway remodeling in severe asthma. Am. J. Respir. Crit. Care Med. *176*, 138–145.

Contreras, F., Prado, C., González, H., Franz, D., Osorio-Barrios, F., Osorio, F., Ugalde, V., Lopez, E., Elgueta, D., Figueroa, A., et al. (2016). Dopamine Receptor D3 Signaling on CD4+ T Cells Favors Th1- and Th17-Mediated Immunity. J. Immunol. *196*, 4143–4149.

Cosentino, M., Fietta, A.M., Ferrari, M., Rasini, E., Bombelli, R., Carcano, E., Saporiti, F., Meloni, F., Marino, F., and Lecchini, S. (2007). Human CD4+CD25+ regulatory T cells selectively express tyrosine hydroxylase and contain endogenous catecholamines subserving an autocrine/paracrine inhibitory functional loop. Blood *109*, 632–642.

Cote-Sierra, J., Foucras, G., Guo, L., Chiodetti, L., Young, H.A., Hu-Li, J., Zhu, J., and Paul, W.E. (2004). Interleukin 2 plays a central role in Th2 differentiation. Proc. Natl. Acad. Sci. USA *101*, 3880–3885.

de Kleer, I.M., Kool, M., de Bruijn, M.J., Willart, M., van Moorleghem, J., Schuijs, M.J., Plantinga, M., Beyaert, R., Hams, E., Fallon, P.G., et al. (2016). Perinatal Activation of the Interleukin-33 Pathway Promotes Type 2 Immunity in the Developing Lung. Immunity *45*, 1285–1298.

Dettman, E.J., Simko, S.J., Ayanga, B., Carofino, B.L., Margolin, J.F., Morse, H.C., 3rd, and Justice, M.J. (2011). Prdm14 initiates lymphoblastic leukemia after expanding a population of cells resembling common lymphoid progenitors. Oncogene *30*, 2859–2873.

Fahy, J.V. (2015). Type 2 inflammation in asthma–present in most, absent in many. Nat. Rev. Immunol. *15*, 57–65.

Felten, D.L., Felten, S.Y., Carlson, S.L., Olschowka, J.A., and Livnat, S. (1985). Noradrenergic and peptidergic innervation of lymphoid tissue. J. Immunol. *135* (2, Suppl), 755s–765s.

Ferreira, M.A., Vonk, J.M., Baurecht, H., Marenholz, I., Tian, C., Hoffman, J.D., Helmer, Q., Tillander, A., Ullemar, V., van Dongen, J., et al.; 23andMe Research Team; AAGC collaborators; BIOS consortium; LifeLines Cohort Study (2017). Shared genetic origin of asthma, hay fever and eczema elucidates allergic disease biology. Nat. Genet. *49*, 1752–1757.

Flierl, M.A., Rittirsch, D., Nadeau, B.A., Chen, A.J., Sarma, J.V., Zetoune, F.S., McGuire, S.R., List, R.P., Day, D.E., Hoesel, L.M., et al. (2007). Phagocyte-derived catecholamines enhance acute inflammatory injury. Nature *449*, 721–725.

Franz, D., Contreras, F., González, H., Prado, C., Elgueta, D., Figueroa, C., and Pacheco, R. (2015). Dopamine receptors D3 and D5 regulate CD4(+)T-cell activation and differentiation by modulating ERK activation and cAMP production. J. Neuroimmunol. *284*, 18–29.

Goto, Y., Otani, S., and Grace, A.A. (2007). The Yin and Yang of dopamine release: a new perspective. Neuropharmacology *53*, 583–587.

Hebel, K., Weinert, S., Kuropka, B., Knolle, J., Kosak, B., Jorch, G., Arens, C., Krause, E., Braun-Dullaeus, R.C., and Brunner-Weinzierl, M.C. (2014). CD4+ T cells from human neonates and infants are poised spontaneously to run a nonclassical IL-4 program. J. Immunol. *192*, 5160–5170.

Henriksson, J., Chen, X., Gomes, T., Ullah, U., Meyer, K.B., Miragaia, R., Duddy, G., Pramanik, J., Yusa, K., Lahesmaa, R., and Teichmann, S.A. (2019). Genome-wide CRISPR Screens in T Helper Cells Reveal Pervasive Crosstalk between Activation and Differentiation. Cell *176*, 882–896.e18.

Ho, I.C., Lo, D., and Glimcher, L.H. (1998). c-maf promotes T helper cell type 2 (Th2) and attenuates Th1 differentiation by both interleukin 4-dependent and -independent mechanisms. J. Exp. Med. *188*, 1859–1866.

Huang, Y., Qiu, A.W., Peng, Y.P., Liu, Y., Huang, H.W., and Qiu, Y.H. (2010). Roles of dopamine receptor subtypes in mediating modulation of T lymphocyte function. Neuroendocrinol. Lett. *31*, 782–791.

Hyttel, J. (1983). SCH 23390 - the first selective dopamine D-1 antagonist. Eur. J. Pharmacol. *91*, 153–154.

Ilani, T., Strous, R.D., and Fuchs, S. (2004). Dopaminergic regulation of immune cells via D3 dopamine receptor: a pathway mediated by activated T cells. FASEB J. *18*, 1600–1602.

Josefsson, E., Bergquist, J., Ekman, R., and Tarkowski, A. (1996). Catecholamines are synthesized by mouse lymphocytes and regulate function of these cells by induction of apoptosis. Immunology *88*, 140–146.

Kim, M.N., Hong, J.Y., Shim, D.H., Sol, I.S., Kim, Y.S., Lee, J.H., Kim, K.W., Lee, J.M., and Sohn, M.H. (2018). Activated Leukocyte Cell Adhesion Molecule Stimulates the T-Cell Response in Allergic Asthma. Am. J. Respir. Crit. Care Med. *197*, 994–1008.

Klose, C.S.N., Mahlakõiv, T., Moeller, J.B., Rankin, L.C., Flamar, A.L., Kabata, H., Monticelli, L.A., Moriyama, S., Putzel, G.G., Rakhilin, N., et al. (2017). The neuropeptide neuromedin U stimulates innate lymphoid cells and type 2 inflammation. Nature *549*, 282–286.

Kustrimovic, N., Rasini, E., Legnaro, M., Marino, F., and Cosentino, M. (2014). Expression of dopaminergic receptors on human CD4+ T lymphocytes: flow cytometric analysis of naive and memory subsets and relevance for the neuroimmunology of neurodegenerative disease. J. Neuroimmune Pharmacol. *9*, 302–312.

Le Gros, G., Ben-Sasson, S.Z., Seder, R., Finkelman, F.D., and Paul, W.E. (1990). Generation of interleukin 4 (IL-4)-producing cells in vivo and in vitro: IL-2 and IL-4 are required for in vitro generation of IL-4-producing cells. J. Exp. Med. *172*, 921–929.

Margueron, R., and Reinberg, D. (2011). The Polycomb complex PRC2 and its mark in life. Nature *469*, 343–349.

Moreland, R.B., Patel, M., Hsieh, G.C., Wetter, J.M., Marsh, K., and Brioni, J.D. (2005). A-412997 is a selective dopamine D4 receptor agonist in rats. Pharmacol. Biochem. Behav. *82*, 140–147.

Mori, T., Kabashima, K., Fukamachi, S., Kuroda, E., Sakabe, J., Kobayashi, M., Nakajima, S., Nakano, K., Tanaka, Y., Matsushita, S., et al. (2013). D1-like dopamine receptors antagonist inhibits cutaneous immune reactions mediated by Th2 and mast cells. J. Dermatol. Sci. *71*, 37–44.

Moriyama, S., Brestoff, J.R., Flamar, A.L., Moeller, J.B., Klose, C.S.N., Rankin, L.C., Yudanin, N.A., Monticelli, L.A., Putzel, G.G., Rodewald, H.R., and Artis, D. (2018). β_2-adrenergic receptor-mediated negative regulation of group 2 innate lymphoid cell responses. Science *359*, 1056–1061.

Müller, J., Sperl, B., Reindl, W., Kiessling, A., and Berg, T. (2008). Discovery of chromone-based inhibitors of the transcription factor STAT5. ChemBioChem *9*, 723–727.

Nakano, K., Higashi, T., Takagi, R., Hashimoto, K., Tanaka, Y., and Matsushita, S. (2009). Dopamine released by dendritic cells polarizes Th2 differentiation. Int. Immunol. *21*, 645–654.

Ogren, S.O., Hall, H., Köhler, C., Magnusson, O., and Sjöstrand, S.E. (1986). The selective dopamine D2 receptor antagonist raclopride discriminates between dopamine-mediated motor functions. Psychopharmacology (Berl.) *90*, 287–294.

Ohtake, J., Kaneumi, S., Tanino, M., Kishikawa, T., Terada, S., Sumida, K., Masuko, K., Ohno, Y., Kita, T., Iwabuchi, S., et al. (2015). Neuropeptide signaling through neurokinin-1 and neurokinin-2 receptors augments antigen presentation by human dendritic cells. J. Allergy Clin. Immunol. *136*, 1690–1694.

Papa, I., Saliba, D., Ponzoni, M., Bustamante, S., Canete, P.F., Gonzalez-Figueroa, P., McNamara, H.A., Valvo, S., Grimbaldeston, M., Sweet, R.A., et al. (2017). T_{FH}-derived dopamine accelerates productive synapses in germinal centres. Nature *547*, 318–323.

Patel, K.R., Aven, L., Shao, F., Krishnamoorthy, N., Duvall, M.G., Levy, B.D., and Ai, X. (2016). Mast cell-derived neurotrophin 4 mediates allergen-induced airway hyperinnervation in early life. Mucosal Immunol. *9*, 1466–1476.

Patel, S., Freedman, S., Chapman, K.L., Emms, F., Fletcher, A.E., Knowles, M., Marwood, R., Mcallister, G., Myers, J., Curtis, N., et al. (1997). Biological profile of L-745,870, a selective antagonist with high affinity for the dopamine D4 receptor. J. Pharmacol. Exp. Ther. *283*, 636–647.

Radzikinas, K., Aven, L., Jiang, Z., Tran, T., Paez-Cortez, J., Boppidi, K., Lu, J., Fine, A., and Ai, X. (2011). A Shh/miR-206/BDNF cascade coordinates innervation and formation of airway smooth muscle. J. Neurosci. *31*, 15407–15415.

Rubinstein, M., Phillips, T.J., Bunzow, J.R., Falzone, T.L., Dziewczapolski, G., Zhang, G., Fang, Y., Larson, J.L., McDougall, J.A., Chester, J.A., et al. (1997). Mice lacking dopamine D4 receptors are supersensitive to ethanol, cocaine, and methamphetamine. Cell *90*, 991–1001.

Sarkar, C., Das, S., Chakroborty, D., Chowdhury, U.R., Basu, B., Dasgupta, P.S., and Basu, S. (2006). Cutting Edge: Stimulation of dopamine D4 receptors induce T cell quiescence by up-regulating Kruppel-like factor-2 expression through inhibition of ERK1/ERK2 phosphorylation. J. Immunol. *177*, 7525–7529.

Sherrill, J.D., Gao, P.S., Stucke, E.M., Blanchard, C., Collins, M.H., Putnam, P.E., Franciosi, J.P., Kushner, J.P., Abonia, J.P., Assa'ad, A.H., et al. (2010). Variants of thymic stromal lymphopoietin and its receptor associate with eosinophilic esophagitis. J. Allergy Clin. Immunol. *126*, 160–165.e3.

Stern, D.A., Morgan, W.J., Halonen, M., Wright, A.L., and Martinez, F.D. (2008). Wheezing and bronchial hyper-responsiveness in early childhood as predictors of newly diagnosed asthma in early adulthood: a longitudinal birth-cohort study. Lancet *372*, 1058–1064.

Talbot, S., Abdulnour, R.E., Burkett, P.R., Lee, S., Cronin, S.J., Pascal, M.A., Laedermann, C., Foster, S.L., Tran, J.V., Lai, N., et al. (2015). Silencing Nociceptor Neurons Reduces Allergic Airway Inflammation. Neuron *87*, 341–354.

Tortorolo, L., Langer, A., Polidori, G., Vento, G., Stampachiacchere, B., Aloe, L., and Piedimonte, G. (2005). Neurotrophin overexpression in lower airways of infants with respiratory syncytial virus infection. Am. J. Respir. Crit. Care Med. *172*, 233–237.

Tuck, M.L. (1986). The sympathetic nervous system in essential hypertension. Am. Heart J. *112*, 877–886.

Tumes, D.J., Onodera, A., Suzuki, A., Shinoda, K., Endo, Y., Iwamura, C., Hosokawa, H., Koseki, H., Tokoyoda, K., Suzuki, Y., et al. (2013). The polycomb protein Ezh2 regulates differentiation and plasticity of CD4(+) T helper type 1 and type 2 cells. Immunity *39*, 819–832.

Van Dyken, S.J., Nussbaum, J.C., Lee, J., Molofsky, A.B., Liang, H.E., Pollack, J.L., Gate, R.E., Haliburton, G.E., Ye, C.J., Marson, A., et al. (2016). A tissue checkpoint regulates type 2 immunity. Nat. Immunol. *17*, 1381–1387.

Verjans, E., Ohl, K., Reiss, L.K., van Wijk, F., Toncheva, A.A., Wiener, A., Yu, Y., Rieg, A.D., Gaertner, V.D., Roth, J., et al. (2015). The cAMP response element modulator (CREM) regulates TH2 mediated inflammation. Oncotarget *6*, 38538–38551.

Wang, H., Yu, M., Ochani, M., Amella, C.A., Tanovic, M., Susarla, S., Li, J.H., Wang, H., Yang, H., Ulloa, L., et al. (2003). Nicotinic acetylcholine receptor alpha7 subunit is an essential regulator of inflammation. Nature *421*, 384–388.

Watanabe, T., Fajt, M.L., Trudeau, J.B., Voraphani, N., Hu, H., Zhou, X., Holguin, F., and Wenzel, S.E. (2015). Brain-Derived Neurotrophic Factor Expression in Asthma. Association with Severity and Type 2 Inflammatory Processes. Am. J. Respir. Cell Mol. Biol. *53*, 844–852.

Zheng, W., and Flavell, R.A. (1997). The transcription factor GATA-3 is necessary and sufficient for Th2 cytokine gene expression in CD4 T cells. Cell *89*, 587–596.

Zhu, J., Cote-Sierra, J., Guo, L., and Paul, W.E. (2003). Stat5 activation plays a critical role in Th2 differentiation. Immunity *19*, 739–748.

STAR★METHODS

KEY RESOURCES TABLE

REAGENT or RESOURCE	SOURCE	IDENTIFIER
Antibodies		
Mouse monoclonal anti-Stat5 (Y694), FITC, clone SRBCZX	eBioscience	Cat#11-9010-41; RRID: AB_2572520
Rat monoclonal anti-MHC II, FITC, clone M5/114.15.2	eBioscience	Cat#11-5321-82; RRID: AB_465232
Armenian hamster monoclonal anti-CD3e, FITC, clone 145-2C11	eBioscience	Cat#11-0031-82; RRID: AB_464882
Rat monoclonal anti-CD62L, FITC, clone MEL-14	eBioscience	Cat#12-0621-81; RRID: AB_465720
Rat monoclonal anti-CD45, FITC, clone 30-F11	eBioscience	Cat#11-0451-82; RRID: AB_465050
Rat monoclonal anti-CD25, Alexa Fluor® 488, clone eBio3C7 (3C7)	eBioscience	Cat#53-0253-82; RRID: AB_763471
Rat monoclonal anti-CD8a, PE, clone 53-6.7	eBioscience	Cat#12-0081-83; RRID: AB_465531
Rat monoclonal anti-IL-5, PE, clone TRFK5	eBioscience	Cat#12-7052-81; RRID: AB_763588
Rat monoclonal anti-IL-13, PE, clone eBio13A	eBioscience	Cat#12-7133-41; RRID: AB_10852712
Mouse monoclonal anti-NK1.1, PE, clone PK136	eBioscience	Cat#12-5941-81; RRID: AB_466049
Rat monoclonal anti-MHC II, PE, clone M5/114.15.2	eBioscience	Cat#12-5321-81; RRID: AB_465927
Rat monoclonal anti-CD4, APC, clone RM4-5	eBioscience	Cat#17-0042-82; RRID: AB_469323
Rat monoclonal anti-CD44, APC, clone IM7	eBioscience	Cat#17-0441-81; RRID: AB_469389
Armenian hamster monoclonal anti-CD11c, APC, clone N418	eBioscience	Cat#17-0114-81; RRID: AB_469345
Rat monoclonal anti-CD11b, PE-Cy7, clone M1/70	eBioscience	Cat#25-0112-82; RRID: AB_469588
Mouse monoclonal anti-CD3, clone OKT3	eBioscience	Cat#16-0037-85; RRID:AB_468855
Armenian hamster monoclonal anti-FceR1α, PE-Cy7, clone MAR-1	eBioscience	Cat#25-5898-80; RRID: AB_2573492
Rat monoclonal anti-CD45, PE-Cy7, clone 30-F11	BioLegend	Cat#103114; RRID: AB_312979
Armenian hamster monoclonal anti-CD3e, APC-Cy7, clone 145-2C11	BioLegend	Cat#100329; RRID: AB_1877171
Rat monoclonal anti-CD19, APC, clone 6D5	BioLegend	Cat#115511; RRID: AB_313646
Rat monoclonal anti-Ly6G, APC, clone 1A8	BioLegend	Cat#127613; RRID: AB_1877163
Mouse monoclonal anti-CD45.2, APC-Cy7, clone 104	BioLegend	Cat#109823; RRID: AB_830788
Rat monoclonal anti-CD4, PE-Cy7, clone GK1.5	BioLegend	Cat#100421; RRID: AB_312706
Rat monoclonal anti-CD11b, APC, clone M1/70	Millipore	Cat# MABF520
Rat monoclonal anti-IFN-γ, FITC, clone XMG1.2	BD Biosciences	Cat#562019; RRID: AB_10893998
Mouse monoclonal anti-Siglec-F, PE, clone E50-2440	BD Biosciences	Cat#562068; RRID: AB_10896143
Rat monoclonal anti-Siglec-F, APC-Cy7, clone E50-2440	BD Biosciences	Cat#565527; RRID: AB_2732831
Rat monoclonal anti-c-Kit, PE, clone ACK45	BD Biosciences	Cat#553869; RRID: AB_395103
Armenian hamster monoclonal anti-CD3e, clone 145-2C11	BD Biosciences	Cat#553058; RRID:AB_394591
Armenian hamster monoclonal anti-CD28, clone 37.51	BD Biosciences	Cat#553295; RRID:AB_394764
Mouse monoclonal anti-CD28, clone CD28.2	BD Biosciences	Cat# 555725; RRID:AB_396068
Mouse monoclonal anti-Stat6 (pY641), clone J71-773.58.11	BD Biosciences	Cat#558241; RRID:AB_647299
Mouse monoclonal anti-DRD4, clone 2B9	Millipore	Cat#MABN125; RRID: AB_10917077
Rabbit polyclonal anti-tyrosine hydroxylase	Millipore	Cat#AB152; RRID: AB_390204
Rabbit polyclonal anti-dopamine beta hydroxylase	Millipore	Cat#AB1585; RRID: AB_90805
Rabbit polyclonal anti-trimethyl-Histone H3 (Lys27)	Millipore	Cat#07-449; RRID:AB_310624

(*Continued on next page*)

Continued

REAGENT or RESOURCE	SOURCE	IDENTIFIER
Mouse monoclonal anti-neural class III beta-tubulin, Clone Tuj1	R&D Systems	Cat#MAB1195; RRID: AB_357520
Rabbit polyclonal anti-CD4	Novus	Cat#NBP1-19371SS; RRID: AB_10011114
Rabbit polyclonal anti-vesicular acetylcholine transporter	Abcam	Cat#ab68986; RRID:AB_1143827
Rabbit polyclonal anti-DRD4	Sigma-Aldrich	Cat#SAB4500672; RRID: AB_10743979
Rabbit polyclonal anti-calcitonin gene related peptide	Sigma-Aldrich	Cat#C8198; RRID:AB_259091
Mouse monoclonal anti-β-actin	Sigma-Aldrich	Cat#A5441; RRID:AB_476744
Goat polyclonal anti-rabbit, HRP	Santa Cruz Biotechnology	Cat#sc-2004; RRID:AB_631746
Goat polyclonal anti-mouse, HRP	BD Biosciences	Cat#554002; RRID:AB_395198
Biological Samples		
Human donor lungs	International Institute for the Advancement of Medicine	https://www.iiam.org/
Chemicals, Peptides, and Recombinant Proteins		
OVA	Sigma-Aldrich	Cat#A5503
Dispase II	Sigma-Aldrich	Cat#4942078001
Red blood cell lysis buffer	Sigma-Aldrich	Cat#R7757
L-745,870 hydrochloride	Sigma-Aldrich	Cat#L131
Raclopride	Sigma-Aldrich	Cat#R121
SCH-23390 hydrochloride	Sigma-Aldrich	Cat#D054
A-412997 dihydrochloride	Sigma-Aldrich	Cat#SML0608
CAS285986-31-4	Sigma-Aldrich	Cat#573108
Epinephrine	Sigma-Aldrich	Cat#E4250
Norepinephrine	Sigma-Aldrich	Cat#A7257
Methacholine	Sigma-Aldrich	Cat#A2251
Imject alum	Thermo Fisher	Cat#77161
Dopamine	Thermo Fisher	Cat#35-485-0
RIPA buffer	Thermo Fisher	Cat#PI89900
Pierce Protein A/G Agarose	Thermo Fisher	Cat# 20421
Salmon sperm DNA	Thermo Fisher	Cat#15632011
DZNep	EMD Millipore	Cat# 252790-2MG
Forskolin	Tocris	Cat#1099
6-Hydroxydopamine hydrobromide	Tocris	Cat#2547
Collagenase Type 4	Worthington-Biochem	Cat#LS004188
DNase I	NEB	Cat#439807
cOmpleteproteinase inhibitor cocktail	Roche	Cat#11697498001
Proteinase K	Roche	Cat#14164600
RNase A	QIAGEN	Cat#1031301
Fixable Viability Dye eFluor 520	eBioscience	Cat#65-0867-18
Fixable Viability Dye eFluor 780	eBioscience	Cat#65-0865-14
Cell Stimulation Cocktail (plus protein transport inhibitors)	eBioscience	Cat#00-4975-03
Fixation/permeabilization solution	BD Biosciences	Cat#554722
Perm/Wash solution	BD Biosciences	Cat#554723
Murine IL-4	BioLegend	Cat#574302
Murine IL-2	R&D Systems	Cat#402-ML-010
Murine IL-12	R&D Systems	Cat#419-ML-010
Murine IL-6	R&D Systems	Cat#406-ML-005
Murine IL-23	R&D Systems	Cat#1887-ML-010
Human IL-4	R&D Systems	Cat#204-IL-010
Human IL-2	R&D Systems	Cat#202-IL-010

(*Continued on next page*)

Continued

REAGENT or RESOURCE	SOURCE	IDENTIFIER
Human TGF-β	R&D Systems	Cat#240-B-002
HDM	Greer Laboratories	Cat#XPB70D3A25
Critical Commercial Assays		
Naive $CD4^+$ T cells isolation kit, mouse	Miltenyi Biotec	Cat#130-104-453
Naive $CD4^+$ T cells isolation kit, human	Miltenyi Biotec	Cat#130-094-131
$CD4^+$ T cells isolation kit, mouse	Miltenyi Biotec	Cat#130-104-454
CD90.2 MicroBeads, mouse	Miltenyi Biotec	Cat#130-049-101
LS columns	Miltenyi Biotec	Cat#130-042-401
Lympholyte®-Mammal Cell Separation Media	Cedarlane®	Cat#CL5115
Mouse on Mouse Kit	Vector Laboratories	Cat#BMK-2202
Hematoxylin QS	Vector Laboratories	Cat#H-3404
Standard ABC kit	Vector Laboratories	Cat#PK-6100
DAB Peroxidase Substrate Kit	Vector Laboratories	Cat# SK-4100
PAS Staining Kit	Sigma-Aldrich	Cat#395B-1KT
IgE Ready-SET-Go! ELISA set	eBioscience	Cat#88-50460-88
IL-4 Ready-Set-Go! ELISA set	eBioscience	Cat#88-7044-86
IL-5 Ready-Set-Go! ELISA set	eBioscience	Cat#88-7054-88
IL-13 Ready-Set-Go! ELISA set	eBioscience	Cat#88-7137-76
Norepinephrine ELISA Kit	Abnova	Cat#89-028-610
Dopamine ELISA kit	Abnova	Cat#89-028-620
cAMP XP® Assay Kit	Cell signaling	Cat#4339S
Mouse OVA Specific IgE ELISA Kit	BioLegend	Cat#439807
CFSE Cell Division Tracker Kit	BioLegend	Cat#423801
RNeasy kit	QIAGEN	Cat#74106
Superscript III Reverse Transcriptase Kit	Thermo Fisher	Cat#18080-044
PicoPure RNA isolation kit	Thermo Fisher	Cat#KIT0204
SuperScript IV VILO Master Mix	Thermo Fisher	Cat#11756050
SuperSignal West Pico PLUS Chemiluminescent Substrate	Thermo Fisher	Cat#34577
Deposited Data		
Raw and analyzed data	This paper	GEO: GSE137968
Full genome sequences for *Mus musculus* (UCSC version mm10)	UCSC	https://genome.ucsc.edu/cgi-bin/hgGateway?db=mm10
Experimental Models: Organisms/Strains		
Mouse: *Drd4*$^{-/-}$: B6.129P2-Drd4 < tm1Dkg > /J	The Jackson Laboratory	JAX:008084
Mouse: OT-II: B6.Cg-Tg(TcraTcrb)425Cbn/J	The Jackson Laboratory	JAX:004194
Oligonucleotides		
Primers for ChIP PCR and qPCR	Dettman et al., 2011; Tumes et al., 2013	See the listed, previous publications for detail
Software and Algorithms		
FlowJo Software (version 10.5.3)	FlowJo	https://www.flowjo.com/
GraphPad Prism 6	GraphPad Software	https://www.graphpad.com
ImageJ 1.49v	ImageJ	https://imagej.nih.gov
R (version 3.2.5)	The R Foundation	https://www.r-project.org/
FastQC v.0.11.2	Babraham Institute	https://www.bioinformatics.babraham.ac.uk/projects/fastqc/
TopHat (version 2.0.13)	Johns Hopkins University	https://ccb.jhu.edu/software/tophat/index.shtml
HTSeq v.0.6	Anders et al., 2015	https://htseq.readthedocs.io

LEAD CONTACT AND MATERIALS AVAILABILITY

Further information and requests for resources and reagents should be directed to and will be fulfilled by the Lead Contact, Xingbin Ai (xai@partners.org). This study did not generate new unique reagents.

EXPERIMENTAL MODELS AND SUBJECT DETAILS

Mice

C57BL/6 (B6), *Drd4*$^{+/-}$ mice (stock number: 008084) and OT-II mice (stock number: 004194) were purchased from The Jackson Laboratories and were maintained in the SPF animal facility at Brigham and Women's Hospital, Harvard Medical School. All animal experiments were approved by the Institutional Animal Care and Use Committee. *Drd4*$^{+/-}$ mice were bred to produce *Drd4*$^{-/-}$ mice and control, wild-type littermates. Both male and female mice were used for experiments. Unless specified for the age of mice, adult mice at 3-4 months of age were used.

Human donor lungs

Lungs from de-identified male and female donors between 0-65 years of age were purchased from International Institute for the Advancement of Medicine (IIAM), a non-profit institute that provides non-transplantable human tissues for medical research. 4 adult lungs (1 female and 3 male donors of 40-65 years of age) and 4 lungs from children (1 female, 2 males and 1 unknown, 0-13 years of age) were used in this study. These donors were healthy volunteers, had no previous lung diseases, and mostly died of brain injuries and heart failure. All the information regarding the donor is anonymous. Because the experiment involves no intervention or interaction with the donors and relates to no living individuals, this project is deemed non-human subject research by the IRB committee at Brigham & Women's Hospital.

METHOD DETAILS

Neonatal and adult mouse models of allergic inflammation

For the neonatal model of OVA exposure (Aven et al., 2014), pups were sensitized by intraperitoneal injection of 10 μg OVA (Sigma Aldrich, A5503) in Imject alum (Thermo Scientific, 77161) at post-natal day 5 (P5) and P10. Mice were subjected to aerosolized challenges of 3% OVA solution between P18-P20, 20 min per day. For the neonatal model of HDM exposure (Barrios et al., 2017), pups were sensitized intra-nasally with 2 μg HDM (Greer Laboratories, XPB70D3A25) in PBS at P5 and P10. Mice were then intra-nasally challenged on 5 consecutive days between P16- P20, each day with 10 μg HDM. For both neonatal models of allergen exposure, mice were euthanized at P21. For the adult model of OVA exposure, adult mice were sensitized with 50 μg OVA in Imject alum on experimental day 0 (D0) and Day 5 followed by 3 aerosolized OVA challenges between D13-D15. For the adult model of HDM exposure, mice were sensitized intra-nasally with 10 μg HDM in PBS at D0 and D5. Mice were then intra-nasally challenged on 5 consecutive days between D11-D15, each day with 25 μg HDM. For both adult models of allergen exposure, mice were euthanized at D16. Non-allergic control mice of both age groups were challenged with saline. For the treatment with the DRD4 antagonist L745870 (Sigma Aldrich, L131), mice were injected intra-peritoneally L745870 at 1 mg/kg body weight (Patel et al., 1997) on a daily basis between P10-P20 for the neonatal model and experimental day 5-day 15 for the adult mouse model. For ablation of dopaminergic nerves, mice were injected subcutaneously 6OHDA (Tocris, 2547) at 100 mg/kg body weight once a day between P1-P7 and got another injection on P14 (Angeletti and Levi-Montalcini, 1972). For the treatment with the DRD4 agonist A412994, adult mice were injected intra-peritoneally with A412994 (Sigma Aldrich, SML0608) once per day between experimental day 12-day 15. A412994 was given at 0.1 μmol/kg body weight (Moreland et al., 2005). For adoptive transfer, donor OT-II mice at 5 weeks of age were sensitized twice and total CD4$^+$ T cells were purified from spleen using an isolation kit (Miltenyi Biotec, 130-104-454). 2×10^6 CD4$^+$ T cells were adoptively transferred to each WT or *Drd4*$^{-/-}$ mouse when the recipients were P14. The recipients were then injected intra-peritoneally L745870 at 1 mg/kg body weight once a day between P14-P20 and challenged with OVA daily between P18-P20. Bronchoalveolar lavage fluid (BALF), lungs and blood samples were collected 24 h after the last challenge in both neonatal and adult models (Aven et al., 2014).

Mouse primary lymphocyte preparation and culture

Mice were sacrificed by over-inhalation of isoflurane followed by cervical dislocation. Spleens were isolated, minced, and digested in RPMI-1640 (Life Technologies, 11875-119) with 10% FBS, 400 U/mL Collagenase Type 4 (Worthington-Biochem, LS004188), 0.1% Dispase II (Sigma, 4942078001) and 20 μg/mL DNase I (NEB, 439807) for 30 min at 37°C. For each sample, 12 mL of digestive solution was used. Digested spleens were mechanically disrupted by pushing through syringe with 18-gauze needle and passage through 100 μm and 40 μm wire meshes. Cells were pelleted by centrifugation and re-suspended in 2 mL red blood cell lysis buffer (Sigma Aldrich, R7757) to remove red blood cells. Naive CD4$^+$ T cells were enriched by negative selection using an isolation kit (Miltenyi Biotec, 130-104-453). CD4$^+$CD25$^-$CD44$^-$CD62L$^+$ cells were deemed naive CD4$^+$ T cells that accounted for ~95% of the purified cell population. Purified cells (2×10^6 per well) were cultured in a 12-well plate pre-coated with 1 μg/mL αCD3 (BD Biosciences, 553058). RPMI-1640 medium was supplemented with 10% FBS, 100 U/mL penicillin, 0.1 mg/mL streptomycin, 2 mM 2-mercaptoethanol. For Th0 condition, cells were cultured at the presence of 1 μg/mL αCD28 (BD Biosciences, 553295). For Th2 (Th0+IL-4)

condition, cells were cultured at the presence of 1 μg/mL αCD28, 5 ng/mL rmIL-2 (R&D Systems, 402-ML-010) and 10 ng/mL rmIL-4 (BioLegend, 574302). For Th1 condition, cells were cultured at the presence of 1 μg/mL αCD28, 5 ng/mL rmIL-2 (R&D Systems, 402-ML-010) and 10 ng/mL rmIL-12 (R&D Systems, 419-ML-010). For Th17 condition, cells were cultured at the presence of 1 μg/mL αCD28, 5 ng/mL rmIL-2 (R&D Systems, 402-ML-010), 2 ng/mL rhTGF-β (R&D Systems, 240-B-002) and 20 ng/mL rmIL-6 (R&D Systems, 406-ML-005) for 48h. And then 10 ng/mL rmIL-23 (R&D Systems, 1887-ML-010) was added to the culture. For treatment, individual neurotransmitter was added daily to T cell cultures on day 0 to day 2. These included dopamine (0.1- 25 μM, Fisher Scientific, 35-485-0), epinephrine (10 μM, Sigma Aldrich, E4250) and norepinephrine (10 μM, Sigma Aldrich, A7257). For most of cultures with dopamine, 10 μM dopamine was used. Other pharmaceutical reagents used in culture to modulate the dopamine pathway include: L-745,870 hydrochloride (300 nM, Sigma Aldrich, L131), raclopride (50 nM, Sigma Aldrich, R121), SCH-23390 hydrochloride (50 nM, Sigma Aldrich, D054), A-412997 dihydrochloride (100 nM, Sigma Aldrich, SML0608), forskolin (1 μM, Tocris, 1099), CAS285986-31-4 (20 μM, Sigma Aldrich, 573108), DZNep (7.5 nM, EMD Millipore, 252790-2MG). For treatment with CAS285986-31-4, cultures were analyzed on day 2. For all other cultures, cells and the conditioned media were harvested for gene and cytokine expression assays after 4 days in culture.

Primary human lymphocyte isolation and culture

Mediastinal lymph nodes associated with healthy donor lungs were dissected digested with 400 U/mL Collagenase Type 4, 0.1% Dispase II and 20 μg/mL DNase I for 30 min at 37°C. Digested samples were mechanically disrupted by pushing through syringe with 18-gauze needle and passage through 100 μm and 40 μm wire meshes. Naive $CD4^+$ T cells were enriched by negative selection using isolation kits (Miltenyi Biotec, 130-094-131). Purified cells (2×10^6 per well) were cultured in a 12-well plate pre-coated with 2 μg/mL αCD3 (eBioscience, 16-0037-85). RPMI-1640 medium was supplemented with 10% FBS, 100 U/mL penicillin, 0.1 mg/mL streptomycin, 2 mM 2-mercaptoethanol. For Th0 condition, cells were cultured at the presence of 2 μg/mL αCD28 (BD Biosciences, 555725). For Th2 (Th0+IL-4) condition, cells were cultured at the presence of 2 μg/mL αCD28, 5 ng/mL rhIL-2 (R&D Systems, 202-IL-010) and 10 ng/mL rhIL-4 (BioLegend, 204-IL-010).

Histology and antibody staining

Lungs and mediastinal lymph nodes associated with donor lungs were fixed in 4% paraformaldehyde in PBS overnight. After washing, tissues were processed for paraffin embedding and cryopreservation before paraffin sections (5 μm) and frozen sections (15 μm), respectively, were collected. Frozen sections were used for visualizing nerve fibers in Figure 1. For staining of cells in culture, cells were spun onto histological slides using a cytospin centrifuge before fixation. The procedure of antibody staining was previously described (Aven et al., 2014). Primary antibodies included: mouse anti-DRD4 (1:100; EMD Millipore, MABN125), rabbit anti-tyrosine hydroxylase (1:200; EMD Millipore, AB152), rabbit anti-DBH (1:100; EMD Millipore, AB1585), mouse anti–neural class III b-tubulin (TUBB3) antibody (1:200; R&D Systems, MAB1195) and rabbit anti-CD4 (1:400; Novus Biologicals, NBP1-19371SS). For staining of mouse tissue sections using mouse monoclonal primary antibodies, tissue sections were blocked using the Mouse on Mouse Kit (Vector Laboratories, BMK-2202). Biotinylated secondary antibodies and secondary antibodies conjugated with Alexa Fluor®488 and 546 were purchased from Thermo Fisher Scientific. For fluorescence staining, nuclei were stained with Hoechst dye (1:1000) and images were collected by confocal microscopy (Carl Zeiss, LSM 710). For DAB staining, sections were treated with standard ABC kit (Vector Labs, PK-6100) and DAB Peroxidase Substrate Kit (Vector Labs, SK-4100). After DAB staining, samples were counterstained with Hematoxylin QS (Vector Laboratories, H-3404). Mucus in lung sections was stained using periodic acid–Schiff (PAS) staining kit (Sigma-Aldrich, 395B-1KT). Bright field images were taken using a digital camera (Nikon DS-Fi2). To quantify sympathetic innervation, the immunoreactive areas of tyrosine hydroxylase and TUBB3 was quantified from non-overlapping images using ImageJ (National Institutes of Health, Bethesda, MD, USA) followed by the calculation of the ratio between tyrosine hydroxylase and TUBB3. To quantify pathological features of the lung (Cohen et al., 2007), 3 non-overlapping areas were quantified from one section, 3 sections for each mouse. The thickness of the airway epithelium was measured using ImageJ. The peri-vascular nuclear density was measured by quantifying the number of infiltrating cells in the peri-vascular area based on nuclear staining and then normalizing the number of nuclei to the size of the area measured by ImageJ.

Flow cytometry analysis of T cell cultures, BALF and lung samples

Mouse lungs were enzymatically dissociated into single cell preparation, as described in the preparation of mouse lymphocytes from the spleen. For cell surface marker staining, cells were first stained with eBioscience Fixable Viability Dye eFluor 520 or 780 (1:2000) in PBS at 4°C for 30 min. After washing twice, cells were subjected to cell surface markers staining in FACS buffer (5% BSA and 0.1% sodium azide in PBS) at 4°C for 30 min. For intracellular cytokine staining, cells were treated with eBioscience Cell Stimulation Cocktail (plus protein transport inhibitors) (eBioscience, 00-4975-03) for 4 hr before live/dead cell staining. Cells were then treated with fixation/permeabilization solution (BD Biosciences, 554722) before staining. For nuclear staining, cells were fixed in 4% paraformaldehyde for 30 min, permeabilized in 90% methanol at 4°C for 45 min and then stained with the antibody in FACS buffer at 4°C for 30 min. After staining, cells were first gated on CD45 and viability dye for live leukocytes. Doublets were excluded based on FSC-A versus FSC-H and SSC-W versus SSC-H. Among $CD3^+CD4^+$ T cells, the $CD62L^+CD44^-CD25^-$ population were deemed naive $CD4^+$ T cells. Eosinophils were the Siglec F^+CD11c^{low} population. Macrophages were $CD11c^+$Siglec F^+MHC II^{low}. Dendritic cells were $CD11c^+$Siglec F^+MHC II^{high}. Neutrophils were $CD11b^+Ly6G^+$Siglec F^-MHC II^-. Mast cells were FceR1α $^+$c-$Kit^+CD11b^-CD11c^-$. Lymphocytes include T cells ($CD3^+CD19^-$), B cells ($CD19^+CD3^-$) and NK cells ($NK1.1^+CD3^-$). For flow cytometry analyses of DRD4

expression, cells were treated with the Mouse on Mouse Kit before incubated with the mouse anti-DRD4 antibody (1:100; EMD Millipore, MABN125) and a fluorescent secondary antibody. Cells were then double labeled for surface markers of $CD4^+$ T cells, $CD8^+$ T cells, B cells, eosinophils, mast cells, macrophages, and dendritic cells. After staining, cells were analyzed on BD FACSCANTO II. Flowjo v.10.5.3 was used for data analysis. All the antibodies used for flow cytometry were listed in Key Resources Table.

ILCs isolation and culture

Cells from the dissociated adult mouse lungs were incubated with CD90.2 microbeads (Miltenyi Biotec, 130-049-101) for 17 min on ice and enriched for $CD90.2^+$ cells by positive selection using LS columns (Miltenyi Biotec, 130-042-401). $CD90.2^+$ cells were stained with antibodies for 20 min on ice, washed, and resuspended in complete medium. ILCs were defined as $CD45^+$ $CD90.2^+CD127^+ST2^+$ and negative for CD3, CD4, CD8, CD11b, CD11c, CD19, NK1.1, TCRβ, TCRγδ. ILCs were isolated by fluorescence activated cell sorting using a BD FACS Aria III. Cells were plated at a density of 6,000 cells per well in complete medium and cultured with IL-7, IL-7 + dopamine, IL-7 + IL-33 or IL-7 + IL-33 + dopamine. IL-7 was used at a final concentration of 20 ng/ml, IL-33 at 200 ng/ml and dopamine at 10 μM. After 3 days in culture, ILCs were subjected to gene expression analyses and the supernatant was analyzed by ELISA.

Physiological measurements of airway reactivity

For airway resistance assay, mice were injected with xylazine (10 mg/kg body weight), pentobarbital (100 mg/kg body weight) and pancuronium (0.5 mg/kg body weight), intubated and placed on a mechanical ventilator (Legacy flexiVent, SCIREQ). Ventilation was at 300 breaths/min (tidal volume 6–7 mL/kg body weight). Airway resistance was measured after airway delivery of nebulized methacholine in PBS (5 mg/mL, 15 mg/mL and 25 mg/mL). Data are presented as relative peak resistance to baseline within each experimental group. For airway contractility assay using lung slices, mouse lungs were infused with 1.5% low-melting agarose and sliced at 150 μm thickness using a tissue slicer (Precisionary Instruments Inc.). After overnight recovery in DMEM/F-12 (1:1; Life Technologies, 11320-033), lung slices were stimulated with increasing doses of methacholine (Sigma-Aldrich, A2251). Mid-sized airways with the diameter between 200-500 μm were imaged before stimulation and 5 min after stimulation with an inverted microscope (DMI6000B; Leica Microsystems, Buffalo Grove, IL, USA). The luminal area of the imaged airway was measured with ImageJ (National Institutes of Health, Bethesda, MD, USA). Airway contraction in response to methacholine was calculated as the percentage of reduction in the luminal area from the baseline.

Cell proliferation assay

Cell proliferation was analyzed with CFSE Cell Division Tracker Kit (BioLegend, 423801) following the manufacturer's protocol. Briefly, freshly isolated lymphocytes were incubated with 5 μM CFSE in PBS containing 5% FBS for 20 min at room temperature and protected from light. The staining was quenched by washing twice with RPMI-1640 with 10% FBS. The labeled lymphocytes were then cultured before flow cytometry analysis.

Quantitative Real Time PCR (qPCR)

Total RNA was extracted from cultured T cells and lungs using a RNeasy kit (QIAGEN, 74106) followed by reverse transcription using Superscript III Reverse Transcriptase (Thermo Fisher Scientific, 18080-044). For ILCs in culture, total RNA was extracted using PicoPure RNA isolation kit (Thermo Fisher Scientific, KIT0204) and reverse transcribed using SuperScript IV VILO Master Mix (Thermo Fisher Scientific, 11756050). Real time PCR was performed using CFX96 real-time system (Bio-Rad). TaqMan primers for mouse *Il13* (Mm00434204_m1), mouse *Il4* (Mm00445259_m1), mouse *Il5* (Mm00439646_m1), mouse *Areg* (Mm00437583_m1), mouse *Il2ra* (Mm01340213_m1), mouse *Muc5ac* (Mm01276704_m1), mouse *Ifng* (Mm01168134_m1), mouse *18S* rRNA (Mm03928990_g1), human *Il13* (Hs00174379_m1) and human *18S* rRNA (Hs99999901_s1) were purchased from Thermo Fisher Scientific. SYRB green primers for mouse *Th* gene (Mm.PY.58.33106186), mouse *Drd1* (Mm.PT.58.43576955.g), *Drd2* (Mm.PT.58.7811767), *Drd3* (Mm.PT.58.12468013), *Drd4* (Mm.PT.58.10440082) and *Drd5* (Mm.PT.58.43058779.g) were purchased from Integrated DNA Technologies. Relative gene expression was measured by normalizing to *18S* rRNA using ΔΔCt (cycle threshold difference). Expression of *Il4*, *Il5*, *Il13* and *Areg* in ILCs was normalized to the housekeeping gene *Actb* (Thermo Fisher Scientific, 4352341E).

Western Blot

Lungs and cells were homogenized in RIPA buffer with cOmpleteproteinase inhibitor cocktail (Roche, 11697498001) followed by standard western blot assays. Primary antibodies include rabbit anti-tyrosine hydroxylase (1:1000; EMD Millipore, AB152), rabbit anti-DBH (1:1000; EMD Millipore, AB1585), rabbit anti-VAChT (1:1000; Abcam, AB68986), rabbit anti-CGRP (1:1000; Sigma Aldrich, C8198), mouse anti-p-STAT6 (pY641) (1:1000; BD Biosciences, 558241), rabbit anti-DRD4 (1:1000; Sigma Aldrich, SAB4500672-100UG), mouse anti-DRD4 (1:1000; EMD Millipore, MABN125) and mouse anti-β-actin (1:3000; Sigma Aldrich, A5441). HRP–conjugated secondary antibodies include: goat anti-rabbit (1:3000; Santa Cruz Biotechnology, sc-2004) and goat anti-mouse (1:3000; BD Biosciences, 554002). The antigen-antibody complex was detected by SuperSignal West Pico PLUS Chemiluminescent Substrate (Thermo Fisher, 34577).

ELISAs

Serum was collected from blood samples of mice and the amount of OVA-specific IgE and total IgE were analyzed using ELISA Kits (BioLegend, 439807 and eBioscience, 88-50460-88). BALF was collected and the amount of IL-4, IL-5 and IL-13 were analyzed using Ready-Set-Go! ELISA sets (eBioscience, 88-7044-86, 88-7054-88 and 88-7137-76). For dopamine and norepinephrine assays, the lung was homogenized in cold RIPA buffer (Thermo Scientific, PI89900) and the amount of dopamine and norepinephrine in the supernatant were analyzed by ELISA kits (Abnova, 89-028-620 and 89-028-610). For the measurement of intracellular cAMP, naive $CD4^+$ T cells were cultured under Th0 condition overnight followed by the treatment with dopamine (10 μM) and forskolin (1 μM) for 1 hr. Cells were lysed with 100 μL RIPA buffer with 1 mM phenylmethylsulfonyl fluoride. The supernatant was collected before assays using the cAMP XP® Assay Kit (Cell signaling, 4339S).

RNA-seq analyses

Naive mouse $CD4^+$ T cells in Th0 culture with and without dopamine treatment were harvested on day 4. Total RNA was purified with a RNeasy kit (QIAGEN) followed with DNase I treatment. RNA-seq libraries were prepared with the TruSeq Stranded Total RNA with Ribo-Zero Globin kit (Illumina) following the manufacturer's instructions. Quality of the libraries was validated by quantitation with picogreen, size analysis on an Agilent Bioanalyzer or Tapestation 2200 and qPCR quantitation against a standard curve. Bar-coded cDNA libraries were pooled together in equal concentrations in one pool per biological triplicates and were sequenced on a HiSeq2500 (Illumina) at the Translational Genomics Core of Partners HealthCare Personalized Medicine (Cambridge, MA, USA). Briefly, raw reads were pre-processed using FastQC v.0.11.2, and then mapped to the mouse genome (*Mus musculus* UCSC version mm10) using the TopHat version 2.0.13. The read count table was produced using HTSeq v.0.6. Differentially expressed gene transcripts were selected based on an adjusted p value less than 0.05. Heatmap and volcano plot were performed using R-3.2.5. For pathway analysis, a list of all genes detected in the samples was ranked on the t-statistic. This list was analyzed with the fGSEA package in R using the complete Molecular Signatures Database MSigDB v6.1 gene set (http://software.broadinstitute.org/gsea/index.jsp). We only showed those pathways that had an FDR < 0.05.

Quantitative Chromatin precipitation (ChIP)-qPCR

Cultures of naive $CD4^+$ T cells were harvested on day 4. Histone was cross-linked to DNA with 1% paraformaldehyde in PBS for 10 min at 37°C. After washing with cold PBS, cells were re-suspended in 100 μL SDS lysis buffer per 1 million cells that contained 1% SDS, 10mM EDTA, 50mM Tris-HCl (pH 8.1) and cOmpleteproteinase inhibitor cocktail. Cells in suspension were sonicated using QSONICA Model Q125(50A with 14 cycles of 30 s on and 30 s off) to break genomic DNA into fragments between 200-500 bp in length. 100 μL of each sample was used as template for measurement of input DNA. Another 100 μL of each sample was diluted with 900 μL of ChIP dilution buffer (0.01% SDS, 1.1% Triton X-100, 1.2 mM EDTA, 16.7 mM Tris-HCl (pH 8.1), 150mM NaCl) and pre-cleared with 60 μL salmon sperm DNA (Invitrogen, 15632011) /protein-A agarose slurry (Thermo Fisher, 20421) for 1 h at 4°C with rotation. After centrifugation, pre-cleared samples were incubated with 5 μg of anti-trimethyl-Histone H3 (Lys27) antibody (Millipore, 07-449) overnight at 4°C with rotation followed by 2 hr incubation with protein A agarose slurry pretreated with salmon sperm DNA. The beads were then pelleted and washed extensively using buffers with increasing concentrations of NaCl. Immune complexes were eluted twice by addition of 250 μL of elution buffer (1% SDS, 0.1M $NaHCO_3$) and incubation for 15 min with rotation at room temperature. Cross-linking was reversed by adding 20 μL NaCl (5 M) and incubating at 65°C overnight. The samples were then treated with 1 μL RNase A (QIAGEN, 1031301) at 37°C for 1 hr and 2 μL Proteinase K (Roche, 14164600) at 45°C for 2 hr before DNA extraction using phenol/chloroform and purified using ethanol. The primers used for ChIP q-PCR were previously described (Tumes et al., 2013) and purchased from Integrated DNA Technologies. The relative H3K27me3 binding to the target loci was measured by normalizing to the input material using ΔCt.

QUANTIFICATION AND STATISTICAL ANALYSIS

Quantification and statistical analyzed were described in the Method Details section above and Figure legends associated with each experiment. GraphPad Prism 6 was used for data analysis. Data in all bar graphs represent mean ± SEM from at least 3 independent experiments. For comparisons between two conditions, statistical significance was analyzed using the unpaired Student's t test. For multiple comparisons between treatment and methacholine concentration or genotype (Figures 5H, S5K, and S6J), statistical analysis was performed with one-way ANOVA followed by Tukey's post-hoc test for multiple comparisons. The difference between experimental groups was considered statistically significant if *P value* was less than 0.05.

DATA AND CODE AVAILABILITY

The RNA-seq datasets of Th0 cultures with and without dopamine treatment are generated during this study and are available at the GEO repository with the accession number GEO: GSE137968.

Immunity, Volume *51*

Supplemental Information

Age-Related Dopaminergic Innervation Augments T Helper 2-Type Allergic Inflammation in the Postnatal Lung

Wei Wang, Jonathan A. Cohen, Antonia Wallrapp, Kenneth G. Trieu, Juliana Barrios, Fengzhi Shao, Nandini Krishnamoorthy, Vijay K. Kuchroo, Matthew R. Jones, Alan Fine, Yan Bai, and Xingbin Ai

Figure S1

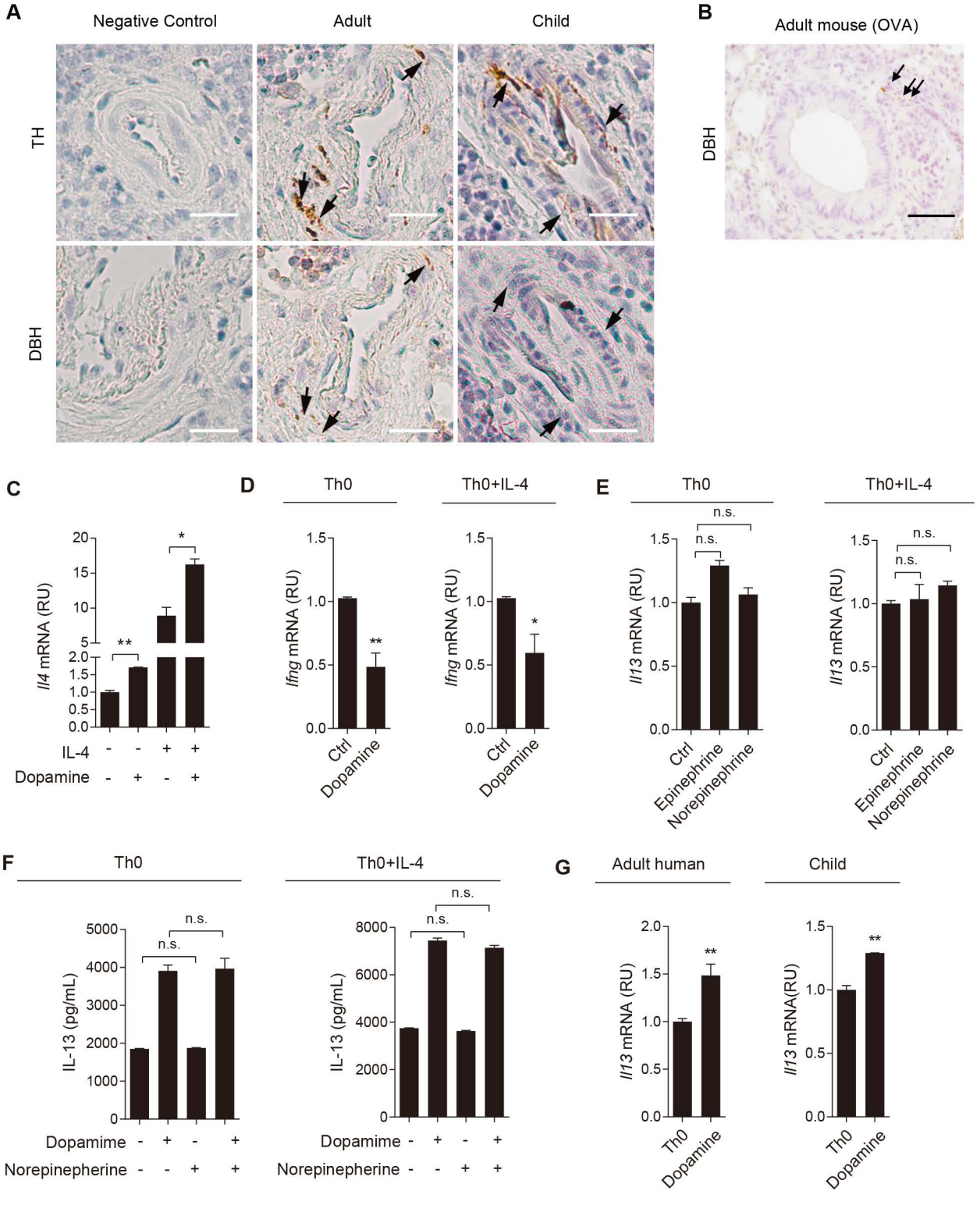
A
Negative Control
Adult
Child
TH
DBH
B
Adult mouse (OVA)
DBH
C
Il4 mRNA (RU)
IL-4
Dopamine
D
Th0
Th0+IL-4
Ifng mRNA (RU)
Ctrl
Dopamine
E
Th0
Th0+IL-4
Il13 mRNA (RU)
Ctrl
Epinephrine
Norepinephrine
n.s.
F
Th0
Th0+IL-4
IL-13 (pg/mL)
Dopamime
Norepinepherine
G
Adult human
Child
Il13 mRNA (RU)
Il13 mRNA(RU)
Th0
Dopamine

Figure S1. DBH is selectively expressed by nerves innervating human lymph nodes and mouse lungs; dopamine, but not norepinephrine and epinephrine, promotes a Th2 phenotype in CD4+ T cells.

Related to Figures 1 and 2. **(A)** Representative images of TH and DBH staining of adjacent tissue sections of lymph nodes associated with donor lungs from adults (40-65 years of age) and children (0-13 years of age). Arrows point to TH+ and DBH+ nerves. Scale bars, 50 μm. Similar results were found in 3 individuals in each age group. (**B**) Representative DBH staining in the adult mouse lung following OVA exposure. Arrows mark DBH+ labelled nerves. Scale bars, 50 μm. For (**C-G**), cultures were treated with neurotransmitters at a concentration of 10 μM and analyzed at day 4 for gene expression by qPCR and for IL-13 production by ELISA. (**C, D**) The expression of *Il4* and *Ifng* genes in mouse Th0 and Th0+IL-4 cultures with and without dopamine treatment. (**E**) *Il13* gene expression in mouse Th0 and Th0+IL-4 cultures with and without the treatment of epinephrine and norepinephrine. (**F)** IL-13 production in mouse Th0 and Th0+IL-4 cultures treated with dopamine and norepinephrine, alone and in combination. (**G**) *Il13* gene expression in human CD4+ T cells in Th0 cultures with and without the treatment of dopamine. Naïve CD4+ T cells were purified from the lymph nodes associated with donor lungs in adults (40-65 years of age) and children (0-13 years of age). For all the bar graphs, data present mean ± SEM of the results in triplicates in each experiment and from at least 3 independent experiments. *$p<0.05$; **$p<0.01$ by two-tailed student's t test. n.s., not significant.

Figure S2

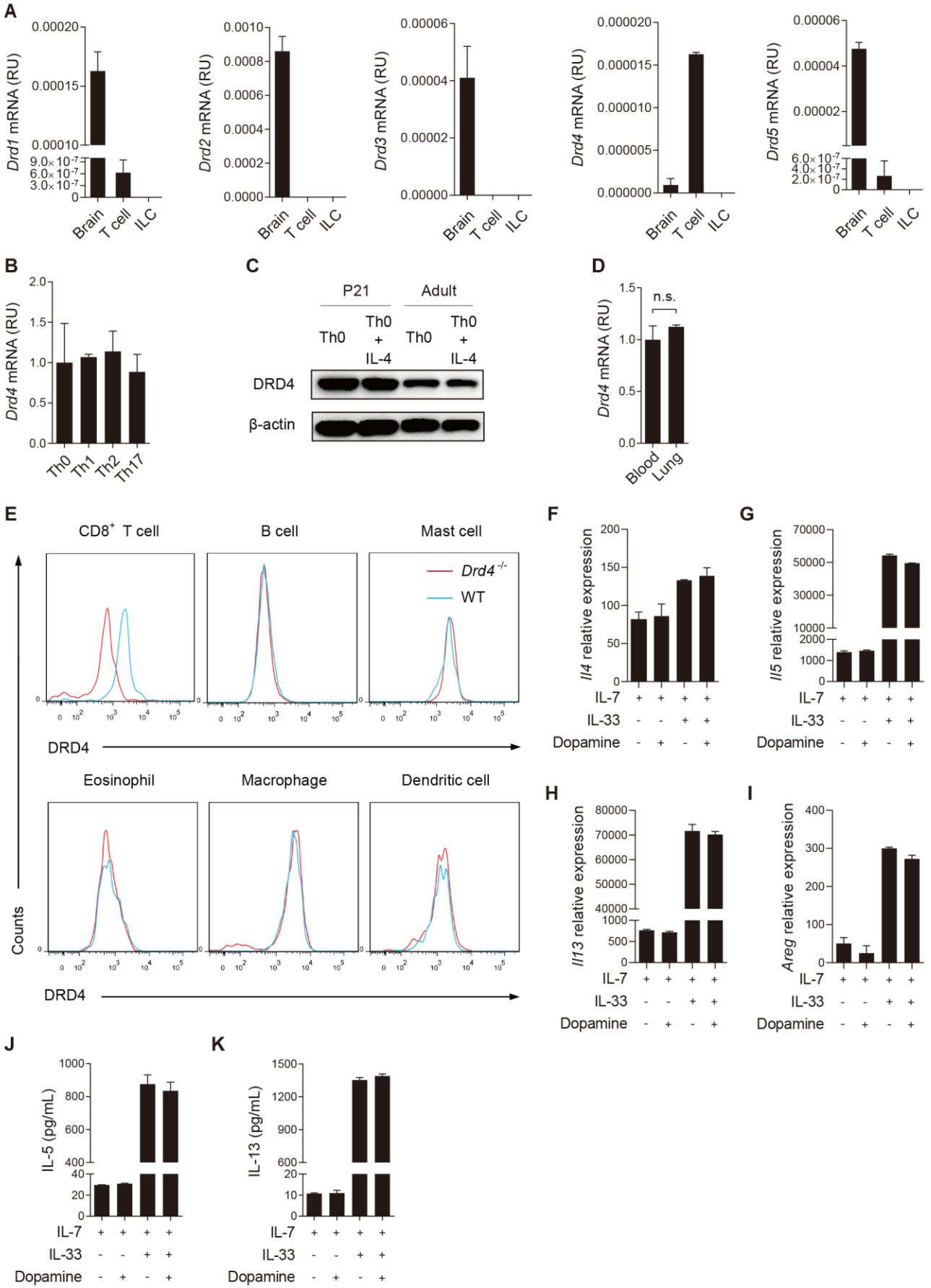
A
Drd1 mRNA (RU)
Drd2 mRNA (RU)
Drd3 mRNA (RU)
Drd4 mRNA (RU)
Drd5 mRNA (RU)
Brain
T cell
ILC
B
Drd4 mRNA (RU)
Th0
Th1
Th2
Th17
C
P21
Adult
Th0
Th0 + IL-4
DRD4
β-actin
D
Drd4 mRNA (RU)
n.s.
Blood
Lung
E
CD8+ T cell
B cell
Mast cell
Drd4 -/-
WT
DRD4
Eosinophil
Macrophage
Dendritic cell
Counts
F
Il4 relative expression
G
Il5 relative expression
H
Il13 relative expression
I
Areg relative expression
IL-7
IL-33
Dopamine
J
IL-5 (pg/mL)
K
IL-13 (pg/mL)

Figure S2. CD4$^+$ T cells and a subset of CD8$^+$ T cells, but no ILCs, express DRD4. Related to Figures 3 and 7. (**A**) qPCR analyses of *Drd1-Drd5* gene expression in purified naïve CD4$^+$ T cells from mouse spleen and ILCs from mouse lung. Mouse brain was positive control. For the analyses in T cells, the results represent mean ± SEM of 3 independent experiments. For the analyses of ILCs, the results represent mean ± SEM of 2 independent experiments. (**B**) *Drd4* gene expression in Th0, Th1, Th2 and Th17 cultures at day 4. Data represent mean ± SEM of 3 independent experiments. (**C**) DRD4 expression in Th0 and Th0+IL-4 cultures prepared from P21 and adult mice by Western blot. β-actin is loading control. Each lane represents one sample. Data represent the results in 3 independent experiments. (**D**) *Drd4* gene expression in CD4$^+$ T cells isolated from blood and lung-associated lymph nodes. Cells were isolated from samples pooled from 5 mice for each experiment. Data represent mean ± SEM of 2 independent experiments. (**E**) Flow cytometry analyses of DRD4 expression in CD8$^+$ T cells, B cells, mast cells, eosinophils, macrophages, dendritic cells. B cells were isolated from mouse spleens and all other immune cells were isolated from mouse lungs. Samples prepared from *Drd4*$^{-/-}$ mice were negative control for the specificity of the DRD4 antibody. Similar results were obtained from 3 independent experiments. (**F-K**) ILCs were isolated from 5 mouse lungs by cell sorting before cells were maintained in media with IL-7 (20 ng/mL), IL-7 + dopamine (10 μM), IL-7 + IL-33 (200 ng/mL) or IL-7 + IL-33 + dopamine. The expression of type 2 cytokine and *amphiregulin* (*Areg*) genes was analyzed at day 3 in culture. Data represent mean ± SEM of cultures in duplicates.

Figure S3

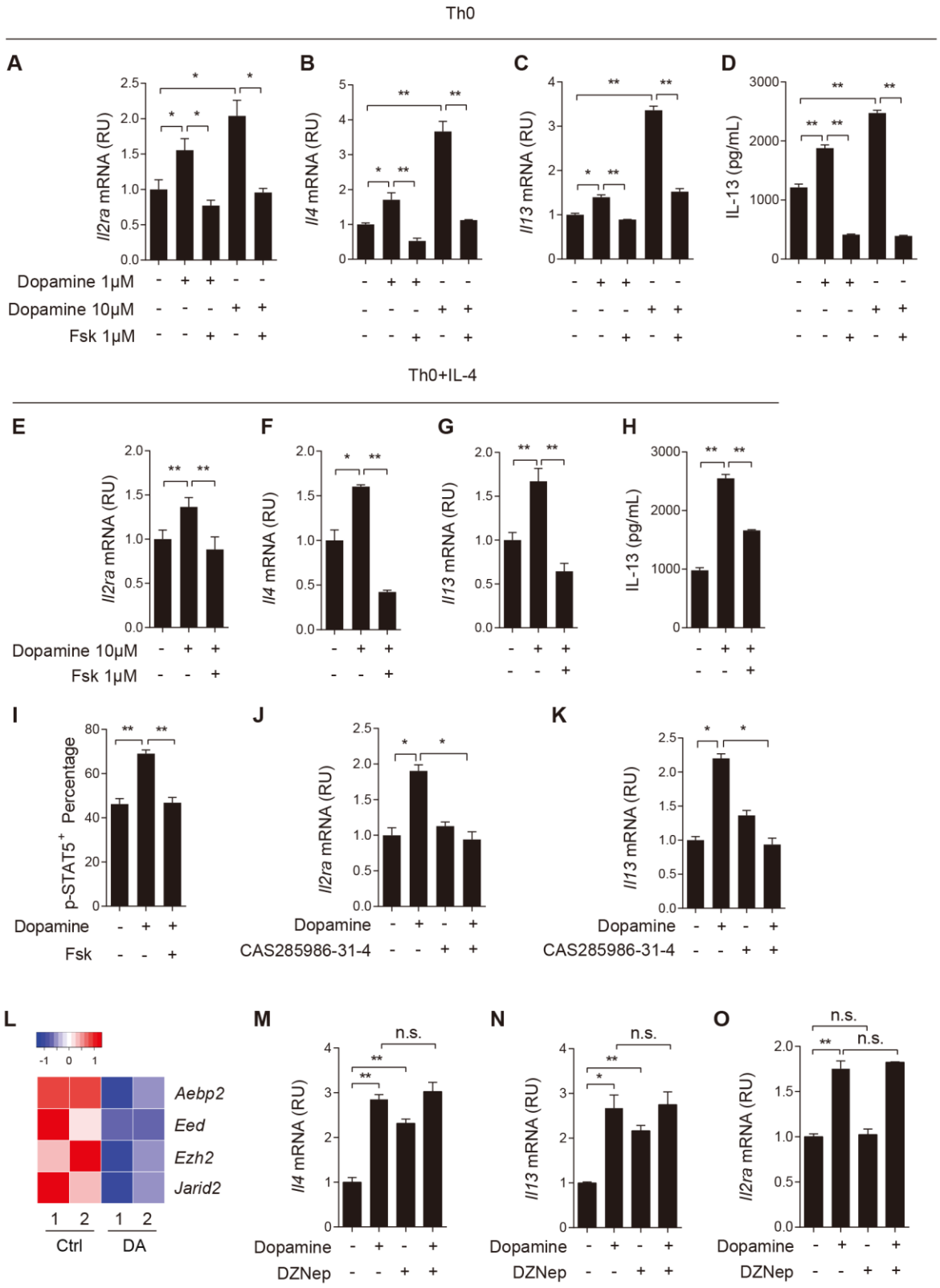

Figure S3. Dopamine signaling downregulates the cAMP and EZH2 pathways. Related to Figures 3 and 4. (**A-C**) Relative expression of *Il2ra, Il4 and Il13* genes in mouse Th0 cultures with and without dopamine and Fsk (1μM) treatment. (**D**) The production of IL-13 in each group was measured by ELISA. (**E-H**) *Il2ra,*

Il4 and Il13 gene expression and IL-13 production in Th0+IL-4 cultures with and without dopamine and Fsk treatment. (**I**) Quantification of the abundance of p-STAT5^{+} cells in Th0+IL-4 cultures treated with dopamine alone and a combination of dopamine and Fsk. Cultures were analyzed by flow cytometry. (**J**, **K**) Relative expression of *Il2ra* and *Il13* genes in Th0 cultures treated with dopamine and CAS285986-31-4 (20 µM), alone and together. (**L**) Heat map of differential gene expression of *Ezh2* and other PRC2 component genes in Th0 cultures treated with dopamine (DA). Data are from the results of RNA-seq. (**M-O**) Relative expression of *Il4, Il13 and Il2ra* genes in mouse Th0 cultures treated with dopamine and DZNep (7.5 nM), alone and in combination. Data were normalized to untreated baseline. All bar graphs represent mean ± SEM of 3 independent experiments. *$p<0.05$; **$p<0.01$ by two-tailed student's t test. n.s., not significant.

Figure S4

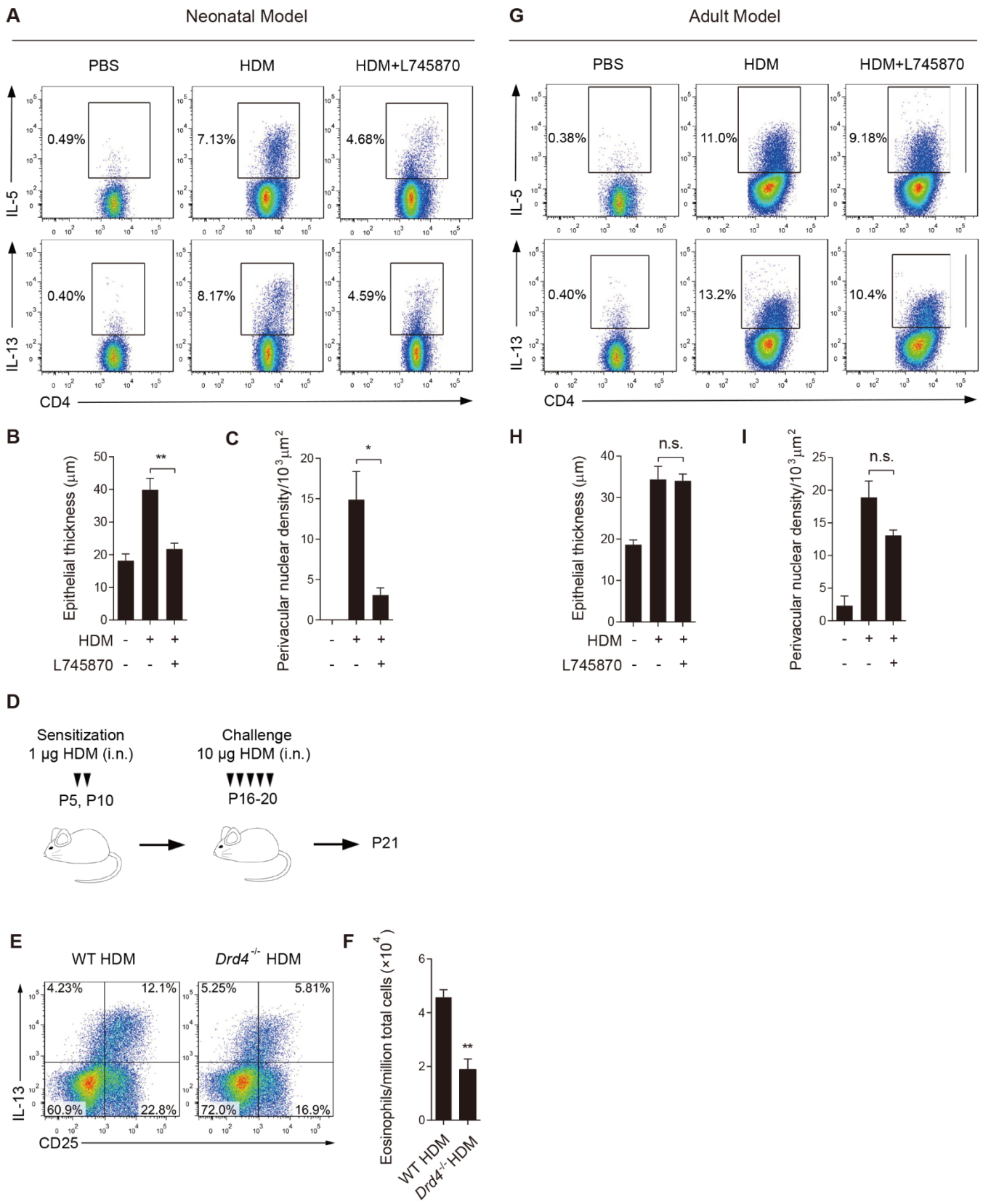

Figure S4. Functional disruption of DRD4 by L745870 and genetic deficiency ameliorates Th2 inflammation in neonatal mice following HDM exposure. Related to Figure 5. (**A**) Flow cytometry

analyses of IL-5^{+}CD4^{+} and IL-13^{+}CD4^{+} T cells in the lung following HDM exposure with and without L745870 treatment in neonates. Results were representative of 3 independent experiments. (**B**, **C**) Pathological measurements of epithelial thickness and peri-vascular nuclear density in each group. Data represent mean ± SEM of 3 non-overlapping histological areas in each mouse, 6 mice in each group from 3 independent experiments. (**D**) Experimental scheme of HDM exposure in WT and *Drd4*$^{-/-}$ neonatal mice. Mice were sacrificed 1 day after the last challenge. (**E**) Representative flow cytometry analyses of IL-13^{+}CD25^{+}CD4^{+} T cells in WT and *Drd4*$^{-/-}$ mice at P21. Similar results were obtained in 3 independent experiments. (**F**) The abundance of eosinophils in the lung of WT and *Drd4*$^{-/-}$ mice following HDM exposure at P21. Data represent mean ± SEM of 6 mice of each genotype in 3 independent experiment. (**G-I**) Assessment of Th2 inflammation in adult mice following HDM exposure by flow cytometry and pathological measurements as described in (**A-C**) for neonatal mice. N=5 adult mice from 2 independent experiments. *$p<0.05$; **$p<0.01$ by two-tailed student's t test. n.s., not significant.

Figure S5

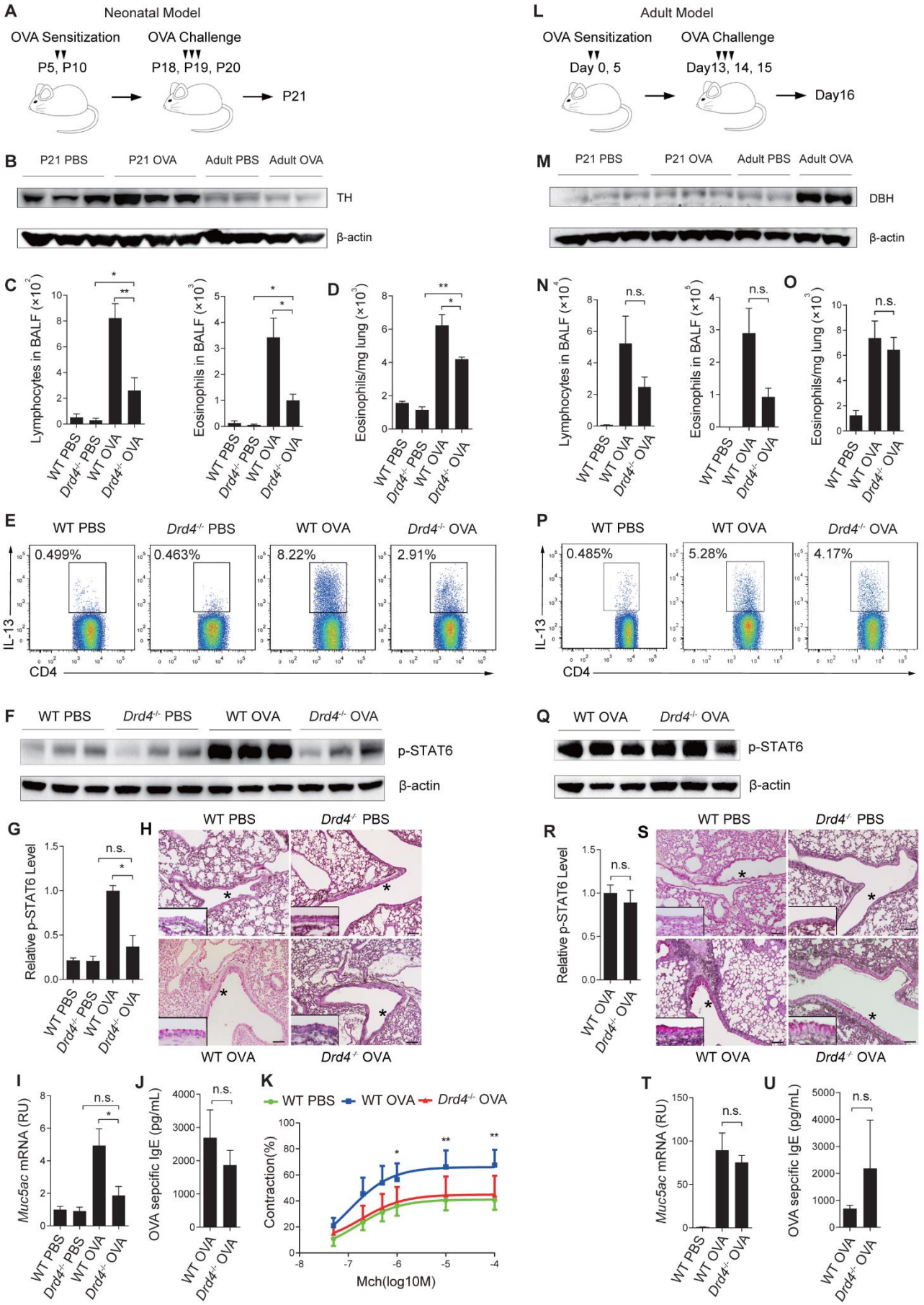
A
Neonatal Model
OVA Sensitization
P5, P10
OVA Challenge
P18, P19, P20
P21
L
Adult Model
OVA Sensitization
Day 0, 5
OVA Challenge
Day13, 14, 15
Day16
B
P21 PBS
P21 OVA
Adult PBS
Adult OVA
TH
β-actin
M
DBH
β-actin
C
Lymphocytes in BALF (×10^2)
Eosinophils in BALF (×10^3)
D
Eosinophils/mg lung (×10^3)
WT PBS
Drd4-/- PBS
WT OVA
Drd4-/- OVA
N
Lymphocytes in BALF (×10^4)
Eosinophils in BALF (×10^5)
O
Eosinophils/mg lung (×10^3)
n.s.
E
0.499%
0.463%
8.22%
2.91%
IL-13
CD4
P
0.485%
5.28%
4.17%
F
p-STAT6
β-actin
Q
G
Relative p-STAT6 Level
H
R
S
I
Muc5ac mRNA (RU)
J
OVA sepcific IgE (pg/mL)
K
Contraction(%)
Mch(log10M)
T
U

Figure S5. DRD4 deficiency ameliorates Th2 inflammation in neonatal mice, but not in adult mice, following OVA exposure. Related to Figure 5. (**A** and **L)** Experimental scheme of OVA sensitization and challenge in neonatal mice (**A**) and adult mice (**L**). Mice were sacrificed 1 day after the last challenge. **(B** and **M)** The amount of tyrosine hydroxylase and DBH in saline and OVA-exposed lungs of WT neonatal and adult mice. β-actin was loading control. Each lane represents one sample. Similar results were obtained in 3 independent experiments. (**C**) Flow cytometry analyses of lymphocytes and eosinophils in BALF of WT and *DRD4*$^{-/-}$ mice following OVA exposure at P21. N=6 in 3 independent experiments. (**D**) The abundance of eosinophils in the lung of WT and *Drd4*$^{-/-}$ mice at P21. Results were normalized to lung weight. N=5 in 3 independent experiments. (**E**) Representative cytometry results of IL-13^{+}CD4^{+} T cells in P21 lungs of each group. Similar results were obtained from 3 independent experiments. (**F**) Western blot analyses of p-STAT6 in the lung of WT and *Drd4*$^{-/-}$ mice at P21. β-actin was loading control. Each lane represents one sample. Similar results were obtained in 3 independent experiments. Data were quantified in **(G**). (**H**) Representative images of PAS staining of tissue sections in P21 lungs from each group. The area of the airway epithelium marked by * is enlarged and shown by the insert. Similar results were obtained in 3 independent experiments. Scale bars, 100 µm. (**I**) Mucus production in WT and *Drd4*$^{-/-}$ P21 lungs assayed by *Muc5ac* qPCR. N=5 for P21 *Drd4*$^{-/-}$ PBS group and N=10-12 for other groups in 3 independent experiments. (**J**) The amount of OVA-specific IgE in serum of WT and *Drd4*$^{-/-}$ mice at P21. N=12 in 3 independent experiments. (**K**) Assessment of airway hypercontractility following OVA exposure in WT and *Drd4*$^{-/-}$ mice at P21 using precision cut lung slices. Airway contractility in response to methacholine was measured by the percentage of reduction in the luminal size from the baseline. N=15-20 airways from 3 mice of each group in 2 independent experiments. (**N**-**U**) Assessment of Th2 inflammation in adult, WT and *Drd4*$^{-/-}$ mice following OVA exposure using flow cytometry, immunological and pathological assays as described for neonatal mice in (**C**-**J)**. N=5-7 for adult WT groups and N=5 for *Drd4*$^{-/-}$ group in 3 independent experiments. For the results in (**K**), data were analyzed by one-way ANOVA for multiple comparisons between treatment and methacholine dosage. For all other panels, data were analyzed by two-tailed student's t test. *$p<0.05$; **$p<0.01$; n.s., not significant.

We noted significant variations in OVA-specific IgE in the neonatal OVA models in (**J**). The variation may contribute to the statistically insignificant difference in OVA-specific IgE between WT and *Drd4*$^{-/-}$ mice.

Figure S6

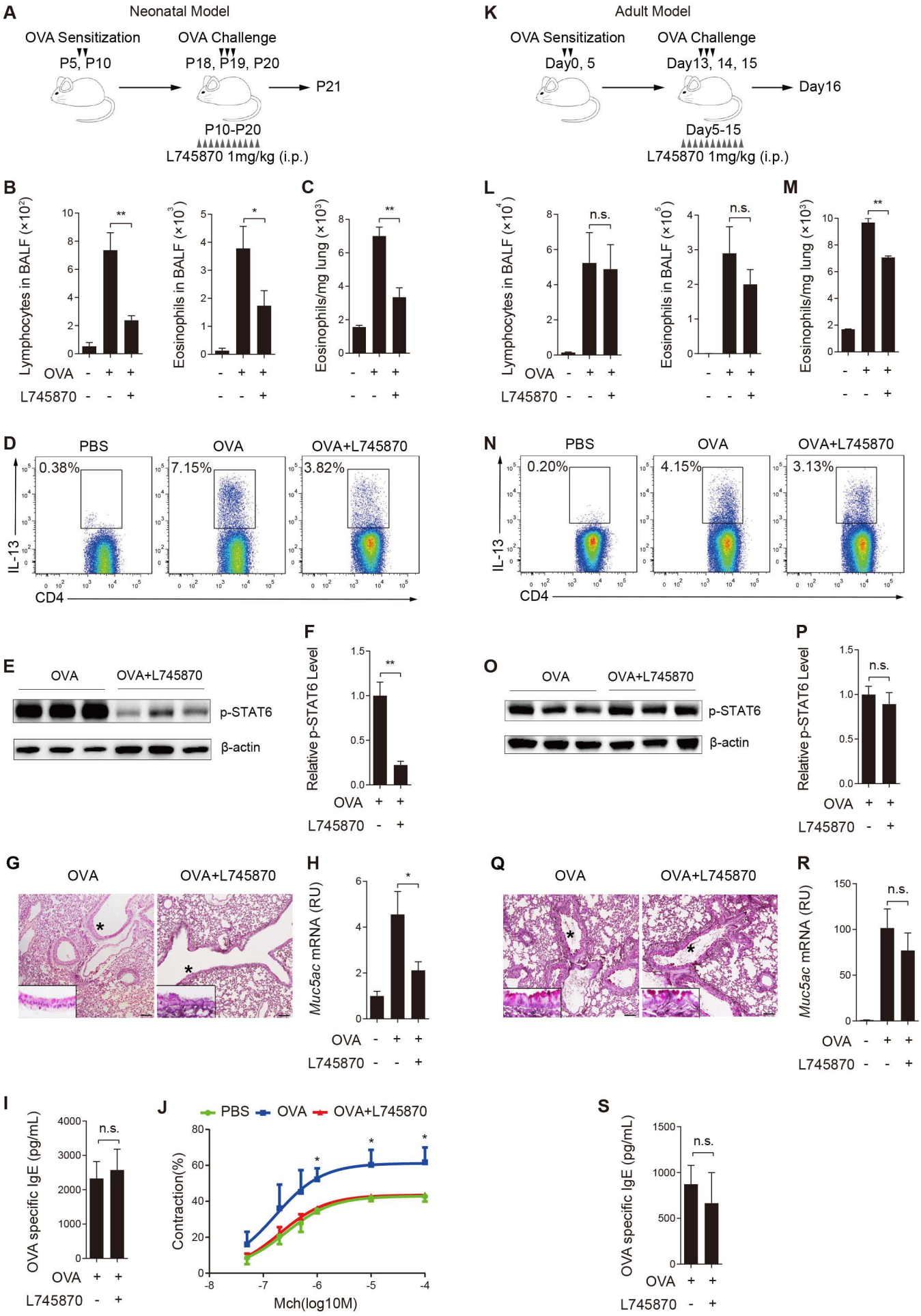
A
Neonatal Model
OVA Sensitization
P5, P10
OVA Challenge
P18, P19, P20
P21
P10-P20
L745870 1mg/kg (i.p.)
K
Adult Model
OVA Sensitization
Day0, 5
OVA Challenge
Day13, 14, 15
Day16
Day5-15
L745870 1mg/kg (i.p.)
B
Lymphocytes in BALF (×10²)
Eosinophils in BALF (×10³)
C
Eosinophils/mg lung (×10³)
OVA
L745870
L
Lymphocytes in BALF (×10⁴)
Eosinophils in BALF (×10⁵)
n.s.
M
Eosinophils/mg lung (×10³)
D
PBS
OVA
OVA+L745870
0.38%
7.15%
3.82%
IL-13
CD4
N
0.20%
4.15%
3.13%
E
p-STAT6
β-actin
F
Relative p-STAT6 Level
O
P
G
H
Muc5ac mRNA (RU)
Q
R
I
OVA specific IgE (pg/mL)
J
Contraction(%)
Mch(log10M)
S

Figure S6. Pharmaceutical blockade of DRD4 signaling ameliorates Th2 inflammation in neonatal mice, but not adult mice, following OVA exposure. Related to Figure 5. (**A**) Experimental scheme of L745870 treatment during OVA sensitization and challenge in neonatal mice. L745870 was given intra-peritoneally at 1 mg/kg body weight daily between P10-P20. Mice were analyzed one day after the last challenge at P21. (**B**) Flow cytometry analyses of lymphocytes and eosinophils in BALF of each group at P21. N=5 for P21 PBS group, N=7 for P21 OVA group and N=7 for P21 OVA+L745870 group in 3 independent experiments. (**C**) The abundance of eosinophils in the lung of each group at P21. Results were normalized to lung weight. N=5 for P21 PBS group, N=7 for P21 OVA group and N=7 for P21 OVA+L745870 group in 3 independent experiments. (**D**) Representative flow cytometry analyses of IL-$13^{+}CD4^{+}$ T cells in P21 lungs of each group. Similar results were obtained from 3 independent experiments. (**E**, **F**) Quantification of p-STAT6 in P21 mouse lungs with and without L745870 treatment by Western blot. β-actin was loading control. Each lane represents one sample. Similar results were obtained from 5-7 mice in 3 independent experiments. (**G**, **H**) Mucus production in different experimental groups assayed by PAS staining and *Muc5ac* qPCR. The area of the airway epithelium marked by * is enlarged and shown in the insert in (**G**). N=9 in 3 independent experiments. Scale bars, 100 µm. (**I**) The amount of OVA-specific IgE in serum from mice at P21 in each group. N=17 in the OVA group and N=12 in OVA+L745870 group from 3 independent experiments. (**J**) Assessment of airway hypercontractility in OVA-exposed mice with and without L745870 treatment at P21 using precision cut lung slices. Airway contractility in response to methacholine was measured by the percentage of reduction in the luminal size from the baseline. N=15-20 airways from 3 mice in 2 independent experiments for each group. (**K**) Experimental scheme of L745870 (1 mg/kg body weight) treatment during OVA sensitization and challenge in adult mice. Adult lungs were analyzed one day after the last challenge at experimental day 16. (**L-S**) Assessment of Th2 inflammation in adult mice with and without L745870 treatment following OVA exposure using similar assays as described in (**B-I**) for neonatal mice. For BALF assays in (**L**), N=7 for each group in 3 independent experiments. For assays in (**M**, **N**), N=5-6 mice in 3 independent experiments. For results in (**O**, **P**), N=3 in 2 independent experiments. For results in (**Q**, **R**), N=8 in 3 independent experiments. For results in (**S**), N=6 in 3 independent experiments. For airway contractility measurement in (**J**), data were analyzed by one-way ANOVA for multiple comparisons between treatment and methacholine dosage. For all other results, data were analyzed by two-tailed student's t test. *$p<0.05$; **$p<0.01$; n.s., not significant.

We noted significant variations in OVA-specific IgE in the neonatal OVA models in (**I**). The variation may explain why the amount of OVA-specific IgE was not statistically significant between WT and *Drd4*$^{-/-}$ mice at P21, although Th2 inflammation was diminished. For panel (**M**), the reduction in eosinophilic infiltrates in the adult lung reached statistical significance in L745870-treated model. However, in other adult exposure

experiments (Figures 5**K** and S5**O**), there was a consistent trend of mild reduction in the number of eosinophils by DRD4 deficiency without reaching statistical significance. The discrepancy may be contributed by technical variations among multiple repeats of the experiment. It is important to note that comparing neonatal and adult mice (Figures S6**C** and S6**M**), L745870 treatment caused a greater reduction in the number of eosinophils in neonates than adults. These findings support our conclusion that the dopamine-DRD4 pathway contributes significantly to the Th2 inflammation in the early lung.

Figure S7

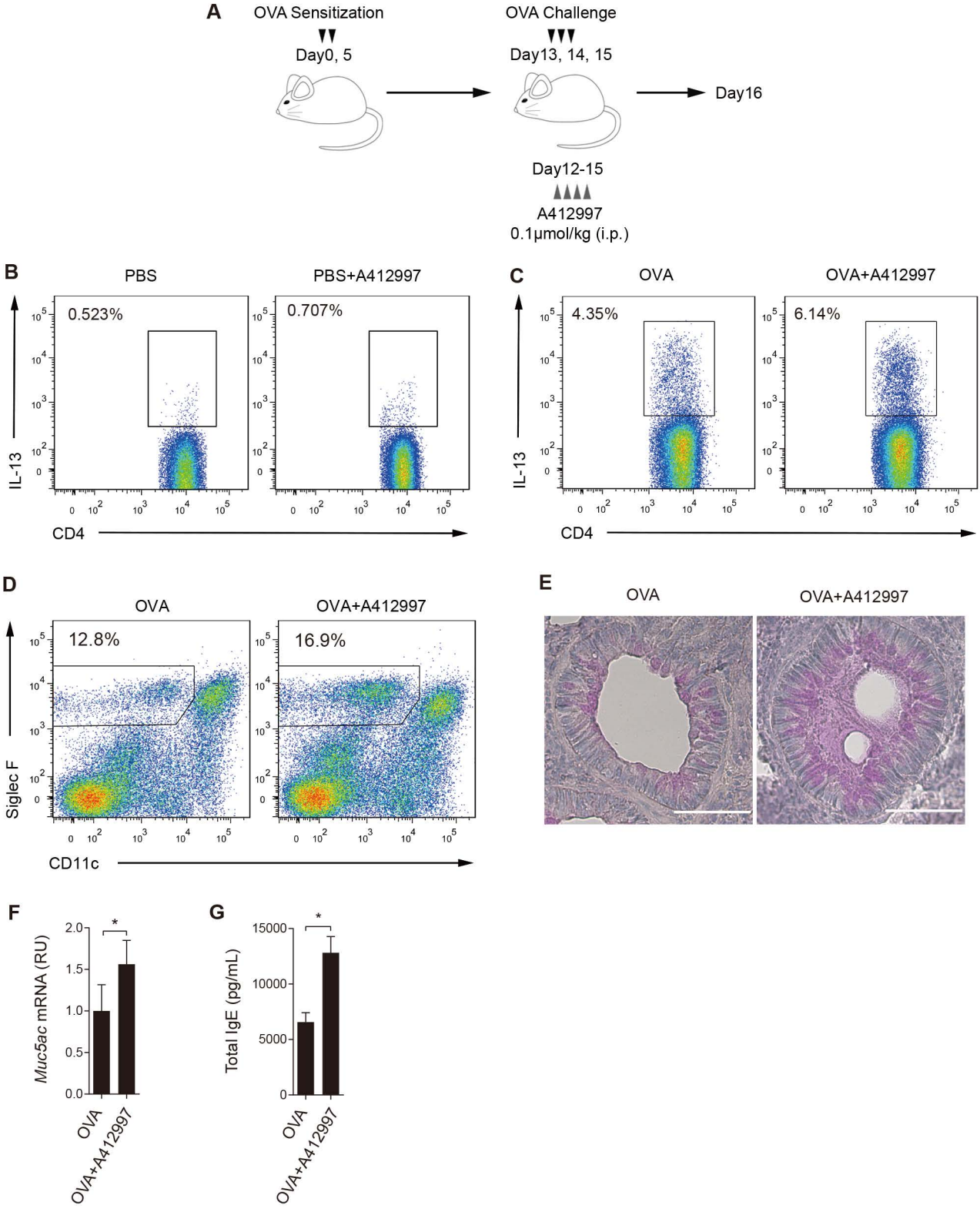
A
OVA Sensitization
Day0, 5
OVA Challenge
Day13, 14, 15
Day16
Day12-15
A412997
0.1μmol/kg (i.p.)
B
PBS
PBS+A412997
0.523%
0.707%
IL-13
CD4
C
OVA
OVA+A412997
4.35%
6.14%
IL-13
CD4
D
OVA
OVA+A412997
12.8%
16.9%
Siglec F
CD11c
E
OVA
OVA+A412997
F
Muc5ac mRNA (RU)
OVA
OVA+A412997
G
Total IgE (pg/mL)
OVA
OVA+A412997

Figure S7. Activation of DRD4 in adult mice by an agonist A412997 worsens Th2 inflammation following OVA exposure. Related to Figure 6.
(**A**) Experimental scheme of A412997 treatment during OVA sensitization and challenge in adult mice. A412997 was given intraperitoneally to adult mice between experimental day 12 -15. A412997 was given once per day at a dose of 1 μmol/kg body weight. Mice were analyzed one day after the last challenge on experimental day 16. (**B-D**) Representative flow cytometry analyses of IL-13^{+}CD4^{+} T cells and eosinophils in the lung of saline- and OVA-exposed mice with and without A412997 treatment. Similar results were obtained from 3 independent experiments. (**E, F**) Mucus overproduction assayed by PAS staining and *Muc5ac* gene expression in OVA-exposed mice with and without A412997 treatment. N=6 in 3 independent experiments. Scale bars, 50 μm. (**G**) The amount of total IgE in serum of OVA-exposed mice with and without A412997 treatment. N=6 in 3 independent experiments. *$p<0.05$ by two-tailed student's t test.